Distribution Agreement

In presenting this thesis or dissertation as a partial fulfillment of the requirements for an advanced degree from Emory University, I hereby grant to Emory University and its agents the non-exclusive license to archive, make accessible, and display my thesis or dissertation in whole or in part in all forms of media, now or hereafter known, including display on the world wide web. I understand that I may select some access restrictions as part of the online submission of this thesis or dissertation. I retain all ownership rights to the copyright of the thesis or dissertation. I also retain the right to use in future works (such as articles or books) all or part of this thesis or dissertation.

Signature:

_____ _____

Andrea R. Pack Date

Measuring and Understanding Muscular Control of Vocal Production in Songbirds
(The neuromuscular dynamics of avian karaoke)

By
Andrea R. Pack
Doctor of Philosophy

Graduate Division of Biological and Biomedical Sciences (Neuroscience)

Samuel Sober, Ph.D.
Advisor

Gordon Berman, Ph.D.
Committee Member

Edelle Field-Fote, Ph.D.
Committee Member

Simon Sponberg, Ph.D.
Committee Member

Lena Ting, Ph.D.
Committee Member

Accepted

Kimberly J. Arriola, Ph.D., MPH
Dean of the James T. Laney School of Graduate Studies

Measuring and Understanding Muscular Control of Vocal Production in Songbirds

By

Andrea R. Pack
B.S. University of Vermont, VT, 2011

Advisor: Samuel Sober, Ph.D.

An abstract of
A dissertation submitted to the Faculty of the
James T. Laney School of Graduate Studies of Emory University
in partial fulfillment of the requirements for the degree of
Doctor of Philosophy
in Graduate Division of Biological and Biomedical Sciences (Neuroscience)
2022

Abstract

Measuring and Understanding Muscular Control of Vocal Production in Songbirds

By Andrea R. Pack

Motor control requires the brain to rapidly process sensory signals and coordinate precise patterns of muscle activity. A central objective in neuroscience is to establish how the brain controls muscle activity and modifies muscle output during motor skill learning. Our prior work in songbirds quantified the timescale at which patterns of neural and muscle activity control vocal and respiratory behavior and demonstrated that millisecond-scale variations in spike patterning in cortical neurons and respiratory muscle fibers are correlated with the upcoming motor output (Srivastava et al., 2017; Tang et al., 2014). However, it is still unknown whether and how muscle fibers transform these precisely timed spikes patterns into variations in behavior. The first set of experiments mentioned above targeted a larger, superficial muscle in the songbird which controls the exhalation phase in a breathing cycle (i.e., expiratory muscle group). My dissertation extends this line of inquiry by investigating whether millisecond-scale differences in activation patterns to vocal organ muscles affect motor output (e.g., singing). Conventional implantable fine-wire electrodes and non-invasive surface skin electrodes are not capable of recording electromyography (EMG) activity from the muscles of interest due to the small size of vocal organ muscles and the deep, internal location of the songbird's vocal organ. To address these limitations, we developed an innovative bipolar electrode array made from extremely flexible and strong carbon nanotube fibers (CNTFs) to simultaneously measure EMG activity from multiple small vocal organ muscles in songbirds during an acute experimental paradigm. As detailed in Chapter 2, the new bipolar CNTF electrode array recordings successfully recorded single-unit spike trains and yielded multi-unit recordings with higher signal-to-noise ratios compared to stainless steel electrodes. We then experimentally induced two- and three-pulse stimulation patterns in fiber bundles from a vocal organ muscle *in vitro* and measured and compared the corresponding changes in force output to determine whether millisecond-scale differences in muscle stimulation patterns modulate force output. These experiments demonstrated that songbird vocal organ muscles exhibit strong timing-based nonlinear force output during short interpulse intervals (IPIs; i.e., IPIs < 15 ms), and suggest that these nonlinearities, along with nonlinearities we have previously described in songbird respiratory muscles, are a crucial feature of vocal behavior. These results will guide future studies to examine how muscle activity is organized across time and space as a skilled behavior is learned, offering new insights into motor control.

Measuring and Understanding Muscular Control of Vocal Production in Songbirds

By

Andrea R. Pack
B.S. University of Vermont, VT, 2011

Advisor: Samuel Sober, Ph.D.

A dissertation submitted to the Faculty of the
James T. Laney School of Graduate Studies of Emory University
in partial fulfillment of the requirements for the degree of
Doctor of Philosophy
in Graduate Division of Biological and Biomedical Sciences (Neuroscience)
2022

Acknowledgments

First, I would like to thank my advisor, Dr. Sam Sober, for his insight and support throughout the entire PhD process. Thank you for all of the opportunities you have given me throughout the last 7.5 years: working with collaborators, attending and presenting at conferences all over the world, and teaching at Phillips State Prison through Common Good Atlanta (CGA). Your enthusiasm and approach to science has created a welcoming and positive lab environment that inspires creative and collaborative research. My project was incredibly exciting and extremely hard, and if something could go wrong, it did. Although the project did not go as planned, you helped me embrace the many challenges with a positive attitude.

I would like to thank my committee, Dr. Gordon Berman, Dr. Edelle Field-Fote, Dr. Simon Sponberg, and Dr. Lena Ting, for your thoughtful feedback, expertise, scientific conversations, time, and advice (not limited to scientific) throughout my PhD. Thank you for providing me with space and support to navigate my PhD while figuring out how to address my health. Yours and Sam's understanding and guidance are the reasons I was able to successfully defend my PhD.

I would also like to thank my collaborators, Dr. Coen Elemans and Dr. Iris Adam, at the University of Southern Denmark. I was fortunate enough to work in their lab for an extended period of time. Their excitement and dedication to science continues to inspire me. It was in their lab where I learned a deep appreciation for birds.

A lab isn't a lab without all of its members. I am so grateful to have worked with the Sober lab members, both past and present. It was a wonderful environment to be in while pushing through the challenges of grad school. Thank you for the encouragement on hard days, endless amounts of advice, and meaningful conversations. My time in the lab was filled with so many laughs (and tears), bad jokes, dangerous lab fun days, and many fun lab dinners at the Sober house. The

welcoming community extended throughout the Biology Department and the Neuroscience program. During my time at Emory, my colleagues have turned into lifelong friends and role models.

The first experience I had working in a lab was with Dr. Randy Nudo. I would not have ventured to grad school without his mentorship, ongoing support, or my experience in the Nudo lab. I am thankful for the people in the Nudo lab who have become friends and have supported me throughout my science career. I gained so much knowledge and discovered my passion in Neuroscience.

I would also like to thank Dr. Sarah Higinbotham, Dr. Elizabeth Beck, Dr. Owen Cantrell, and the Common Good Atlanta community. I am grateful for the opportunity to bring science to curious and gracious students at Phillips State Prison. It has been such an incredible and eye-opening experience that I want to continue doing where ever my life takes me.

Lastly, I want to thank my family and friends. Mom and Dad, thank you for indulging (not always by choice) in the endless amounts of questions I asked as a kid. Your constant love and support for my curiosities helped me be the person I am today. I am grateful for my community of people that provide me with continuous encouragement and support. You all continued to motivate and help me throughout this difficult and sometimes defeating process. Without you all, I wouldn't be here.

Table of Contents

List of Figures

List of Supporting Figures

List of Tables

List of Symbols and Abbreviations

ACh	acetylcholine
AFP	anterior forebrain pathway
ATP	adenosine triphosphate
BMI	brain machine interface
Ca^{2+}	calcium
CM	medial mesopallium
CNT	carbon nanotube
CNTF	carbon nanotube fiber
CNS	central nervous system
DLM	dorsolateral nucleus of the medial thalamus
dph	days post hatch
DDS	deep dorsal syringeal muscle (*musculus syringealis dorsalis profundus*); one of three DS muscles
DS	dorsal syringeal muscle (*musculus syringealis dorsalis*)
DTB	dorsal tracheobronchial muscle (*musculus tracheobronchialis dorsalis*)
DVTB	deep ventral tracheobronchial muscle (*musculus tracheobronchialis ventralis profundus*); one of two VTB muscles
EMG	electromyography
HVC	used as a proper noun; the nucleus upstream of RA
IPI	interpulse interval
ISI	interspike interval
LDS	lateral dorsal syringeal muscle (*musculus syringealis dorsalis lateralis*); one of three DS muscles

LMAN	lateral magnocellular nucleus of the anterior nidopallium
M1	primary motor cortex
MEAD	myo-elastic aerodynamic theory
MDS	medial dorsal syringeal muscle (*musculus syringealis dorsalis medialis*); one of three DS muscles
MU	multi-unit
NCM	caudal medial nidopallium
NMF	non-negative matrix factorization
NMT	neuromuscular transform
PCA	principle component analysis
Pt-Ir	platinum iridium
RA	robust nucleus of the arcopallium
SCI	spinal cord injury
SD	standard deviation
SDU	University of Southern Denmark
SEM	standard error of the mean
SNR	signal-to-noise ratio
SR	sarcoplasmic reticulum
SSW	stainless-steel wire
STB	short trachealbronchial muscle (*musculus tracheobronchialis brevis*)
SU	single-unit
SVTB	superficial ventral tracheobronchial muscle (*musculus tracheobronchialis ventralis superficialis*); one of two VTB muscles
$nXII_{ts}$	tracheosyringeal portion of the hypoglossal motor nucleus

VAF variance accounted for

VS ventral syringeal muscle (*musculus syringealis ventralis*)

VTB ventral tracheobronchial muscle (*musculus tracheobronchialis ventralis*)

wfANOVA wavelet-based functional ANOVA

Dissertation Overview

- **Chapter 1** provides an introduction and review of literature on the insights and challenges of deciphering the neural control of skilled behavior, specifically focusing on how the electrical activity is translated to behavioral output (i.e., motor code) in the muscle.
- **Chapter 2** characterizes the recording parameters of a novel EMG bipolar electrode array, where each bipolar electrode is made from two single Parylene-C CNTFs twisted together. First, we present two designs to build CNTF bipolar electrode arrays and a protocol for collecting bipolar EMG activity from small, deep muscles in the vocal organ in an acute experimental paradigm. We then report how the unique characteristics of the CNTFs, such as extreme flexibility, high electrical conductivity, and mechanical strength, make for excellent electrodes. The data demonstrates that the bending stiffness of CNTFs is 8 times lower when compared to the standard stainless-steel wire (SSW) used in EMG recordings. Additionally, we show that CNTFs provide a higher signal-to-noise ratio (SNR) and can record both single-unit (SU) and multi-unit (MU) activity. Lastly, we discuss an interpretation of these results and arguments supporting the use of CNTFs as a material for EMG bipolar electrodes.
- **Chapter 3** pursues answers to whether millisecond-scale differences in songbird vocal muscle stimulation patterns modulate the force output of muscle fibers. To do this, we experimentally induced double- and triple-pulse stimulation patterns in fiber bundles from a vocal muscle *in vitro* and measured the corresponding changes in force output. We found that every double- and triple-pulse stimulation pattern produced distinguishable force waveforms, which was supported by our wavelet-based functional ANOVA (wfANOVA)

results where all contrast curves derived from the analysis showed a significant effect. Furthermore, the data demonstrates muscles of the songbird vocal organ exhibit strong timing-based nonlinear force output during short interpulse intervals (IPIs; i.e., IPIs < 15 ms). We then discuss the importance of these results, which suggest that the vocal organ muscles in songbirds can translate millisecond-scale differences in neural activity to meaningful changes in their vocal behavior.

- **Chapter 4** summarizes the data presented in Chapters 2 and 3, and then examines potential future research questions and directions that emerged as a result of this dissertation.
- A comprehensive list of references cited in this dissertation.

Chapter 1

Introduction and Literature Review

1.1 The neurobiology of motor control

1.1.1 What is motor control?

A fundamental problem in neuroscience is understanding how neural signals coordinate muscle activity to produce behavior. Some complex behaviors require the animal to participate in motor skill learning, which refers to the increasing accuracy, speed, and adaptability of intentional movements with practice. In most cases, many motor commands can be used to achieve the same goal, requiring the brain to develop strategies to flexibly coordinate the actions of groups of muscles. Without the precise integration of neural signals to execute coordinated motor output, animals lose their ability to perform learned behaviors.

The organization and production of movement is a complex problem because of the necessity to coordinate multiple body systems (e.g., central processing and the peripheral motor system output) and multiple levels (e.g., pallium, brain stem, and muscles). Complex motor control includes both involuntary, spontaneous movements (e.g., reflexes), automatic motor behaviors (e.g., breathing), and voluntary movements (e.g., directed movements), which typically involve sensorimotor learning. This thesis will focus on motor skills that are acquired through sensorimotor learning. To perform a learned motor skill, first, the brain gathers sensory information from the environment. The afferent sensory information determines an appropriate plan of action that is executed via the primary motor cortex (M1). M1 Neurons send information (via electrical activity) to the motor

neurons, which are located in the brain stem or spinal cord, and the motor neurons directly innervate the necessary muscles. We then use sensory feedback to correct any errors in the behavior, resulting in a modified plan of action.

In the mid-20th century, the motor system community emphasized the importance of understanding the interactions between the brain, musculoskeletal, internal forces, and external forces (e.g., environment, goal, and gravity) to comprehend complex motor control (Bernshteĭn, 1967; Thomas, 1967). As mentioned above, there are multiple solutions to executing behaviors (e.g., multiple motor commands can be used to achieve the same goal). This is known as the degrees of freedom problem (i.e., motor equivalence problem), where the degrees of freedom is the sum of all independent ranges of motion at each joint (Bernshteĭn, 1967; Scholz & Schöner, 1999). One difficulty in understanding the mechanisms underpinning motor control is deciphering how the motor system organizes, simplifies, and selects which solution it will use to complete the task. To address this problem, Bernstein (Bernshteĭn, 1967) proposed that the brain controls muscles by reducing degrees of freedom through ensembles (i.e., synergies; units for organization and simplification) (Davies, 1968; Kelso, 2009; Kelso, 1995; Thomas, 1967; Turvey & Carello, 1996). I will specifically focus on the concept of muscle ensembles, where one ensemble is a pattern of relative levels of muscle activation that can be scaled up or down over time (Torres-Oviedo & Ting, 2007).

Past research has shown that the complex stimulation patterns observed across muscles can be explained by time-varying combinations of a muscle ensemble representing a consistent pattern of activity across multiple muscles (Ting, 2007). Muscles can engage in more than one muscle ensemble, and the activation of multiple muscle ensembles at varying levels is required to produce complex motor behavior (Torres-Oviedo & Ting, 2007). The number of muscle ensembles has

been shown to increase as motor learning progresses (Dominici et al., 2011; Sawers et al., 2015; Torres-Oviedo & Ting, 2007). Many neurological disorders affecting the motor system, such as stroke and spinal cord injury (SCI), disrupt neural output signals to muscles, consequently affecting the person's ability to coordinate activity across muscles and perform motor behaviors (Gowland et al., 1992). Research has demonstrated that some people with stroke and SCI have shown a decrease in the number of muscle ensembles, which correlates with abnormal coupling of muscles and motor deficits (Clark et al., 2010; Fox et al., 2013). A large body of literature demonstrates how skeletal muscle ensembles are activated during motor performance (Berniker et al., 2009; Israely et al., 2018; Sawers et al., 2015; Sharif Razavian et al., 2019; Ting, 2007; Ting & Chiel, 2017; Ting & McKay, 2007; Torres-Oviedo & Ting, 2007), but there is little known about the origins and uses of intermuscular coordination and how patterns of coordinated activity across multiple muscles emerge when learning and performing a skilled behavior.

There are two main challenges to studying how the brain controls skilled behavior. The first challenge is recording motor commands at the level of the muscle. To understand how complex muscle stimulation patterns produce various motor behaviors, it is necessary to collect a large number of concurrent recordings within and across multiple muscles. Unfortunately, current muscle recording technology typically relies on non-invasive skin-level surface electrodes or the insertion of fine wires into the muscles. Surface electrodes are unable to record activity from deep or small muscles, and wire electrodes are stiff and tend to injure the muscle at the implant site. Moreover, traditional EMG methods are often unable to isolate spike trains from individual motor units within muscles. The second challenge is understanding the information the motor commands are carrying at the level of the muscle. We know that motor units transmit information about the upcoming behavior by modulating the timescales of the spike patterns. Recent work from many

labs has demonstrated the importance of milliseconds-scale spike timing in motor control, particularly at the level of the muscles (Putney et al., 2019; Sober et al., 2018; Srivastava et al., 2017; Tang et al., 2014; Zhurov & Brezina, 2006). Because muscles have been shown to be sensitive to the timing of the activity patterns, it is essential to be able to record and isolate single spikes. To address both of these challenges, we need new recording technology that is small, flexible, and strong. Understanding how muscles modulate spike patterns will help the motor systems community explain the biomechanical bases of precise motor control.

1.1.2 Dissertation objectives

Our goal is to contribute to the understanding of how patterns of muscle activity control behaviors attained through sensorimotor learning. The focus of this thesis will address the two main challenges mentioned above. In chapter 2, we developed and characterized a novel electrode array that can be used to record fine-scale muscle activity from multiple small, deep muscles. In chapter 3, we begin to address how changes in the time-scale of activation patterns at the level of the muscle alter behavior by experimentally inducing activation timing patterns with variations in the IPIs and measuring the force output. In this thesis, the terms ‘activation (timing) patterns’ and ‘IPI(s)’ refer to experimentally induced stimulation to the muscle, whereas, the terms ‘spike (timing) patterns’ and ‘ISI(s)’ refer to biologically induced stimulation to the muscle. We hope the work reported in this dissertation impacts the understanding of the interactions between neural control and biomechanics.

1.2 Songbirds as a model system for vocal control and sensorimotor learning

1.2.1 Motivations to study bird vocal production

Birdsong and human speech are complex acoustic signals. The sounds are produced by the flow of air during expiration through a vocal motor organ (e.g., syrinx and larynx, respectively). Bengalese finches (*Lonchura striata domestica*), a species of songbirds, provide an ideal model system for studying complex motor control for three primary reasons. First, there are very few animals, including songbirds (Brainard & Doupe, 2002), bats (Boughman, 1998; Boughman & Wilkinson, 1998), elephants (Poole et al., 2005), and cetaceans (Janik, 2014), that learn and produce vocal behaviors similar to humans (Kuhl & Meltzoff, 1996; P. Marler, 1970). Songbirds acquire their vocal behavior through sensorimotor learning, which is characterized by a reduction in variability and a convergence of the motor program on a specific target behavior (D. M. Wolpert et al., 2011). Similar to human speech, birdsong is divided into syllables with sounds of silence in between syllables. Song develops during a critical period that occurs once in the bird's life, approximately 25-90 days post hatch (dph) (A. J. Doupe & P. K. Kuhl, 1999; Kroodsma & Pickert, 1980). The bird learns its song from a tutor, an adult male songbird, in two stages: sensory acquisition and sensorimotor learning. During sensory acquisition, the juvenile bird listens to and memorizes one or more tutor songs, creating a song template. During sensorimotor learning, the juvenile gradually matches its highly variable, "plastic song" to the memorized template using auditory feedback (A. J. Doupe & P. K. Kuhl, 1999). A "crystalized song" marks the end of sensorimotor learning, at which time the juvenile songbird has learned the tutor song (Brainard & Doupe, 2002). After the song is crystalized, the bird produces a less variable song that stays stable

throughout adulthood as long as no sensory manipulation is introduced to the song (Hoffmann et al., 2012).

Secondly, the finch species song repertoire consists of one song that is spontaneously produced hundreds of times per day with slight variations depending on sensory input, environmental influence, and stage of learning (Kroodsma, 1980). Birds have the ability to modify their song in social contexts (i.e., direct song – less variable and intended for courtship vs. indirect song – extremely variable, usually produced when the bird is alone, and considered the exploratory or practice state) (Dunn & Zann, 1996a, 1996b; Jarvis et al., 1998) and in response to sensory manipulations (e.g., auditory feedback) (Hoffmann et al., 2012; Sober & Brainard, 2009; Zhu et al., 2019). Not only is their song highly quantifiable, but we are also able to understand how the acoustic and sequential (i.e., ordering of syllables) features change over learning from their plastic to crystalized song (Kao & Brainard, 2006). Lastly, songbirds have well-defined circuitry that is exclusively dedicated to the learning and production of song (Scharff & Nottebohm, 1991). This allows us to develop an array of experiments that can manipulate brain areas involved with song

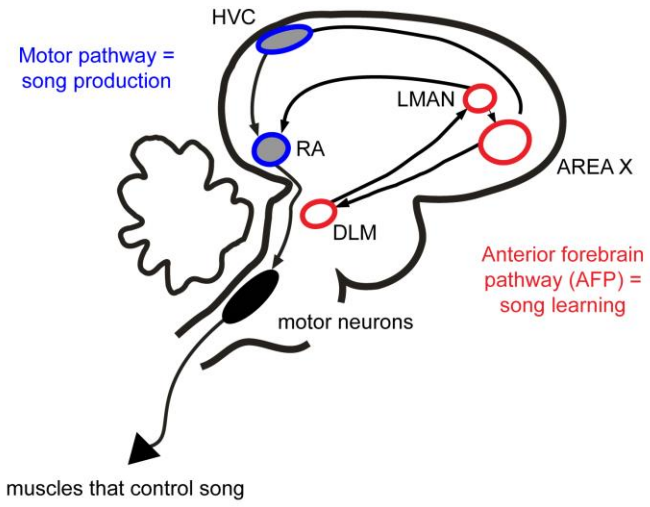

Figure 1.1: Songbird Neuroanatomy. The motor pathway (blue), required for vocal production, contains the robust nucleus of the arcopallium (RA), which projects to brainstem motoneurons (black) innervating the vocal muscles. The anterior forebrain pathway (AFP; red) is a basal ganglia circuit, including lateral magnocellular nucleus of the anterior nidopallium (LMAN), Area X, and dorsolateral nucleus of the medial thalamus (DLM), controlling vocal learning.

without altering other behaviors (Nottebohm et al., 1976). The next section will detail brain areas and muscles involved in song learning and production.

1.2.2 Overview of song system circuitry

Vocal learners (i.e., humans, bats, cetaceans, and songbirds) have cortical brain regions that control vocal behavior in addition to regions that control innate vocal behavior. This differs from non-vocal learners (e.g., chickens) who only have midbrain and brainstem regions that control innate vocalizations. The songbirds' song system circuitry is unique in that it is the only known motor system that has two spatially separated pathways only dedicated to vocal learning (anterior forebrain pathway, AFP) and vocal production (motor pathway) (Brainard & Doupe, 2013) (Figure 1.1). The AFP, which is analogous to the basal ganglia thalamocortical circuit, consists of three nuclei – Area X, dorsolateral nucleus of the medial thalamus (DLM), and lateral magnocellular nucleus of the anterior nidopallium (LMAN). Previous studies have shown that lesions to LMAN disrupt juvenile song learning (Bottjer et al., 1984; Kittelberger & Mooney, 1999) and adult song plasticity (Brainard & Doupe, 2002, 2013). Similarly, lesions to Area X impaired song learning (Scharff & Nottebohm, 1991; Sohrabji et al., 1990) and song variability (Olveczky et al., 2005). Lesions to the AFP disrupt song learning but have no significant effect on song production. The AFP actively generates exploratory song variability and consolidates learning via LMAN to the robust nucleus of the arcopallium (RA).

The motor pathway consists of two pallial nuclei – HVC (used as a proper name) and RA (Vu et al., 1994; Wild, 1997). HVC is analogous to the pre-motor cortex in mammals and projects to RA via HVC_{RA} neurons and Area X (AFP) via HVC_{X} neurons, playing an important role in both song production and song learning, respectively. Research has shown that a population of HVC_{RA} neurons control the entire time course of a song (Long & Fee, 2008), including the respiratory

timing, where the same individual neurons fire once per song motif (Hahnloser et al., 2002; Long & Fee, 2008), suggesting that HVC contains a pattern generator for song (Vu et al., 1994). RA is analogous to M1 in mammals and projects to brainstem nuclei that control vocal (tracheosyringeal portion of the hypoglossal motor nucleus - $nXII_{ts}$) and respiratory (ventral respiratory group - VRG) muscles. $nXII_{ts}$ projects to the vocal organ (syrinx), the nucleus retroambigualis projects to the expiratory muscle group, and the nucleus parambigualis projects to the inspiratory muscles. Those three muscle groups are essential for song production (Schmidt & Martin Wild, 2014; Wild, 1997).

Many stimulation and lesion studies have contributed to our understanding of the motor pathway. Any lesion to the motor pathway directly affects song production, either leading to a non-discernable song or muteness. Stimulation of HVC during song interrupts and resets the song program, whereas stimulation to RA during song disrupts the syllable the bird is singing but has no effect on the temporal pattern set by HVC (Vu et al., 1994). These results suggest that HVC_{RA} neurons encode the sequencing of syllables, whereas activity in RA neurons is correlated with elements (Yu & Margoliash, 1996) and spectral features of the song, such as fundamental frequency, amplitude, and spectral entropy (i.e., a measure to characterize the audio spectrum from pure tone to white noise) (Sober et al., 2008; Tchernichovski et al., 2001; Wild, 1997).

The songbird community has concentrated their efforts on understanding how the brain changes during juvenile song acquisition and performance, but there is little knowledge regarding shifts in activity patterns in the muscles, specifically breathing muscles and the vocal organ, from subsong to crystalized song. In contrast to our lack of knowledge about muscle changes, neural recordings have shown considerable changes during song acquisition. The firing patterns of RA from subsong to crystalized song change quite drastically. During subsong, RA neurons discharge sporadically

and are more likely to spike evenly across the motif with occasional bursts of activity. As their song crystalizes, RA neurons become highly stereotyped and precise bursts of activity, typically active in only one part of the song (i.e., increase in sparseness) (Leonardo & Fee, 2005; Olveczky et al., 2005). In addition, the average firing rate of neurons in RA during song increase from 36.2 ± 22.8 Hz to 71.1 ± 25.0 Hz as the behavior is learned (Olveczky et al., 2005).

As mentioned earlier, songbirds learn and maintain their song through sensorimotor learning. Although our lab recently demonstrated that songbirds can make changes to their song from non-auditory (e.g., cutaneous electric shocks) feedback (McGregor et al., 2022), most research has focused on how auditory feedback affects song and how the AFP and motor pathway interact with auditory feedback. Researchers have demonstrated deafening birds cause their song to degrade over time, suggesting that auditory feedback is essential to learn and maintain a stable (i.e., crystalized) song (A. J. Doupe & P. K. Kuhl, 1999;

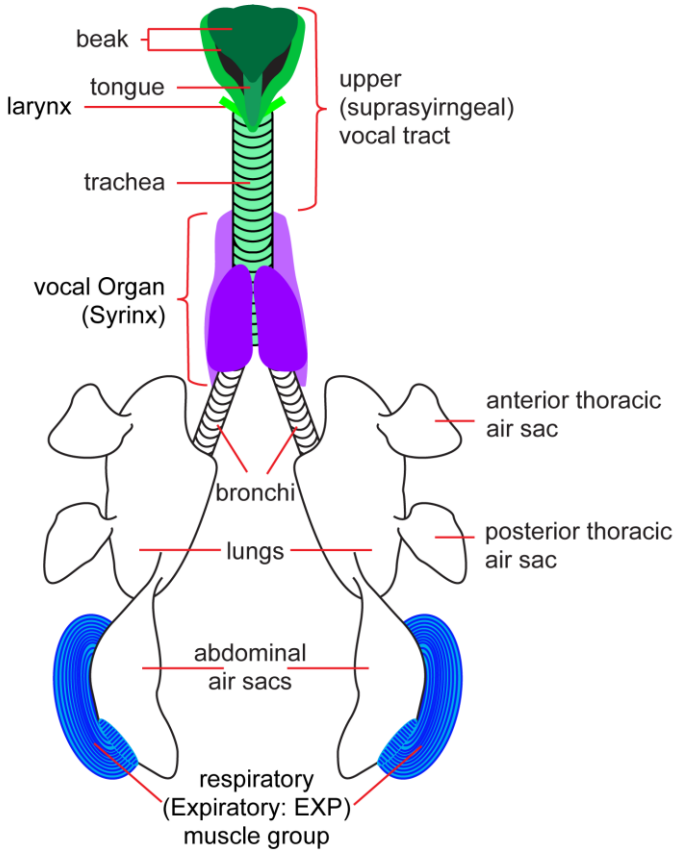

Figure 1.2: Respiratory system, vocal organ, and upper vocal tract schematic. The respiratory (i.e., air pressure system) system controls breathing and consists of lungs, air sacs, and respiratory muscles (shown in blue). The vocal organ (shown in purple) controls the vocal behavior and consists of seven bilateral muscles. Lastly, the upper (i.e., suprasyringeal) vocal tract (shown in green) acts as a variable resonant filter and consists of trachea, larynx, oropharyngeal cavity, beak, and tongue.

Nordeen & Nordeen, 1992; Winkler, 2001). Through many synapses, starting at the hair cells, songbirds' auditory feedback pathway connects to the thalamic nucleus ovoidalis which in turn connects to the primary auditory cortex (i.e., L2 of Field L). Although controversial, it is thought that L2 of Field L has an indirect connection to HVC via nucleus interfacialis, one of three secondary auditory areas, where auditory feedback is integrated into the AFP and the motor pathway (Kelley & Nottebohm, 1979; Vates et al., 1996). The other two secondary auditory areas are caudal medial nidopallium (NCM) and caudal mesopallium (CM), two nuclei that aid with the perceptional processing of novel song and familiar song, respectively (Gobes et al., 2010; Mooney, 2009). Additionally, lesions to NCM and CM cause a decrease in a bird's ability to form auditory memories of previously heard songs, which is necessary for song learning (Gobes & Bolhuis, 2007).

1.2.3 Vocal organ anatomy and function

Singing in birds, like human speech, requires three subsystems outside of the central nervous system (CNS): the respiratory system, the vocal organ, and the upper vocal tract (Figure 1.2). First, I will briefly discuss the components of the three subsystems, and then I will talk about how the systems work together to produce vocalizations in songbirds. Lastly, I will discuss the similarities and differences between bird and human vocal motor mechanisms.

Producing vocalization requires precise coordination between the respiratory system and the vocal motor pathway (Andalman et al., 2011; Schmidt & Martin Wild, 2014). The respiratory system plays a crucial role in birds producing complex song patterns, allowing the birds to produce sound for long durations and manipulate temporal features of the song. The air pressure system controls respiration and consists of lungs, air sacs, and respiratory muscles (Düring et al., 2013; Goller & Cooper, 2004; Schmidt & Martin Wild, 2014) (Figure 1.2). Air sacs are internal membranous

structures that hold air and facilitate internal airflow. There are two groups of air sacs: 1) the cranial group consisting of bilateral cervical, clavicular, and cranial thoracic sacs, and 2) the caudal group consisting of bilateral caudal thoracic and abdominal sacs. Lastly, the expiratory muscle group (*m. obliquus externus abdominis, m. obliquus internus, and m. transversus abdominis*) controls ventilation in the exhalation phase of the breath cycle, and the inspiratory muscles (mostly made up of external intercostal muscles) control ventilation in the inhalation phase (Düring et al., 2013; Goller & Cooper, 2004; Hartley, 1990; Schmidt & Martin Wild, 2014; Srivastava et al., 2017).

The syrinx, or the bird's vocal organ, is located at the bifurcation of the trachea into two bronchi (Figure 1.3) and surrounded by an air sac (Düring et al., 2013; Riede et al., 2019). Each bronchus has a set of independently controlled labia (i.e., vibrating membranes) that oscillate with airflow (Fee et al., 1998; Goller & Larsen, 1997, 2002; Riede & Goller, 2010a). With two sets of labia, songbirds can either produce syllables by oscillating the bilateral membranes simultaneously or by oscillating each pair of membranes independently, leading to two independent sound sources (M.

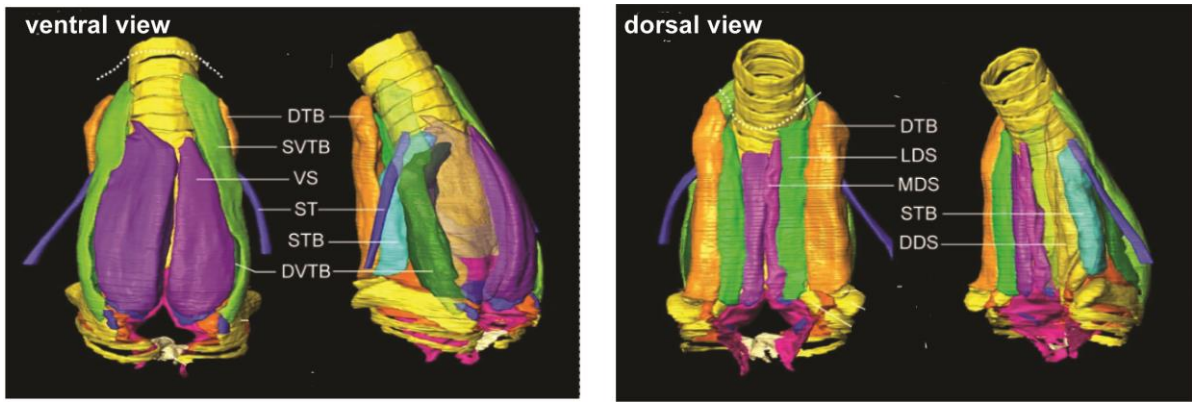

Figure 1.3: Syrinx (vocal organ) schematic. Ventral (left panel) and dorsal (right panel) view of male zebra finch syrinx. Muscle abbreviations: deep dorsal syringeal muscle - DDS: yellow; dorsal tracheobronchial muscle - DTB: orange; deep ventral tracheobronchial muscle - DVTB: dark green; lateral dorsal syringeal muscle - LDS: neon green; medial dorsal syringeal muscle - MDS: violet; sternotracheal muscle - ST: blue; short tracheobronchial muscle - STB: cyan; superficial ventral tracheobronchial muscle SVTB: light green; ventral syringeal muscle - VS: purple. Adapted from (Düring et al., 2013).

S. Fee, 2002; Fee et al., 1998; Goller & Larsen, 1997, 2002; Goller & Suthers, 1995; Suthers et al., 2004). Ten pairs of muscles make up the syrinx, which modulates and regulates airflow from the air sacs to the upper vocal tracts to produce sound (Düring et al., 2013; Suthers & Zollinger, 2004) (Figure 1.3). This includes five bilateral intrinsic muscles (i.e., muscles with both attachment sites on the syrinx) and two bilateral extrinsic muscles (i.e., muscles with one attachment site outside of the syrinx). Each muscle can control several acoustic parameters related to song (e.g., fundamental frequency, amplitude, and spectral entropy), and the function of each muscle can vary with each syllable (Srivastava et al., 2015). Additionally, the vocal organ controls the fast and fine temporal dynamics of song.

There are five intrinsic muscles. The ventral syringeal muscle (*musculus syringealis ventralis*; VS), ventral tracheobronchial muscle (*musculus tracheobronchialis ventralis*; VTB), dorsal syringeal muscle (*musculus syringealis dorsalis*, DS), dorsal tracheobronchial muscle (*musculus tracheobronchialis dorsalis*; DTB), and short trachealbronchial muscle (*musculus tracheobronchialis brevis*, STB) (Düring et al., 2013; Larsen & Goller, 2002; Vicario, 1991a, 1991b). VS is the largest vocal muscle (i.e., 2 x 4 mm) and is highly correlated with fundamental frequency, or pitch, of the song (Adam & Elemans, 2020; Srivastava et al., 2015). It is thought VS regulates the tension of the medial vibrating membrane (i.e., labia) located in each bronchi to control pitch during vocalization. The DS muscle is made up of 3 parts: deep dorsal syringeal muscle (*musculus syringealis dorsalis profundus*; DDS), medial dorsal syringeal muscle (*musculus syringealis dorsalis medialis*; MDS), and lateral dorsal syringeal muscle (*musculus syringealis dorsalis lateralis*, LDS) (Düring et al., 2013). These muscles initiate sound production by rotating the bronchial cartilages and adducting the vibrating membranes (Goller & Suthers, 1996). VTB is made up of two parts, the superficial ventral tracheobronchial muscle (*musculus*

tracheobronchialis ventralis superficialis; sVTB) and the deep ventral tracheobronchial muscle (*musculus tracheobronchialis ventralis profundus*; dVTB) (Düring et al., 2013). VTB abducts the vocal membrane, increasing airflow and modulating syringeal resistance during phonation (Goller & Suthers, 1995; Goller & Suthers, 1996). This muscle group is active during the inspirations that occur during silent periods of the song. Previous research demonstrated that DTB adducts the lateral labia in response to microstimulation, with the capability of modulating and decreasing airflow and sound amplitude (C. P. H. Elemans et al., 2008; Larsen & Goller, 2002). The two extrinsic muscles, muscles with one attachment site outside of syrinx, are the sternotracheal muscle (*musculus sternotrachealis*, ST) and tracheolateral muscle (*musculus tracheolateralis*; TL) (Düring et al., 2013). Research suggests that the ST muscle is used to alter the length of the trachea during breathing, and the TL muscle contributes to controlling membrane tension (Goller & Cooper, 2004; Riede & Goller, 2010b) (Figure 1.3). The last subsystem required for producing sound is the suprasyirngeal (i.e., upper) vocal tract, which includes the trachea, larynx, oropharyngeal cavity, beak, and tongue (Düring et al., 2013; Suthers & Zollinger, 2004; Vicario, 1991b). The larynx in a bird, not to be confused with the larynx in a human, is located above the trachea, lacks sound generating labia, and functions as a respiratory valve that protects the airway. Not only does the vocal tract create a distinctive sound for each bird, but it also filters acoustic properties to control the spectral composition, such as harmonics, of song (Nowicki, 1987; Riede et al., 2006).

1.2.4 Superfast muscles

Many songbirds produce syllables and/or songs that are complex (e.g., trills) and require extraordinarily fast control (Goller & Suthers, 1996; Greenewalt, 1968; Podos, 1996). Although the structural properties of the syrinx aid with motor control (Michale S. Fee, 2002; Fee et al.,

1998), the modulations of song (e.g., intra-specific variability) can only be accomplished by superfast muscle control (Elemans et al., 2004; Elemans et al., 2011; C. P. H. Elemans et al., 2008; Greenewalt, 1968). Superfast muscles are the fastest known synchronous muscle phenotypes in vertebrate muscles. These muscles have been shown to control the tail shaker in a rattlesnake (Rome et al., 1996) and the swimbladder muscle in the toadfish (Fine et al., 2001). Previous work has demonstrated that the muscles of the songbird vocal organ contain superfast muscle properties, allowing them to deliver a very fast force modulation required to directly control individual sound elements. Songbird vocal organ muscles have fast synchronous contraction rates ranging from 200 to 250 Hz and fast isometric contraction speeds around 4.7 ± 0.8 ms (Elemans et al., 2008; Mead et al., 2017). Additionally, syringeal muscles have a maximum stress during tetanic contraction (5 mN/mm2) that is 60 times lower than mammalian limb muscles, allowing the muscle to contract faster (Ward et al., 2007). Approximately 87% of all muscle fibers in the vocal organ express the superfast phenotype (Adam et al., 2021). In the VS muscle, the superfast motor unit is extremely small and contains 1 to 11.6 ± 2.6 muscle fibers per motor unit. 1/5 of all motor neurons in VS innervate only one single superfast syringeal muscle fiber (Adam et al., 2021), making the motor neurons in $nXII_{ts}$ the highest controlled resolution in the vertebrate nervous system (C. P. H. Elemans et al., 2008). Lastly, data shows the motor units in syringeal muscles can control acoustic features at the resolution of 50 mHz to 4.2 Hz (Adam et al., 2021). These properties suggest that muscles in the syrinx are sensitive to the spike timing of activity patterns and use precise millisecond-spike timing to control behavior.

1.2.5 Calcium dynamics

Rapid activation and relaxation of superfast muscles require multiple additional structural and molecular systems, including larger quantities of mitochondria, sarcoplasmic reticulum, and t-

tubules (Young et al., 2003). Additionally, previous research in other species with superfast muscles (e.g., toadfish) determined that calcium (Ca^{2+}), a molecule essential for muscle contraction, uses different mechanisms to move Ca^{2+} within the muscle when compared to a standard muscle (Harwood et al., 2011; Young & Rome, 2001). Here, I will briefly go over the main uses of Ca^{2+} in a muscle. First, when an action potential occurs in the motor neuron, voltage-gated Ca^{2+} channels at the motor endplate release Ca^{2+} into the terminal to release acetylcholine (ACh), which is the neurotransmitter essential for initiating action potentials along the muscle fibers (Berchtold et al., 2000; Gehlert et al., 2015; Stein et al., 1988). When the action potential runs across T tubules, the sarcoplasmic reticulum (SR) releases more Ca^{2+} increasing cytosolic Ca^{2+}, which initiates the binding of Ca^{2+} to the troponin protein, the movement of actin and myosin, and the contraction of the muscle fiber (MacLennan et al., 1997; Shoshan-Barmatz & Ashley, 1998). This is followed by Ca^{2+} ion pumps removing Ca^{2+} from the cytosol back into the SR, causing the muscle fiber to relax (Baylor & Hollingworth, 2012). Additionally, Ca^{2+} is needed to produce adenosine triphosphate (ATP), energy supply for the muscles, protein synthesis and degradation, and to initiate the release of transcription factors (Berchtold et al., 2000; Gehlert et al., 2015; Stein et al., 1988).

Ca^{2+} must be released and taken up with each muscle contraction. The maximal SR-Ca^{2+} pumping rate in a skeletal muscle is 2 mmol kg^{-1} s^{-1}. A muscle with contraction rates at 100 Hz requires a SR-Ca^{2+} pumping rate of 7 mmol kg^{-1} s^{-1}, suggesting that superfast muscles with contraction rates up to 250 Hz (e.g., VS muscle in songbirds) can not rely on the traditional mechanisms used in skeletal muscles to release and reuptake of Ca^{2+} (Harwood et al., 2011; Young et al., 2003). Research has identified this biological phenomenon as Ca^{2+} kinetics. When looking at the swimbladder muscle of a toadfish (a superfast muscle with contraction rates around 80-100 Hz

and up to 250 Hz), Hardwood et al., found two alternative mechanisms used in superfast muscles for Ca^{2+} release and reuptake. First, the amount of Ca^{2+} released at the start of a contraction is reduced, allowing more Ca^{2+} to be stored in the SR (Rome, 2006). The second mechanism temporarily binds the Ca^{2+} that was released during a toadfish call to the parvalbumin protein, which has a higher concentration in superfast muscles, and only pumps the released Ca^{2+} back to the SR after the muscle has relaxed during the silent interval (Tikunov & Rome, 2009). Superfast muscular control, along with nonlinear intrinsic dynamics of the syrinx, allows the vocal organ muscles to create rapid transitions during song (in the order of ~ 1 ms) and produce precise and complex motor behaviors (e.g., singing).

1.2.6 Vocal organ mechanisms in birds

In general, vocalizations in songbirds (and humans) are generated by the expiratory airflow moving into the bronchi and inducing self-sustained oscillations of the labia and vibration of the suprasyringeal vocal tract (Nowicki, 1987; Riede & Goller, 2010a; Riede et al., 2006). This is described as the myoelastic-aerodynamic (MEAD) theory of phonation, which explains how a steady stream of air from the lungs sets the vocal membranes into vibration, revealing the interaction between muscle force, elastic force, and aerodynamic force of the syrinx (Titze, 1980; Titze, 2006; Van den Berg, 1958). To produce sound, first, the expiratory muscle group contracts, which compresses the abdomen and thorax (i.e., subglottal component) and increases air pressure through the air sacs, sending the airflow through the bronchi and syrinx (Düring et al., 2013; Goller & Cooper, 2004; Schmidt & Martin Wild, 2014; Suthers & Zollinger, 2004). The airflow causes the syrinx to move forward, signaling for the DTB and DS syringeal muscles to contract, ultimately causing the bronchus to rotate into the trachea lumen. This rotation causes the medial and lateral membranes (i.e., labia) to slightly adduct into the expiratory airstream, causing the membranes to

oscillate (Fee et al., 1998; Goller & Cooper, 2004; Goller & Suthers, 1996; Riede & Goller, 2010a; Srivastava et al., 2015). The membranes move laterally until the force of muscle elasticity is greater than air pressure, moving the membranes medially (Riede & Goller, 2010a). The high velocity of the expiratory airstream causes an opening of the labia. This is followed by low pressure, when the force of the muscle elasticity is greater than air pressure, causing the labia to close and release a pulse of air (i.e., Bernoulli effect) (Jiang et al., 2000; Titze, 1988; Van den Berg et al., 1957). The opening and closing of the labia are repeated, producing membrane oscillation. The rapid oscillations of air are amplified as they travel through the suprasyringreal vocal tract, ultimately producing sound. A bird can change their pitch by modulating the frequency of the membrane oscillations (Düring et al., 2017; C. P. Elemans et al., 2008; Goller & Larsen, 2002). For example, increasing the frequency of the oscillations increases the tension, leading to higher-pitch sounds.

1.2.7 Similarities and differences in vocal behavior between birds and humans

As mentioned above, there are many parallels between bird song and human speech. The most notable similarities involve the process by which birds and humans learn their vocal behavior and the brain circuitry involved in learning and producing learned vocalizations. Both birds and humans use sensorimotor learning and rely heavily on social interactions to develop their song. Like humans, birds have a critical period for learning their vocal behavior early in life, making it more difficult to learn new languages or songs later in life (dos Santos, 2018; Gobes et al., 2019; Krashen, 1973; London, 2019; Scovel, 2000; Tyack, 2020). Vocalizations in both humans and songbirds require auditory feedback for 1) learning sounds from others (typically adults) and 2) error correction that allows them to adapt their vocal motor map (Brainard & Doupe, 2000; A. J. Doupe & P. K. Kuhl, 1999; Konishi, 1965). Many research studies have demonstrated that if

infants or fledglings are raised in isolation or are not exposed to early auditory tutoring, they produce simplified, abnormal vocal behaviors that do not reflect their adult contemporaries (Krashen, 1973; P. Marler, 1970; Marler & Sherman, 1983; Marler & Sherman, 1985; P. R. Marler, 1970; Thorpe, 2008). Lastly, both birds and humans have a motor cortex that directly innervates motor neurons located in a brainstem nucleus (i.e., birds – *hypoglossal nucleus* and humans – *hypoglossal nucleus* and *nucleus ambiguus*) which directly innervate vocal organ muscles (Jarvis, 2004; Ludlow, 2005; Ojemann, 1991; Wild, 1997).

There are important features that differ between birds and humans when learning and performing their vocal behavior. First, I will address the differences in the neocortex and neural pathways followed by the differences in their vocal organs and sound production. Although the cortico-basal-thalamo-cortical circuit loop (i.e., vocal learning circuit) is analogous in functional, physiological, and molecular characteristics (Ojemann, 1991), there are several anatomical and structural differences between human and bird brains. A human's neocortex is derived from the pallium as a laminar structure (i.e., six cellular layers), whereas a songbird's neocortex is derived from the pallium as several nuclei (Aamodt et al., 2019; Calabrese & Woolley, 2015; Jarvis, 2004; Prather et al., 2017; Reiner et al., 2004; Reiner et al., 2005). Generally, efferent (i.e., motor) pathways in humans decussate at the brainstem or spinal cord, meaning the right side of the brain controls the left side of the body. Efferent pathways in birds mostly control the ipsilateral side of the body (i.e., the right side of the brain controls the right side of the vocal organ) (Mooney, 2009). The efferent tracts used in humans to innervate structures in the head, face, tongue, and neck derive from the corticobulbar tracts (Kandel et al., 2013). Unlike birds, the neurons controlling efferent pathways in humans have bilateral control (i.e., the right side of the brain controls right and left side of muscles involved in sound production) or contralateral control (i.e., right side of the brain

controls left side of the body). The neurons controlling muscles in the upper half of the face have bilateral control and decussate (cross over) at the midbrain and pons. The neurons controlling muscles in the lower half of the face only have contralateral control and decussate at the brainstem (i.e., medulla) (Kandel et al., 2013; Simonyan, 2014). Contrary to humans, there is evidence of sexual dimorphism in brain areas dedicated to learning and producing song in birds (Devoogd et al., 1993; MacDougall-Shackleton & Ball, 1999; Nottebohm & Arnold, 1976; Riede et al., 2010). In most known species of songbirds, such as the Bengalese finch, only the male birds learn and produce song. Researchers have found that in species of birds where only male birds sing, vocal areas in the brain (i.e., Area X, HVC, RA, and brainstem nucleus $nXII_{ts}$) and the vocal organ are significantly larger in male birds when compared to their female counterparts (Konishi, 1989; Nottebohm & Arnold, 1976; Riede et al., 2010). The size of the female birds' vocal regions are linearly correlated with their ability to learn and produce song (Gahr et al., 1998). Additionally, the vocal learning and production circuitry in humans' overlaps, where birds have two spatially separated pathways for vocal learning (i.e., AFP) and vocal production (i.e., motor pathway).

Although humans and birds are thought to rely on MEAD theory mechanisms to produce sound, humans and birds have different numbers of sound sources (Düring et al., 2013; Titze, 2006; Van den Berg et al., 1957). Humans have one source of sound via one set of membranes that oscillate in the trachea. Birds have two sources for sound, one set of membranes in the right and left bronchia, that can be controlled independently (Fee et al., 1998; Goller & Larsen, 1997; Riede & Goller, 2010a; Titze, 1980; Titze, 2006). As stated earlier, breathing is an important component of vocalization. In humans, the diaphragm, which is positioned between the thorax and abdomen, plays a significant role in breathing (Ludlow, 2005). Instead of a diaphragm, birds rely on air sacs to help move air in and out of the syrinx (Andalman et al., 2011; Nowicki, 1987; Riede et al.,

2006). The most notable difference between humans and birds can be found at the vocal organ. The larynx (i.e., human vocal organ) sits on the cranial end of the airway and is comprised of smooth and striated muscles (Ludlow, 2005). Alternatively, the syrinx (i.e., songbird vocal organ) is located at the base of the airway and contains superfast muscles that have fast synchronous contraction rates up to 250 Hz (C. P. H. Elemans et al., 2008; Andrew F. Mead et al., 2017). The location of the syrinx, type of muscle, and the ability to modulate vocalization with two sets of oscillating membranes independently allow the bird to make complex songs (Riede & Goller, 2010a; Vicario, 1991a). Although humans and birds care about non-auditory feedback (King et al., 2005; Lipkind et al., 2013; Schmidt & Martin Wild, 2014), there is no proof of muscle spindles (i.e., stretch receptors in muscles) in the syrinx muscles (Faunes et al., 2017). Additionally, we have very little information on how mechanoreceptive and other non-auditory somatosensory sources of feedback contribute to motor control of the syrinx and sound production. Despite the structural and anatomical differences, birdsong and speech require the brain to rapidly process sensory signals and coordinate precise patterns of muscle activity in breathing and vocal organ muscles (A. Doupe & P. Kuhl, 1999; A. J. Doupe & P. K. Kuhl, 1999; P. Marler, 1970; Schmidt & Martin Wild, 2014).

1.3 Muscles

Muscles operate as the interface between the CNS and the surrounding external environment (Fye, 1995). The brain must rapidly

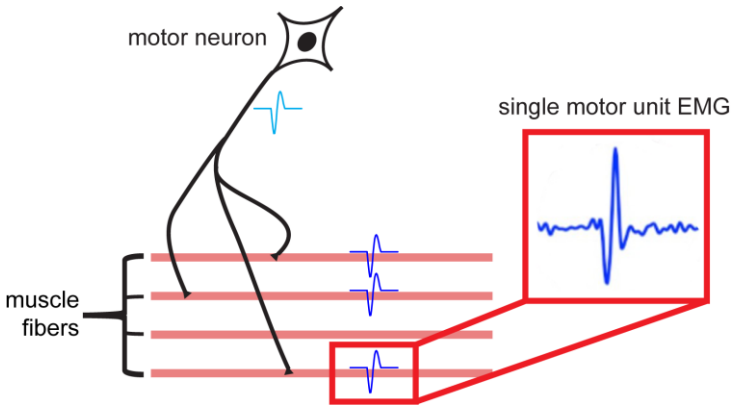

Figure 1.4: Motor unit schematic. A motor unit consists of the muscle fibers (pink) innervated by a single motor neuron. When a motor neuron fires (light blue), synchronous action potentials are produced in the muscle fibers (blue traces).

process sensory signals and coordinate precise patterns of muscle activity to execute accurate motor behaviors. Vertebrates have three types of muscles: striated (i.e., skeletal), smooth, and cardiac muscles. The experiments in this thesis focus on skeletal muscles, which are connected to bones and are engaged in voluntary movements (i.e., movements controlled by the CNS) (Kandel et al., 2013). These muscles are made up of a varying number of muscle fibers, from a few to several thousand depending on the size of the muscle.

1.3.1 Motor Units

Motor units are the basic functional units of skeletal muscle, transmitting the final output of the CNS. Skeletal muscle activation is controlled by alpha motor neurons that are either located in the brain stem or spinal cord. One motor neuron can innervate multiple muscle fibers distributed throughout the muscle, where every fiber is a muscle cell, but a muscle fiber is typically only innervated by one motor neuron. A motor neuron and all the muscle fibers it innervates is called a motor unit (Duchateau & Enoka, 2011; Liddell & Sherrington, 1925) (Figure 1.4). Motor units are defined by contraction speed, maximal force (i.e., strength), and fatigability (i.e., endurance), and these properties vary depending on the type of motor unit (Buchthal & Schmalbruch, 1980). There are three types of motor units found in mammal skeletal muscles: slow (S), fast fatigable (FF), and fast fatigue-resistant (FR) (Burke et al., 1973; Burke & Tsairis, 1974; Schiaffino & Reggiani, 2011). S motor units (Type I) consist of small motor neurons and a small number of small muscle fibers. Small muscle fibers contract slowly, generate a small force, and are resistant to fatigue resulting in a motor unit that is important for movements that require a sustained muscular contraction (e.g., standing). FF motor units (Type IIa) include large motor neurons and a sizable number of large muscle fibers that contract quickly. Large fibers have fewer mitochondria compared to small fibers which causes the fiber to fatigue easily. FF motor units (Type IIb) are

recruited for movements that require a significant amount of force (e.g., jumping). The properties of FR motor units, such as size, fatigability, speed, and force output fall between S and FF motor units. Because S motor units have a lower threshold for activation, it is typically necessary for multiple S motor units to fire to induce muscle contraction or movement. The CNS can increase the strength of muscle contraction by either 1) increasing the number of active motor units, or 2) increasing the firing rate of individual motor units to optimize the summated tension generated (Duchateau & Enoka, 2011).

The motor neuron generates an action potential down its highly branched axons, causing a release of ACh at the neuromuscular junction (i.e., synapse between a motor neuron and skeletal muscle) (Dale, 1914; Zeisel, 2012). The ACh binds to all the muscle fibers innervated by the single motor neuron, called a motor unit, causing the fibers to contract and produce force (Zeisel, 2012). There is a one-to-one relationship between the action potential in the motor neuron and the action potential in the innervated muscle fibers (Kandel et al., 2013). The transform from motor neuron spikes to force is often referred to as the neuromuscular transform (NMT) (Zhurov and Brezina, 2006). Briefly, I will describe the structure of muscle fibers, and then I will describe how muscles contract.

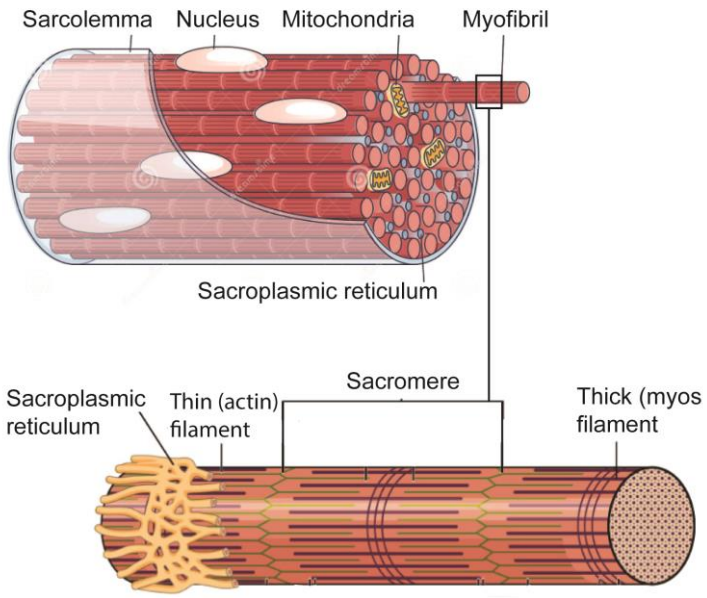

Figure 1.5: Muscle fiber schematic. There are multiple muscle fibers in each muscle. (Top panel) Muscle fiber structure. Skeletal muscle fibers are surrounded by a plasma membrane (i.e., sarcolemma). Each fiber is composed of multiple myofibrils. (Bottom panel) Myofibrils are made up of many sacromeres. Sacromeres are the contractile unit of the fiber. The interaction between thick and thin filaments determines how much force the sarcomere produces. Adapted from (Anatomy and Physiology).

Within each skeletal muscle, there are bundles of muscle fibers (Figure 1.5, top panel) and each fiber contains many myofibrils. Myofibrils are made up of many sacromeres, the contractile unit of the fiber, which area made up of two protein filaments, actin (thin filaments) and myosin (thick filaments) (Kandel et al., 2013; Szent-Györgyi, 2004) (Figure 1.5, bottom panel). Actin filaments contain a myosin binding site (Szent-Gyorgyi, 1949). Additionally, troponin and tropomyosin proteins run along the actin filaments, controlling when the acting binding site will be exposed to bind to myosin (Straub, 1943; Szent-Gyorgyi, 1949). The actin filaments are anchored to the outer edges of the sarcomere (Hanson & Lowy, 1963). Alternatively, myosin filaments are anchored at the center of the sarcomere. Myosin filaments are composed of two myosin heavy chains and four light chains. The heavy chains contain an actin binding site (i.e., cross bridges) and ATP (energy carrying molecule found in cells) binding site (Engelhardt & Liubimova, 1994). The interaction between thick and thin filaments determines how much force the sarcomere produces.

1.3.2 Sliding filament model of muscle contraction

The sliding filament model, which was first described in 1954, is the most widely accepted model describing how muscle fibers contract (Hanson & Huxley, 1953; Huxley & Niedergerke, 1954; Huxley & Hanson, 1954). As mentioned above, ACh neurotransmitter acts as a stimulus to the muscle, initiating an action potential (Dale, 1914; Zeisel, 2012). The action potential causes the release of Ca^{2+} into the sacromeres. Ca^{2+} binds to troponin, causing a conformational change in troponin (i.e., troponin-tropomyosin complex) and exposing the actin binding site (Ebashi et al., 1980; Ebashi & Ohtsuki, 2007; Szent-Györgyi, 1975). Myosin then binds to the actin binding site causing the thin filament to be pulled toward the center of the sarcomere, shortening the sarcomere (Huxley & Niedergerke, 1954; Huxley, 1957). During this process, the chemical energy of ATP transforms into mechanical energy of the contraction (Gergely, 1950). ATP then binds to its

binding site on the myosin cross bridges forcing myosin cross bridges to release from actin (Huxley, 1969). Ca^{2+} is transported back to the sarcomere which shifts the troponin-tropomyosin complex to cover the actin binding site (Huxley, 1957). In short, the myosin filaments pull acting filaments close together, shortening the sacromeres within a fiber ultimately causing the muscle to contract (Kandel et al., 2013). Although the sarcomere changes length throughout the contraction and relaxation of a muscle, the individual proteins and filaments do not. The speed of muscle contraction depends on the distribution, movement, signaling, and regulation of the Ca^{2+} ion (Berchtold et al., 2000; Gehlert et al., 2015). Additionally, the force output from a muscle fiber is modulated by the concentration of Ca^{2+}, known as Ca^{2+} sensitivity (MacIntosh, 2003). Changes in Ca^{2+} sensitivity are driven by muscles' intrinsic properties, such as current state (e.g., length and velocity), fatigue, activity-dependent potentiation, and the muscle state history (Sober et al., 2018; Ting & Chiel, 2017). These timing-dependent nonlinearities in muscles cause millisecond-scale variations in interspike intervals (ISIs) to produce sizable shifts in force output (Sober et al., 2018).

1.3.3 Force generation in muscles

The amount of force produced by a muscle is determined by three primary factors: 1) the length-tension relationship (Herzog & ter Keurs, 1988; Julian & Morgan, 1979; Julian & Moss, 1980), or the instantaneous muscle length, 2) the force-velocity relationship (Alcazar et al., 2019; Hill, 1938), or the muscle velocity during shortening or lengthening, and 3) the degree of muscle activation, or when and in what pattern was the muscle stimulated (Enoka et al., 2020; Vromans & Faghri, 2017). Below, I will explain each of these relationships and how it affects the force output of a muscle. The resting muscle length is the length of the muscle that will produce the most force when the muscle is contracted (Kandel et al., 2013). The length is typically about halfway between contraction and extension. Over contraction of a muscle will reduce the potential for

future contraction because there are no more actin myosin cross-bridges that can form, ultimately causing less force to be produced (Josephson, 1999; Nubar, 1962; Ward et al., 2007). The same outcome occurs when the muscle is over stretched (e.g., less force produced by the muscle) (Minozzo et al., 2013). In this scenario, the sacromeres are so far apart resulting in little to no overlap of myosin and actin. This results in a nonlinear relationship between the length of the muscle and the force output.

The force-velocity relationship describes the relationship between the speed of the muscle contraction and the force of the muscle contraction (i.e., power) (Alcazar et al., 2019; Herzog & ter Keurs, 1988; Josephson, 1999). The force generated by a muscle depends on the number of cross-bridges formed between actin and myosin (Hill, 1938; Huxley, 1969). As muscle velocity decreases, more myosin actin cross-bridges have time to bind, increasing the force output of the muscle. Alternatively, as muscles shorten with increasing velocity, force decreases (Herzog & ter Keurs, 1988; Zajac, 1989). This is caused because the filaments are moving too fast to allow for the myosin actin cross-bridges to bind. A muscle contracting at high velocity would imply that the muscle is contracting with low force, meaning as velocity increases, force and power produced is reduced (Josephson, 1999).

There are many nonlinear properties of muscles, such as the force-length and force-velocity relationships, that would suggest muscles are sensitive to the precise timing of action potentials (Josephson, 1999; Zajac, 1989). Based on the length-tension relationship, the timing of a second spike will directly affect the force production (Herzog & ter Keurs, 1988; Julian & Morgan, 1979; Julian & Moss, 1980). For example, two spikes with smaller interspike intervals (ISIs) will have a larger force output compared to two spikes with larger ISIs. In addition, the NMT is a nonlinear, dynamic, and modifiable filter (Zhurov & Brezina, 2006). Lastly, there are metabolic factors in

muscles, such as the necessity for Ca^{2+} to produce a muscle contraction, that can support the idea that muscles are sensitive to spike timing (Szent-Gyorgyi, 1949; Szent-Györgyi, 1975). The premise of this dissertation is understanding how patterns of muscle activity control behavior. In order to effectively decipher how muscles modulate spike patterns, it is necessary to develop electrodes that can record SU activity.

1.4 Electromyography

Understanding the learning and control of complex movements requires collecting a large number of parallel recordings within and across multiple muscles. Electromyography (EMG) is a research and diagnostic tool that can record the electrical activity generated by active muscle fibers. Alternatively, one can think of EMG as representing the output activity of an active motor neuron. In 1929, the first methodology for recording a single motor unit potential in an anesthetized animal was developed (Kazamel & Warren, 2017). The electrical activity from one fiber of a nerve in a cat hindlimb was recorded by placing the recording end of a concentric needle electrode into the fiber, while the other end was attached to an amplifier and a speaker (Adrian & Bronk, 1929), leading to the invention of the electromyograph.

When used in a diagnostic setting, EMG can help assess the health of muscles and the corresponding nerves (i.e., motor neurons). This technique is used frequently to diagnosis disorders that affect the motor neurons (e.g., ALS), nerve root (e.g., herniated disc), peripheral nerve (e.g., carpal tunnel syndrome), connection between the nerve and muscle (e.g., myasthenia gravis), and muscle (e.g., muscular dystrophy). EMG is also commonly used in research to understand how muscles are controlled by the CNS, the functional role of muscles in movement generation, and how the control of muscles change when learning motor behaviors or after injury

(Jarque-Bou et al., 2021; Mills, 2005). This can be done by observing when various muscles are in/active during specific behaviors and how various parameters of muscle activity, such as duration of activation and amplitude and frequency of EMG signals, change over time (M. B. Raez et al., 2006).

1.4.1 Current EMG methods

At a minimum, EMG equipment includes recording electrodes, a ground or reference electrode, an amplifier, a data acquisition system, and a display system. The specifications of the recording electrodes, including electrode shape, size, inter-electrode distance, material, design, and placement of electrodes on the muscles/skin directly affect the quality of the signal recorded (Mills, 2005; M. B. Raez et al., 2006). Current electromyographic (EMG) methods typically rely on non-invasive skin-level surface electrodes or the insertion of metal wire electrodes into the muscles (Basmajian, 1985; Bogey et al., 2000; Farina & Negro, 2012; Farrell & Weir, 2008; M. B. I. Raez et al., 2006). Although it is possible to collect EMG activity with one electrode and one reference electrode (i.e., monopolar recording), it is most common to use two electrodes (surface) or bipolar electrodes (fine wire) or electrode arrays with a reference electrode (Beck et al., 2007). To reduce noise, a ground wire is placed on an electrically neutral site away from the recording area (Soderberg, 1992). Surface electrodes can either be dry electrodes that are placed directly on the skin or gelled electrodes that use an electrolytic gel as an interface between the skin and recording site on the electrode (Cram, 1998; Jamal, 2012). Insertion electrodes are placed in the muscle with a needle or by applying pressure to the electrode to penetrate the muscle. This can be done with needle electrodes or fine wires. Needle electrodes consists of an insulated wire in the cannula of a needle (M. B. I. Raez et al., 2006). Alternatively, intramuscular EMG can be recorded using a fine-wire electrodes made from insulated wires that are stiff, strong, and have a small diameter (~25-

50 μm), such as SSW or platinum iridium (Pl-Ir). Bipolar fine wire electrode consists of two insulated fine wires that are attached together either with glue or by twisting the wires. The distal end of the fine wires (i.e., recording end) are stripped of insulation and the tips are offset by ~2 mm or cm, depending on the size of the muscle, with the goal of detecting the same motor unit action potential spatially shifted (Mohr et al., 2018). Surface electrodes are applied to the skin (i.e., non-invasive) and use electrolytic conduction to detect the change in chemical equilibrium between the muscle surface and the skin (Chowdhury et al., 2013; Pylatiuk et al., 2009). These electrodes are conductive metal plates (e.g., silver) and range in size form 0.5 to 2.5 cm (Merlo et al., 2003). There are two types of surface electrodes. Gelled surface electrodes require a gelled electrolytic substance, which can improve the electrical conduction, whereas dry surface electrodes don't require a substance (Jamal, 2012). Surface electrodes typically record many action potentials from a population of motor units, known as MU activity, which provides a comprehensive perspective of the activity from the recorded muscle. Insertion electrodes are better at recording activity between individual fibers and have the ability to discriminate SU activity (Cavalcanti Garcia & Vieira, 2011).

Recording and interpreting EMG activity correctly is contingent on the electrode properties (as noted above), the amplifier design, and post-hoc filtering of the signal (Tankisi et al., 2020). EMG signals are high frequency, so an amplifier is used to increase the amplitude, filter, and digitize the signal. The most relevant amplifiers for detecting EMG signal are amplifiers with unipolar or bipolar configurations. The output of a unipolar amplifier is produced by amplifying several (at least two) input electrodes against one reference (Cavalcanti Garcia & Vieira, 2011). Typically, the reference channel is determined post-hoc. A bipolar amplifier, also called a differential amplifier, amplifies the difference between two adjacent input electrodes (i.e., bipolar electrodes).

This ultimately suppresses any signal that is common to both electrodes and increases the signal that is unique to both electrodes (M. B. I. Raez et al., 2006).

1.4.2 Challenges

EMG signals are complex (Amrutha, 2017), thus there are many opportunities to collect poor quality data and misinterpret what the signal depicts. One of the major obstacles to solve is decreasing the noise level, which is caused from electrical noise, motion artifact, or a combination of the two. Electrical noise can come from electromagnetic devices, power supplies, faulty or shorted connections between cables (e.g., connection between electrode and amplifier), and improper grounding (Jamal, 2012). Motion artifact can either be produced by unrelated movement from the subject, muscle tissue migration, or a wire or cable that has been displaced (M. B. Raez et al., 2006). Although newer technology and recording techniques have helped reduce the amount of noise, it is still likely that one will need to perform post-hoc filtering of the recorded EMG data to remove any electrical noise or motion artifact. There are many types of filters that can be applied to EMG data. Commonly used filters are a low pass filter to remove high frequency noise (e.g., motion artifact) and/or a high pass filter to remove low frequency noise (e.g., electrical noise) (M. B. I. Raez et al., 2006; Sanches et al., 2007; Tankisi et al., 2020).

In addition to noise, the traditional electrode technologies (e.g., surface and fine wire electrodes) present limitations. Due to their location, surface electrodes are unable to record activity from deep or small muscles, and it is more difficult to confirm the

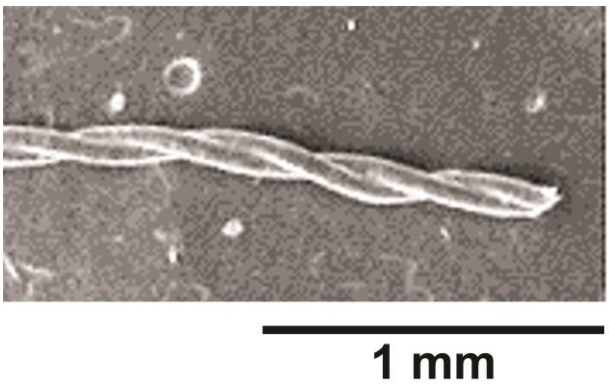

Figure 1.6: Carbon nanotube fibers (CNTFs). Scanning electron microscopy image of two parylene-coated CNTFs twisted together. Single fiber diameters ranged from 14-24 μm.

recorded signal was derived from the muscle of interest (Cram, 1998; De Luca, 1997; Perry et al., 1981). Although recent technology advancements (e.g., multi-channel high density surface EMG) have made it possible to collect more detailed temporal and spatial EMG signal (Lapatki et al., 2019; Martinez-Valdes et al., 2017), it is still difficult to decipher information regarding motor unit morphology (Tankisi et al., 2020). Furthermore, fat tissue can be layered between the skin and muscle, damping down the recorded signal. Insertion of fine wire or needle electrodes do allow for greater specificity in the targeted muscle, but it is invasive, potentially resulting in injury to the muscle fibers at the implant site (Turker, 1993). Fine wire electrodes are stiff, which may cause the electrode to break more easily. Additionally, the stiffness in the wire electrodes could also cause strain and/or damage on the muscle of interest, impeding motor behaviors.

1.4.3 New Technology

To address the challenges mentioned above, researchers have been exploring various materials that are soft and flexible while still being highly conductive. In the early 1990s, three papers popularized a material called carbon nanotubes (CNT), a highly stable cylindrical structure of sp^2 bonded carbon (Bethune et al., 1993; Iijima, 1991; Iijima & Ichihashi, 1993). This material quickly grew attraction across many fields because of its unique properties, such as extreme flexibility (Dresselhaus et al., 2001), high electrical conductivity (Adnan et al., 2018; Behabtu et al., 2013; Vitale et al., 2015), mechanical strength (Yan et al., 2021), chemical and thermal stability (Vitale et al., 2015), and nanoscale size (e.g., as small as ~4 μm in diameter).

Since 2003, researchers have been advancing methods to create pure nanotube fibers (Davis et al., 2004) spun into a textile thread-like material that have properties exceeding metal wires. Carbon nanotube fibers (CNTF) are continuous threads made up of cross sections consisting of tens to hundreds of densely packed CNTs (Yan et al., 2021). To create this strong, flexible, and light-

weight fiber, purified CNTs are dissolved in chlorosulfonic acid and then fabricated into a single fiber via a wet spinning process (Behabtu et al., 2013; Tsentalovich et al., 2017; Vitale et al., 2015). Parylene C is then deposited onto the CNTF, leaving either tip exposed, to insulate the fiber (Behabtu et al., 2013). CNTFs are 5-10 times stronger than graphene fibers (Adnan et al., 2018; Yan et al., 2021), have 15–20 times lower interface impedance (Vitale et al., 2015) and four times more flexural rigidity than platinum-iridium (Pt-Ir) (Zhu et al., 2019), are biocompatible (Behabtu et al., 2013; Tsentalovich et al., 2017; Vitale et al., 2018), and can be made as small as ~14-24 µm in diameter.

CNTs and CNTFs have been tested and are being used for many applications ranging from engineering and biomedicine to material sciences (Voge & Stegemann, 2011). CNTs have been used as cell culture substrates that encourage the attachment and growth of cell types, such as neural stem and glial cells, by controlling neuronal extracellular-molecular interactions (Hu et al., 2004; Jan & Kotov, 2007; Kam et al., 2009; Lee et al., 2015). Additionally, CNTS are being tested as flexible antennas for wireless communication (Bengio et al., 2019). CNTFs have been used as supercapacitors (An et al., 2001; Muralidharan et al., 2018), flexible batteries (Sun et al., 2013; Wang et al., 2015), and wearable electronics to monitor health (Rdest & Janas, 2021; Ryu et al., 2015; Taylor et al., 2021). In the field of neuroscience, CNTF's have been successfully used to record neural activity from mice cortex and thalamic reticular nucleus in acute brain slices (Vitale et al., 2018), chronically stimulate neurons and record SU neural activity in rats (Alvarez et al., 2020), and acutely stimulate and record from nerves in small animal models (Lissandrello et al., 2017). The use of CNTs or CNTFs have countless applications, but they have yet to be tested as a material to collect EMG activity.

1.4.4 Project 1: Develop new EMG technology to record from small, deep muscles

As mentioned earlier, our primary goal is to discover how neurons control muscles to produce complex learned behaviors by deciphering the motor code. To examine this fundamental question in motor control, it is necessary to record EMG activity from the muscles that control the pertinent behavior. We are specifically interested in understanding how motor neurons control muscles of the songbird vocal organ to produce song. Unfortunately, the location of the songbirds' vocal organ (deep in the chest cavity, surrounded by air sacs) and the small size of the muscles (largest muscle, VS, only measuring 2 mm wide by 4 mm long), make it extremely difficult to access. Despite recent advances in tools for monitoring and manipulating neural activity, methods for recording and analyzing EMG signals, especially from small, deep muscles, have changed little in recent decades. To address these concerns, we created bipolar electrodes with CNTFs and characterized the parameters of these electrodes and the resulting EMG data (Figure 1.6). In the section above, we go into detail regarding various unique properties of CNTFs, such as strength, flexibility, small size and low interface impedance, and why the properties could lead to improved EMG recordings. In chapter 2, we introduce a novel approach to record high-resolution EMG signals in small muscles using extremely strong and flexible CNTFs, and test the CNTFs' functionality in songbird vocal organ muscles. Acute EMG recordings successfully yielded MU recordings with higher SNR compared to SSW electrodes. Furthermore, CNTF electrodes recorded SU spike trains, where SSW could not. CNTF electrodes have great potential for chronic EMG studies of small, deep muscles that demand high electrode flexibility and strength.

1.5 Understanding how patterns of activity produce motor behavior

Motor learning requires the brain to rapidly process sensory signals and coordinate precise patterns of muscle activity. As mentioned in the beginning of the introduction, it is still unknown how the CNS performs these computations. These computations are sometimes referred to as neural and/or motor codes. A motor code is defined as the relationship between the electrical activity from individual or ensembles of neurons (i.e., pattern of spikes) and resulting behavior (Gerstner et al., 1997; Kandel et al., 2013; Prescott & Sejnowski, 2008). Chapter 3 in my thesis will focus on the motor code (derived from the recorded MU and SU EMG activity) at the level of the muscle. Understanding the neural code can provide insight into how information (e.g., external stimulus or error correction) is transformed as electrical signals from one area of the brain to another area of the brain or muscles and how the information is represented as a behavior.

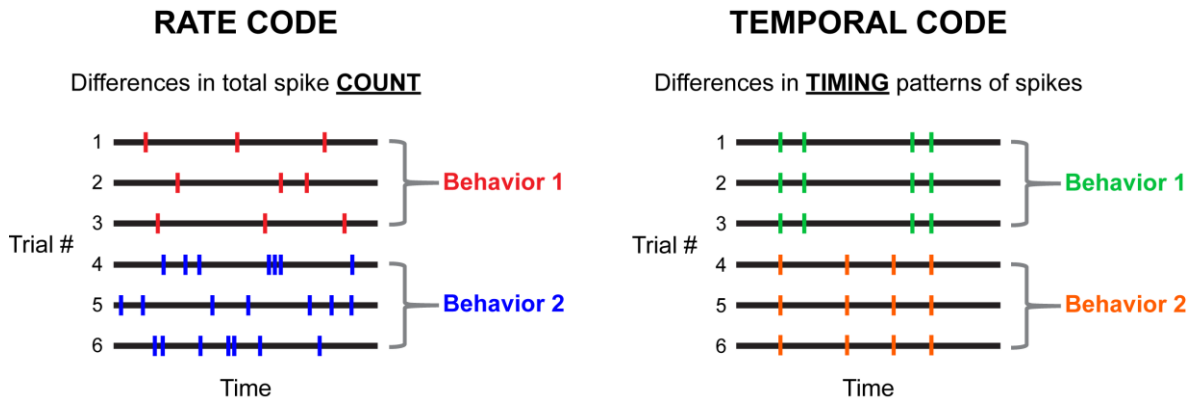

Figure 1.6: Schematic of two possible ways neural and motor unit activity carry information about the upcoming behavior. For each panel, time is along the x-axis and each tick mark represents an action potential. Rate code (left panel) is the total number of action potentials within a time interval, whereas temporal code (right panel) is the timing patterns of the action potentials that occur within a specific time interval. "Behavior 1" and "Behavior 2", as used here, generally refer to variations in the same behavior (e.g., pitch difference in same syllable across two renditions) rather than two completely different behaviors (e.g., singing verses flying). When looking at the left panel, the main difference between behaviors 1 and 2 is the total number of action potentials that occur. When looking at the right panel, the main difference between behaviors 1 and 2 is the timing patterns of the action potentials rather than the total number of action potentials.

1.5.1 Defining patterns of muscle activity

Does the brain use a rate code or spike timing code? This question has inspired considerable debate amongst the motor systems community. In general, there are two non-exclusive ways that spikes can carry information or computations: rate code and temporal (i.e., spike-timing) code. Rate code is the total number of action potentials within a time interval and is defined from individual spikes (Figure 1.6, left panel), whereas spike-timing codes are based on the timing patterns of action potentials within a time interval (Figure 1.6, right panel). In theory, neurons can encode information via spike rate, spike timing, or a combination of the two.

The first reported experiment detecting rate code occurred in the mid-1920s. Experimenters hung different weights from a frog muscle while recording spikes from the corresponding sensory nerve fibers. They found a positive correlation between the weight and response from the sensory nerve. The intensity of a sensory stimulus was correlated with the spiking activity of a sensory neuron. With these results, the experimenters concluded that the frequency of all action potentials, rather than looking at individual spiking events, described how neurons communicate (i.e., neural code). Early theories of brain function relied exclusively on spike rate (rate code) (Prescott & Sejnowski, 2008) to explain sensory input and motor output (Adrian, 1926; Adrian & Zotterman, 1926a). Studies in the sensory system were unable to explain responses to stimuli using spike rate and eventually began to identify characteristics of neural firing via spike timing-based codes (Hallock & Di Lorenzo, 2006; Prescott & Sejnowski, 2008). Eventually, researchers studying sensory coding discovered that millisecond-scale spike timing patterns (timing-based codes) were far more informative about sensory inputs than were spike rates (Figure 1.6) (Strong et al., 1998). This holds true for all of the sensory systems (e.g., visual and auditory). Yet despite the strong evidence for temporal codes in sensory systems, investigators researching the motor system have studied

neuronal activity almost exclusively in terms of spike rate (Arabzadeh et al., 2006). Because the information capacity of rate code is substantially smaller than that of a timing code (Victor, 2005), rate codes may be insufficient for transmitting information about the control of precise skilled motor behaviors.

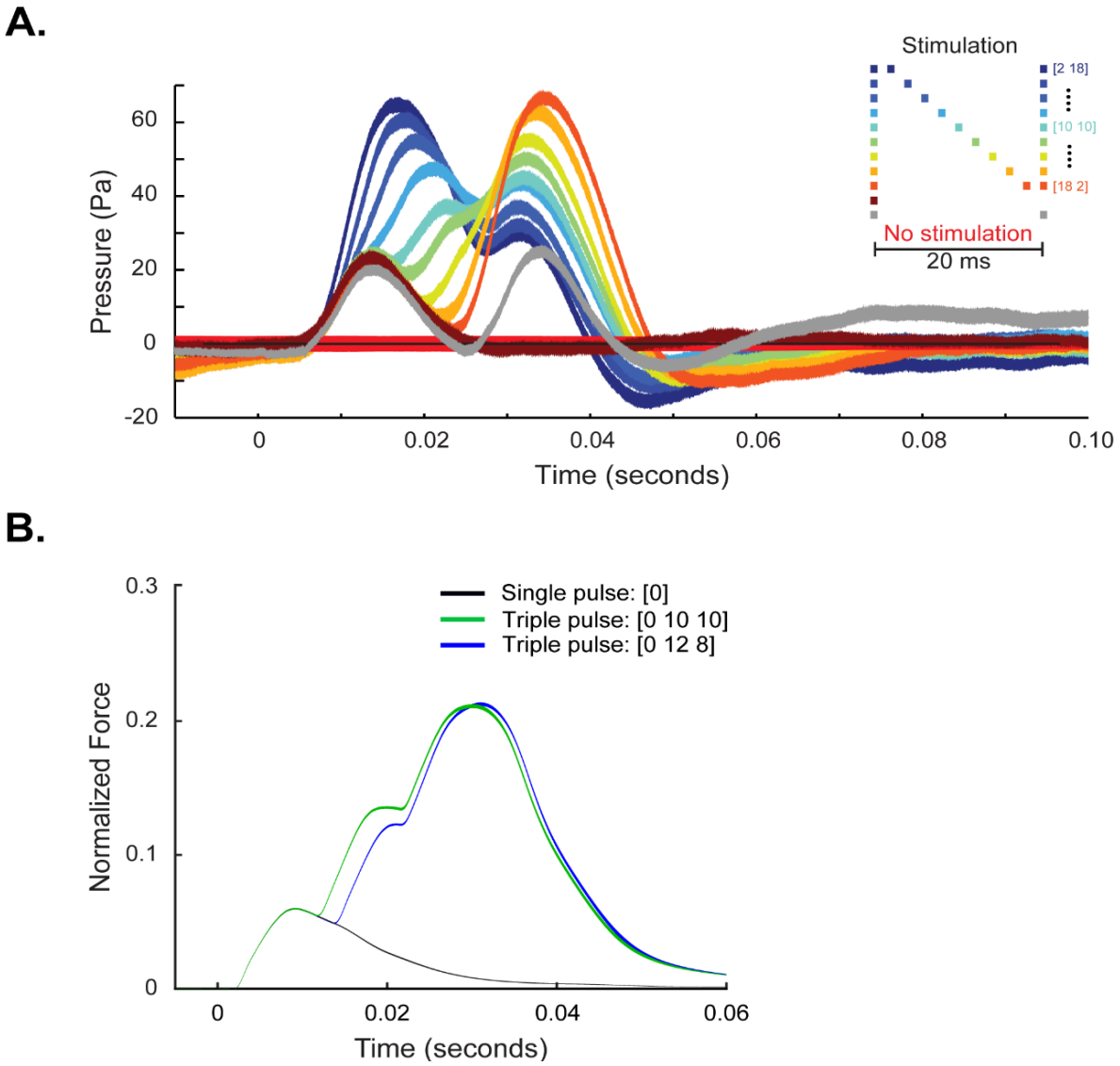

Figure 1.7: Millisecond-scale differences in triple-pulse stimulation patterns modulates behavior. (A) In vivo air pressure responses for each triple-pulse stimulation pattern (legend to right) applied to the expiratory muscle. All stimulation patterns caused different air pressure waveforms, demonstrating that the expiratory muscle is sensitive to millisecond-scale changes in spike timing. (B) In vitro force output of two triple-pulse stimulation patterns where the middle pulse differs by 2 ms differ significantly (wfANOVA). For both figures, full width of line indicates mean ± standard error of the mean (SEM) and time is relative to onset of the stimulation pattern. Figures adapted from (Srivastava et al., 2017).

1.5.2 Project 2: Determine whether muscles of the songbird vocal organ are sensitive to milli-second spike timing

Our lab has combined novel experimental and computational tools to investigate the timescale at which patterns of neural and muscle activity in the motor system control complex behaviors in songbirds. After recording single unit activity in a songbird's cortical vocal motor area (RA), our lab discovered neurons encode significantly more information about upcoming vocal behavior (i.e., singing) by millisecond-scale spike timing patterns compared with spike rate (Tang, et al., 2014). Although these results revealed that millisecond-scale spike timing differences predict variations in behavior, it is still unknown how timing differences cause changes in motor output. We first looked at the expiratory muscle group, examining how the muscle activity is organized across time. These experiments established that recorded motor units control respiratory muscles with millisecond-time scales and variations in spike timing patterns significantly alter breathing behavior (Figure 1.7A) and muscle force output (Figure 1.7B) (Srivastava, et al., 2017).

The labs prior work on understanding the importance of spike coding in bird muscles has been solely focused on the expiratory muscle and the corresponding breathing behavior. Even though breathing is an essential feature in vocalization, we wanted to shift our attention to study syringeal (vocal) muscles and the corresponding vocal behavior, which is a main interest in songbird neuroscience. In Chapter 3, we address whether millisecond-scale differences in songbird vocal organ muscle activation patterns modulate the force output of muscle fibers. We experimentally induced two- or three-pulse stimulation patterns in fiber bundles from a vocal organ muscle (VS) *in vitro* and measured the corresponding changes in force output. These experiments demonstrated that songbird vocal organ muscles can exhibit strong timing-based nonlinear force output during short IPIs (i.e., IPIs < 15 ms). These findings suggest that learning a complex skill such as birdsong

depends on the muscle's ability to organize precisely timed patterns of coordinated activity across muscles. The results, along with the previous results from our lab provide insight into the underlying mechanisms of motor control on both a neural and muscular level.

Chapter 2

A flexible carbon nanotube electrode array for acute in vivo EMG recordings.

2.1 Abstract

Executing complex behaviors requires precise control of muscle activity. Our understanding of how the nervous system learns and controls motor skills relies on recording EMG signals from multiple muscles that are engaged in the motor task. Despite recent advances in tools for monitoring and manipulating neural activity, methods for recording in situ spiking activity in muscle fibers have changed little in recent decades. Here, we introduce a novel experimental approach to recording high-resolution EMG signals using parylene-coated CNTFs. These fibers are fabricated via a wet spinning process and twisted together to create a bipolar electrode. CNTFs are strong, extremely flexible, small in diameter (14 - 24 μm), and have low interface impedance. We present two designs to build bipolar electrode arrays that, due to the small size of CNTF, lead to high spatial resolution EMG recordings. To test the EMG arrays, we recorded the activity of small (4 mm length) vocal organ muscles in songbirds in an acute setting. CNTF arrays were more flexible and yielded MU/bulk EMG recordings with higher SNR compared to SSW electrodes.

Furthermore, we were able to record SU recordings not previously reported in these small muscles. CNTF electrodes are therefore ideal for high-resolution EMG recording in acute settings, and we present both opportunities and challenges for their application in long-term chronic recordings.

2.2 Introduction

Acquiring a skilled behavior requires the development of precise coordination across neurons and muscles. It is unknown how the brain generates, refines, and controls precise patterns of activity during motor skill learning. To examine this fundamental question in motor control, it is necessary to record EMG activity from the muscles (Figure 2.1A) that control the pertinent behavior. Existing methods used to record EMG activity rely on surface electrodes or intramuscular electrodes comprised of fine wires or rigid bipolar needles (Basmajian, 1985; Bogey et al., 2000; Farina & Negro, 2012; Farrell & Weir, 2008; M. B. Raez et al., 2006; Turker, 1993). Surface electrodes can include two contacts (Loeb G.E, 1988) or larger number of electrodes and are non-invasively placed on the subject's skin (Cram, 1998). The location of surface electrodes makes them incapable of recording EMG activity from small or deep internal muscles (Cram, 1998; De Luca, 1997; Perry et al., 1981). Fine wire electrodes are placed in the muscle with a needle or by applying pressure to the electrode to penetrate the muscle. Rigid needle electrodes are similarly inserted directly into the muscle.

For small muscles in small experimental animals, such as songbirds, the stiffness of traditional fine-wire metal electrodes creates a number of difficulties. Muscles of the songbird vocal organ are located deeper in the body than, for example, the muscles of the rodent forelimb, and are thus more prone to muscle injury at the implant site (Turker, 1993). The muscle fibers in the songbird vocal

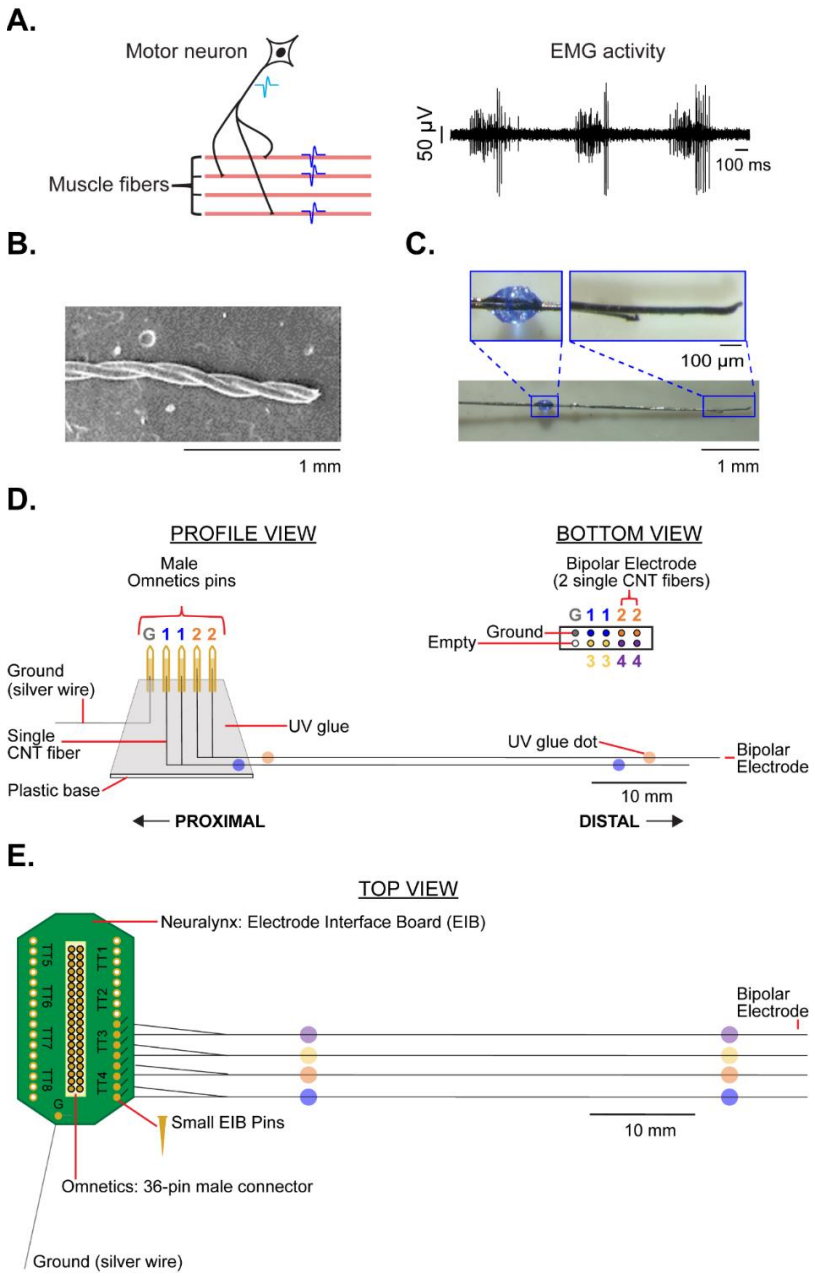

Figure 2.1: Motor units, EMG, and carbon nanotube fibers (CNTF) array construction. (A) (Left Panel) Motor unit schematic, which consists of all muscle fibers (shown in pink) innervated by a single-motor neuron (shown in black). When a motor neuron fires an action potential (light blue waveform), the action potential moves down the axon to the muscle fibers it innervates, causing the innervated muscle fibers to fire a near-synchronous volley of action potentials (dark blue waveforms). (Right Panel) Example recordings of multi-unit EMG activity. (B) Scanning electron microscopy image of two parylene-coated carbon nanotube fibers twisted together, creating a bipolar electrode. (C) Each bipolar electrode was labeled with colored dots of UV glue. Each electrode array consisted of 4 CNTF bipolar electrodes and one ground wire. (E) CNTF array schematic for Design 1. Each proximal end of four CNTF bipolar electrodes and one ground wire were secured into male Omnetics pins with carbon glue, creating a two by five electrode array. (D) CNTF array schematic for Design 2. Each proximal end of a CNTF bipolar electrode was inserted into side-by-side gold plated holes on a Neuralynx electrode board interface and secured with a gold attachment pin.

organ produce 50-100 times lower stress (Adam et al., 2021) and are smaller diameter (A. F. Mead et al., 2017) than skeletal muscles, and thus are impeded more than skeletal muscles by stiff wire implants when contracting. Furthermore, it is important for the lead-out wires to be very flexible to prevent strain on the vocal organ which could interfere with natural singing behavior, a behavior much more sensitive and easily restricted than (e.g., locomotion). The lack of flexibility in fine wire electrodes also limits the number of channels that can be implanted simultaneously. Recording with four fine wire bipolar channels is extremely challenging (Goller & Cooper, 2004), thus songbird vocal organ muscles provide a good test case for more flexible EMG electrode designs.

To address these obstacles, we developed a novel electrode technology that uses CNTFs to create bipolar electrodes (Figure 2.1). CNTFs are five times stronger than graphene fibers and the best conductive polymer (Yan et al., 2021), have a flexural rigidity about four times that of platinum-iridium (Pt-Ir) fine-wire electrodes (Zhu et al., 2019), and can be produced as small as ~14 to 24 µm diameter threads (Figure 2.1B). Electrochemically, CNTF have 15-20 times lower interface impedance than Pt-Ir fine-wire electrodes of the same diameter (Vitale et al., 2015). Compared to Pt-Ir, CNTFs are more biocompatible, producing a reduced inflammatory response (Behabtu et al., 2013; Tsentalovich et al., 2017; Vitale et al., 2015). Additionally, CNTFs have been successfully used to record neural activity from mice cortex and thalamic reticular nucleus in acute brain slices (Vitale et al., 2018), chronically stimulate neurons and record SU neural activity in rats (Alvarez et al., 2020), and acutely stimulate and record from nerves in small animal models (Lissandrello et al., 2017). These properties make CNTFs ideal candidates for constructing multi-channel electrode arrays for EMG recordings of small muscles, allowing EMG recordings in muscles that

were previously not possible. However, we currently do not know whether CNTF bipolar electrodes could be used to record high amplitude EMG activity in such muscles.

In this paper, we introduce two designs to build bipolar electrode arrays with the CNTF technology, where each array consisted of four CNTF bipolar electrodes and one ground wire (Figure 2.1D, E). We measured the bending stiffness of these arrays to be eight times lower than the same array made of SSW electrodes. We furthermore present a procedure to record EMG activity from small muscles in an acute experimental paradigm. Our results show that CNTF electrodes can attain high spatial resolution, recording both bulk (MU) and SU EMG activity across multiple small muscles. In acute recording situations, we observed SNRs in the CNTF bipolar electrodes between 8 - 44 for MU activity, which is up to 7.1 times higher than SSW electrodes, and 39 - 62 for SU activity, which we never observed using traditional SSW electrodes. The SNR of CNTF remained consistent over several hours, demonstrating the stability of the EMG recordings within and across multiple muscles.

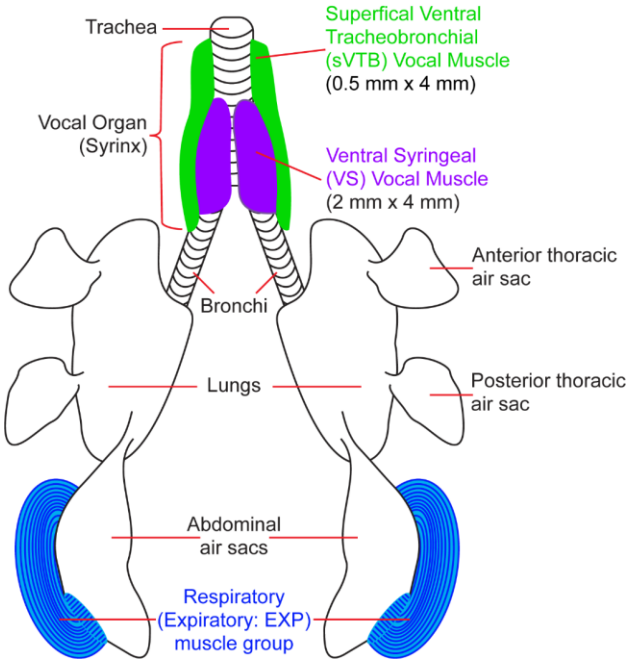

Figure 2.2: Illustration of the respiratory and vocal system of songbirds. We measured EMG activity in either the right or left expiratory (respiratory) muscle group or the right and/or left ventral syringeal (VS) muscles and/or superficial ventral tracheobronchial (sVTB) muscles. VS and sVTB muscles are part of the songbird vocal organ, syrinx.

2.3 Methods

2.3.1 Animals

Fifteen adults (> 90 dph) songbirds were used in this study. Nine birds were used for acute EMG recordings with CNTF bipolar electrodes. Two

female Bengalese finches (*Lonchura striata domestica*; Table 2.1: Birds 1 and 2) were used to record EMG activity from muscles of the songbird vocal organ, the syrinx: *musculus syringealis ventralis* (ventral syringeal – VS) and *m. tracheobronchialis ventralis superficialis* (superficial ventral tracheobronchial – sVTB; Figure 2.2). One male Bengalese finch was used to compare EMG recordings between CNTF and SSW bipolar electrodes in the same vocal muscle (VS) (Bird 3). Three female Bengalese finches (Birds 4, 5, and 6) were used to record EMG activity from one of the respiratory muscles (expiratory muscle group - Exp; Figure 2.2). Bengalese finches were bought from a supplier or bred in our laboratory at Emory University, USA and singly housed in sound-attenuating chambers with food and water. Additionally, two female and one male Zebra finch (*Taeniopygia guttata*; Birds 7, 8, and 9) were used to record EMG activity from VS and sVTB. Six additional male zebra finches (Birds 10-15) were used for acute EMG recordings with SSW bipolar electrodes. All zebra finches were from a breeding colony housed in indoor aviaries at the University of Southern Denmark (SDU), Denmark. Sound chambers and aviaries were kept on a 12-h:12-h light/dark cycle, and ambient temperature was maintained between 24 to 28°C. Bengalese finch experiments were conducted at Emory University, and Zebra finch experiments were conducted at SDU. All experimental protocols were approved by Emory University and SDU Institutional Animal Care and Use Committees.

2.3.2 Carbon nanotube fiber fabrication

Purified CNTs were dissolved in chlorosulfonic acid at 2 weight % and wet-spun into CNTFs (diameter per fiber = 22.1 ± 1.1 μm) as previously described (Behabtu et al., 2013; Tsentalovich et al., 2017; Yan et al., 2021). CNTFs fabricated using this method are strong, flexible, light-weight, conductive, and possess significantly lower interface impedance than metal electrodes (Behabtu et al., 2013; Tsentalovich et al., 2017; Vitale et al., 2015; Yan et al., 2021). Next, 2.5 μm

of Parylene C were deposited onto CNTF for insulation using SCS Labcoter 2 vacuum deposition system, leaving only the ends exposed. High resolution scanning electron microscopy was used to measure single-fiber diameters (Vitale et al., 2018), which range from 14 to 24 μm.

2.3.4 Carbon nanotube fibers array construction

CNTF bipolar electrodes

Two coated CNTFs were twisted around each other at ~20 turns/cm using a cord maker. This bipolar electrode pair was given another layer of coating (~2 μm Parylene C) to hold the twists in place (Figure 2.1B). It is near impossible to precisely cut the CNTF with standard scissors because of their combined strength and flexibility. We used a new #11 scalpel blade on a glass plate under a stereomicroscope to trim the bipolar CNTF electrode to ≈ 6.5 cm. To prepare the electrodes for insertion into muscles, the two CNTF of each bipolar electrode were separated 4 to 6 mm on the distal (recording) end. The two separated CNTFs were then cut so one tip was shorter than the other, creating an offset between the tips that varied between 0.2 to 1 mm (Figure 2.1C). The tips were pushed back together with forceps and then secured to each other with UV glue (Solarez UV-cure thin, hard formula; Solarez, Minneapolis, MN) up until the offset of the tips. A dot of colored UV glue (a mixture of colored acrylic paint and UV glue) was placed approximately 1 cm from the offset of the tips on the distal end (Figure 2.1C) and approximately 2 cm from the proximal end (Figure 2.1D, E) of the bipolar electrode. The colored glue bead helped to identify the electrodes and corresponding recording channels after muscle implantation, as well as to help place the electrode on the muscle.

CNTF electrode array

We used two different designs to construct the CNTF electrode array. For design 1, ten male pins (Omnetics, Minneapolis, MN) were placed in two rows of five pins in a 36-channel female Omnetics connector (NSD 36 VV GS 4; Omnetics, Minneapolis, MN). The two by five male pin configuration created an electrode array consisting of four bipolar CNTF electrodes and one ground wire (Figure 2.1D). The proximal end of two CNTFs of a prepared bipolar electrode was separated 1.5 cm. Each separated CNTF proximal end was placed into individual Omnetics male connector pins side-by-side (Figure 2.1D, Bottom View). The pin and proximal end of the electrode were covered with carbon glue (Wire Glue; Anders product, Andover, MA), making an electrical connection between the CNTF and the Omnetics male connector pin. These steps were repeated for the other three bipolar electrodes; securing one more bipolar electrode on the bottom row and two bipolar electrodes on the top row. A 15 mm, x 139.7 µm diameter perfluoroalkoxy (PFA) coated silver wire (Catalog # 785500; A-M Systems, Sequim, WA) was used for the ground wire. The PFA coating on the silver wire was stripped on both ends, and one end was secured to the male pin with carbon glue. After the carbon glue dried (~8 to 12 hours), the proximal end of the electrode array (excluding the tips of the Omnetics male connector pins) was covered with UV glue. Then, a thin 10 x 15 mm plastic square was secured to the base of the Omnetics male connector pins (opposite of the recording end) with UV glue (Figure 2.1D, Profile view). The plastic square was used to create a base to handle and secure the CNTF electrode array. The electrode array was then removed from the 36-channel female Omnetics connector with forceps.

Although design 1 was lightweight and small (10 mm x 14 mm), the design presented a few disadvantages including the average amount of time to build the electrode array (approximately eight hours over two days) and the fragility of the structure. To address these challenges, we

created an alternative design that was easier and faster to build (Figure 2.1E). For design 2, the ends of two CNTF of a prepared bipolar electrode were separated 1.5 to 2 cm on the proximal end. Each proximal end was inserted into side-by-side gold plated holes from the bottom of an electrode interface board (EIB) (EIB-36-PTB; Neuralynx, Bozeman, MT). The output of the Omnetics end is a 36-pin male Omnetics connector (NPD-36-AA-GS 4 Guide Posts; Omnetics, Minneapolis, MN). A gold electrode attachment pin (Small HEAD PLATE Pins; Neuralynx, Bozeman, MT) was then placed in the hole from the top of the head plate, catching the CNTF. Pliers with offset tips were used to push the pin further into the hole and pinch the CNTF. This action stripped off a small section of Parylene C coating, making an electrical connection between the CNTF and gold on the EIB, securing the CNTF into place. We continued attaching the CNTF for the remainder of the CNTF electrodes (maximum of 15 bipolar electrodes and ground). A 15 mm PFA coated silver wire was used for the ground wire. Both ends of the coating were stripped off the wire, and one end of the wire was soldered to the ground connection on the EIB. In addition to being faster to assemble, the larger base (20 mm x 11 mm) of the EIB makes design 2 easier for the experimenter to grasp and manipulate during the experiment. While both designs are reusable, the use of the attachment pin in design 2 to secure the CNTF in place (compared with UV glue in design 1) allows for the experimenter to remove and replace the used CNTF with unused CNTF by using the offset tip pliers to push the attachment pin from the underside of the 36-pin male Omnetics connector, removing the pin.

Fine wire electrode array

To compare the performance of the CNTF electrode arrays and standard fine wire electrode arrays, we built the same arrays as described in detail above with 25 µm diameter, Teflon insulated SSW electrodes (California Fine Wire Company, CA, USA).

2.3.5 Mechanical testing of array flexibility

We compared the mechanical resistance to bending of an intact CNTF versus SSW electrode arrays by measuring the force needed to bend the combined electrodes of assembled arrays (Fischer et al., 2012). We used 4-channel assembled arrays and placed them horizontally on a raised aluminum platform. The electrodes were clamped between two 1mm thick, 20 mm wide glass microscope slides to prevent them from moving. The array connector was placed on one end of the glass and the bundle consisting of four free electrodes exited on the other side. At 1.0 mm from the exit point we depressed the bundle with a dual-mode ergometer (model 300C, Aurora Scientific, Canada) that measured force and displacement. All signals were digitized at 6 kHz and 16 bit (USB-6259, National Instruments). All control and analysis software were written in Matlab.

We applied 20 sinusoidal cycles with 1.0 mm peak-to-peak amplitude. Force signals were lowpass filtered at 1kHz (2^{nd} order Butterworth filter with zero-phase shift). The loading curves of cycles 5 to 20 were isolated and a linear regression curve was fitted to each cycle. We report the mean slope of the 15 cycles per array.

2.3.6 EMG data collection

Prior to surgery, arrays were connected to a 36-pin female Omnetics connector that interfaced with the Intan digital 16-channel bipolar recording headstage (RHD2216, Intan technologies, Los Angeles, CA). A flexible clamp was used to hold the plastic base (design 1) or the Omnetics EIB (design 2) of the CNTF or fine wire array during acute recordings. The EMG signals were digitized at 30 kHz at the headstage and delivered to a computer via the RHD recording controller (Intan technologies). All recordings were terminated by experimenter when the signal SNR was still robust because sufficient data had been collected, except for three recordings, which were terminated due to signal loss.

2.3.7 Acute EMG surgery

Birds were water and food deprived an hour before the start of surgery. Each bird was anesthetized initially with ketamine (40 mg/kg) and midazolam (3 mg/kg) intramuscular. Anesthesia was maintained throughout the experiment using 0 to 3% (vol/vol) isoflurane in oxygen gas and/or injections of midazolam as needed. Breathing rate was monitored throughout the surgery. All birds participated in acute experiments to either record EMG activity from the vocal organ muscles or respiratory muscles.

Syrinx exposure and electrode implant

Following anesthesia, the bird was placed on its back and secured to the surgery table. A vertical 2 to 3 mm incision was made in the skin from the furcula to the base of the trachea. Any fat was carefully separated with blunt forceps and retractors, revealing the interclavicular air sac. An 8-0 suture was loosely tied midway down the trachea. The bipolar electrodes were routed through the suture tied around the trachea to secure the electrodes in place while recording EMG activity. This positioned the electrodes to be parallel to the long axis of the trachea, and the distal (recording) end of the electrodes were located where the trachea and air sac connect.

Prior to opening the air sac, isoflurane was reduced to 0.5% followed by an intramuscular injection of midazolam (3 mg/kg). Approximately five minutes after injection, the interclavicular air sac was cut, the syrinx was exposed, and the isoflurane was turned off. Thereafter, intramuscular injections of midazolam were used as needed for anesthesia maintenance. We placed individual CNTF bipolar electrodes or SSW bipolar electrodes on top of vocal organ muscles without removing fascia surrounding the targeted muscle. The exposed distal tip of the ground wire was placed subcutaneously near by the implanted muscles. Muscle activity was recorded from *Musculus syringealis ventralis* (VS) and/or *M. tracheobronchialis ventralis superficialis* (sVTB).

VS is located on the ventral portion of the syrinx near the midline, and sVTB is located directly lateral to VS (Figure 2.2).

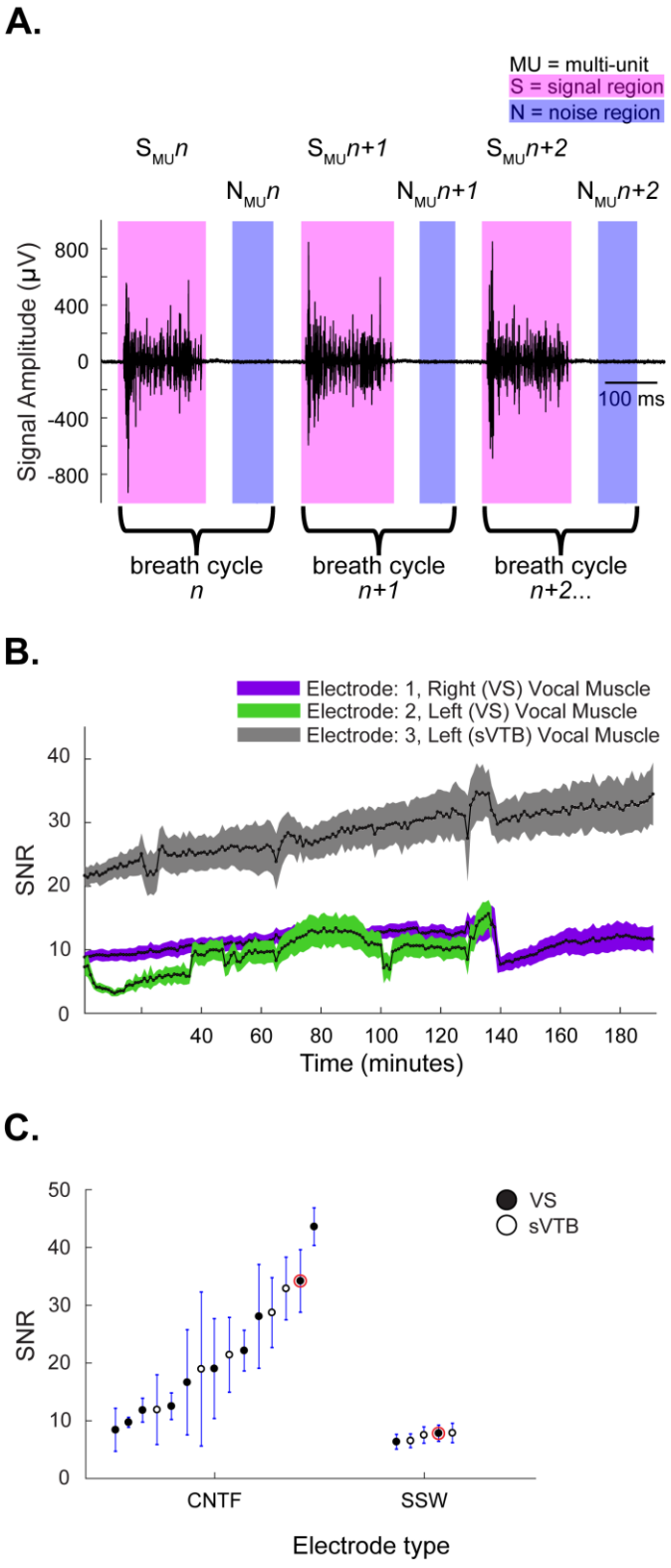

Figure 2.3: Multi-unit data analysis and results. (A) An example recording (Table 1: Bird 1, Recording 1, Electrode 3) of multi-unit EMG activity from VS muscle. The signal (pink shaded regions) and noise (blue shaded regions) regions were used to calculate the SNR (see Methods). (B) Example recording (Table 1: Bird 1, Recording 1, Electrodes 1, 2, and 3) of the multi-unit SNR values for an extended continuous recording in three vocal muscles. All SNR values for each complete breath cycle were averaged across one minute. (C) The SNR of CNTFs (Birds 1,2, 7-9) in vocal muscles ranged from 8.4 ± 3.7 to 43.6 ± 3.3 and was significantly higher (One-way ANOVA, $p = 0.032$) compared to SSW (Birds 10-12) with SNR of 6.2 ± 1.2 to 7.9 ± 1.7. In one animal (Bird 3, shown circled in red), we recorded EMG of a SSW bipolar electrode implanted in the muscle (L. VS, SNR: 7.8 ± 1.8) and a CNTF bipolar electrode on top of the fascia (SNR; 34.2 ± 6.1).

Expiratory muscle group exposure and electrode implant

Following anesthesia, the bird was placed on either its right or left side and secured to the surgery table. A 10 to 12 mm incision was made rostral to the pubic bone and dorsal to the femoral joint, exposing the expiratory muscle group (Figure 2.2) in the same manner as previous studies (Srivastava et al., 2017). Forceps were used to place individual CNTF bipolar electrodes or SSW bipolar electrodes on top the left or right expiratory muscle group without removing fascia. The exposed distal tip of the ground wire was placed subcutaneously near by the implanted muscles.

2.3.8 EMG data analysis

In songbirds, the expiratory muscle group (*m. obliquus externus abdominis, m. obliquus internus, and m. transversus abdominis*) controls ventilation in the exhalation phase of the breath cycle, where one breath cycle is one inhalation and one exhalation. This group of muscles contract around the abdominal air sacs during expiration (Figure 2.2), controlling pressure through the air sac system that drives sound production and surrounds the vocal organ (During et al., 2013; Goller & Cooper, 2004; Hartley, 1990; Schmidt & Martin Wild, 2014; Srivastava et al., 2015; Srivastava et al., 2017). The expiratory muscle group and vocal organ muscles are typically rhythmically active when the animal is fully anesthetized (Srivastava et al., 2015; Srivastava et al., 2017).

Defining signal and noise regions in EMG data

The rhythmic activity of the muscles allowed us to track the amplitude of segments of signal and noise within a breathing cycle. The recorded EMG signals were band-pass filtered between 350 and 7,500 Hz, rectified by taking the absolute value of the signal, and then smoothed with a square filter of width 17.5 ms (smoothing window). We refer to the periods were the expiratory muscle group and the vocal organ muscles were active as the “signal”. We fitted a gaussian mixture model

to the distribution of voltage amplitude, using either three or four gaussian functions, to fit the bimodal distribution. The intersection of the two gaussians directly after the first peak in the histogram was used to set the threshold value between signal and "noise" (i.e., low threshold). All data greater than the low threshold were considered signal. This produced region boundaries for each defined signal phase for every recorded breath cycle in the filtered data. The noise floor (i.e., noise phase) was determined by taking the data points between each defined signal phase for every recorded breath cycle. In order to make sure that no noise data points were included in the signal phase and vice versa, we adjusted the region boundaries for each signal and noise phase by ± 3*smoothing windows (3*17.5 = 52.5 ms), defining the signal regions and noise regions for each breath cycle used to calculate SNR (Figure 2.3A).

Signal to noise ratio – multi-unit activity

To determine the SNR for MU activity, we calculated the root-mean-square (rms) value of the

$$\text{rms} = \sqrt{\frac{\sum_{i=1}^{n} a_i^2}{n}}$$

amplitude for the signal region and the rms of the amplitude for the corresponding noise region. To find the rms of a set of values (a), take the square root of the arithmetic mean of the squared values. We then divided the rms of the signal region of one breath cycle (Sn) by the rms of the corresponding noise region (Nn).

$$\text{SNR} = \frac{rms(S\ n)}{rms(Nn)}$$

One SNR value was computed for each individual breath cycle. We were unable to differentiate the signal region from the noise region in the SSW bipolar electrodes of three birds (Table 2.1: Birds 13-15), who were omitted from further analysis,

Signal to noise ratio – single-unit activity

We identified single-motor units in the recorded EMG data with a previously published spike sorting algorithm (Sober et al., 2008). Briefly, we performed principal components analysis (PCA) on EMG voltage waveforms and examined their projections along the first two principal components and used k-means clustering to identify clusters of waveforms that corresponded to individual motor units or undifferentiated, MU background signals. We then quantified the extent of overlap between clusters. Waveform clusters with overlaps of less than 1% were classified as SU, and recordings with larger overlaps were classified as MU recordings. This technique yielded

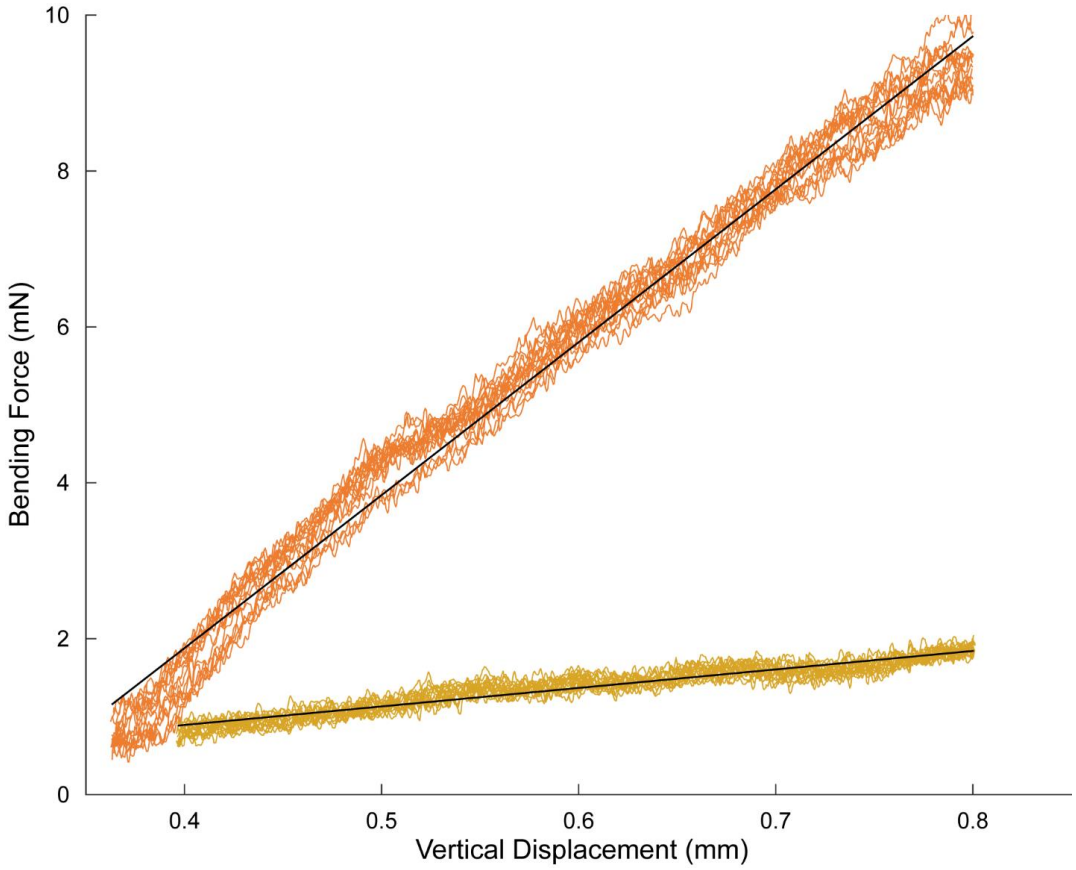

Figure 2.4: The bending stiffness of CNTF arrays is over eight times lower than SSW. The bending stiffness of a 4-channel array electrode bundle (black lines) was 2.4 ± 0.1 mN/mm for CNTF (yellow, $p<<0.01$, $R2=0.91$) and 19.6 ± 0.5 mN/mm for SSW arrays (orange, $p<<0.01$, $R2=0.99$). The CNTF arrays thus required 8.3 times less force to bend the same amount compared to a SSW array.

quantitative estimates of motor unit isolation that agreed well with both qualitative assessments of unit isolation and estimates based on spike refractory periods. After isolating the spikes from single motor units, we then computed the SNR of each spike by dividing the peak spike amplitude by the rms of voltage in the adjacent noise region, where the latter quantity is computed as described above in "Signal to noise ratio – multi-unit activity." All values presented are mean ± standard deviation (SD).

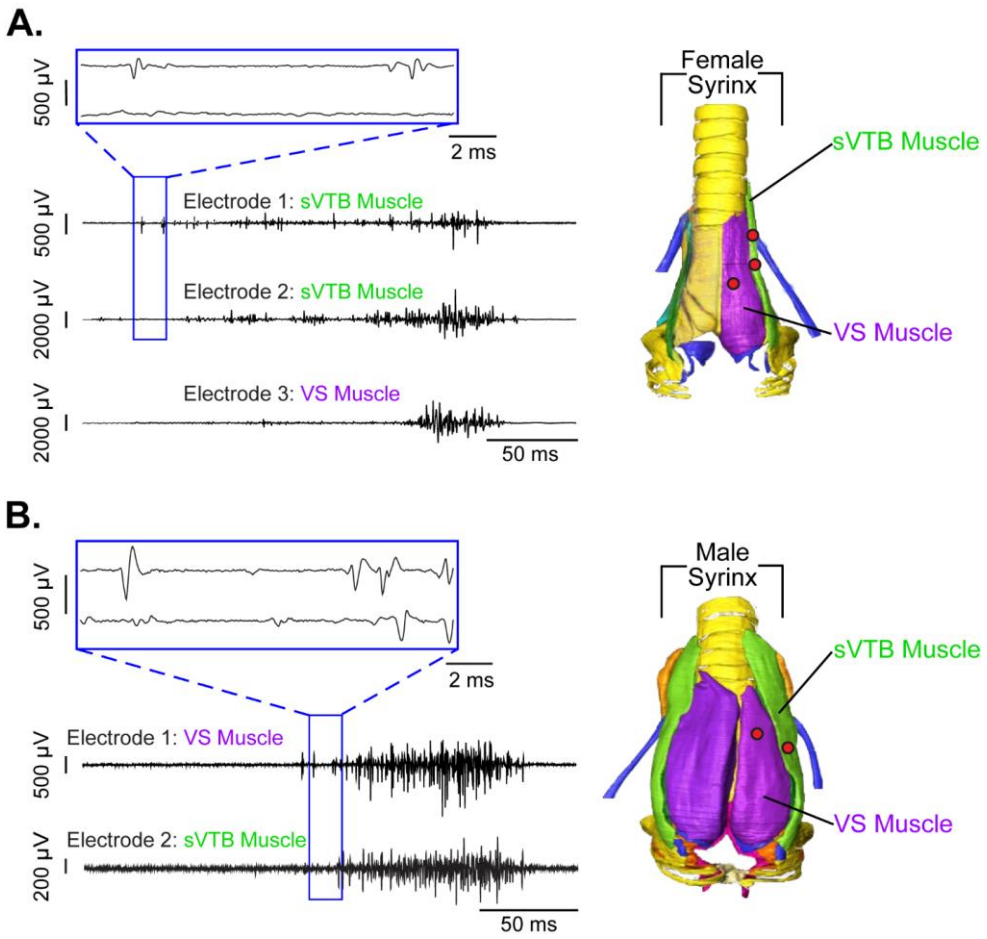

Figure 2.5: Recording distinct motor unit populations within and across muscles. (A) The left panel is an example recording (Table 1: Bird 7, Recording 2, Electrodes 1, 2, and 3) of different MU EMG activity within (Electrodes 1 and 2) and across (Electrode 3) multiple vocal muscles simultaneously in a female ZF bird. (B) The left panel is an example recording (Table 1: Bird 9, Recording 1, Electrodes 1 and 2) of different MU EMG activity across two vocal muscles (VS and sVTB) in a male ZF bird. In both examples, all electrodes are picking up different motor units in the identified muscle. The right panels in both A and B are ventral views of the female and male syrinx (adapted from (During et al., 2013)), respectively, and the corresponding muscles shown in the example recordings. The female and male syrinx have uniform muscle definitions and muscle attachment sites. The red dots on the syrinx represent the location of the recording electrodes.

2.4 Results

To determine whether bipolar CNTF electrode arrays can record MU and SU motor activity from multiple small muscles, we recorded acute EMG in songbird vocal and respiratory muscles. We tested 25 CNTF electrodes in six muscles (left and right VS, sVTB, and expiratory muscle group) across nine birds (Table 2.1). In addition, we tested 12 SSW electrodes in 4 muscles (left and right VS and sVTB) across 7 animals. Acute recordings lasted between 3-249 minutes, and in most cases were terminated by the experimenter while signal amplitude was still high, rather than ending due to a loss of EMG signal (see Methods). In addition, we compared the mechanical bending stiffness of four-channel bipolar CNTF arrays to SSW arrays. We found that the bending stiffness of CNTFs were 8.3 times lower compared to SSW arrays (Figure 2.4).

The CNTF bipolar electrodes can record MU motor activity within and across multiple small muscles of the songbird vocal organ simultaneously (Figures 2.3, 2.5). Not only were we able to record from three bipolar electrodes in two vocal organ muscles, but we were also able to record different ensembles of activity from the same muscle while the recording sites were less than 2 mm from one another**.** As illustrated by the MU recording shown in Figure 2.5A (top, blue inset boxes), two bipolar electrodes inserted into sVTB recorded different ensembles of motor units, as illustrated by the different waveforms in the highlighted channels. The SNR of the CNTF electrodes remained stable or increased over several hours in acute recordings. Figure 2.3B shows the SNR value for three electrodes recording muscle activity on a different vocal muscle simultaneously within the same bird (Table 2.1: Bird 1) over an extended (>3 hour) period (Electrode 1: N = 29,255 breath cycles, Electrode 2: N = 21,540 breath cycles, Electrode 3: N = 29,311 breath cycles). Taking the longest recording of 8 individuals, their MU SNR for all the

electrodes ranged from 3-44 (Figure 2.3C). These recordings demonstrate that the CNTFs can record discrete motor unit populations in multiple small bird muscles.

To compare the recording quality of the CNTFs to commonly used SSW electrodes, we quantified and compared SNR values of acute EMG recording between CNTFs (Table 2.1: Birds 1, 2, 7-9)

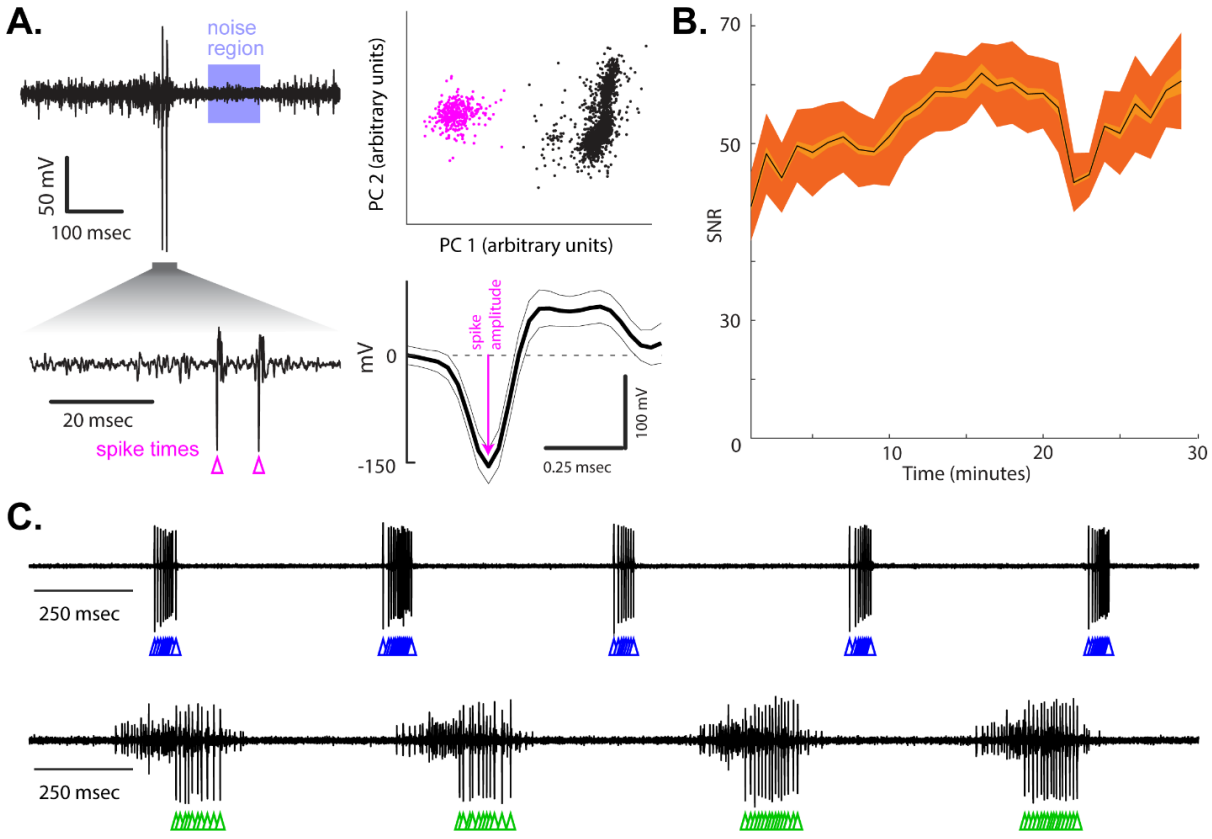

Figure 2.6: CNTF electrodes successfully record the activity of single-motor units in small muscles. (A) Top left, example recording (Table 1: Bird 4, Recording 1, Electrode 3) of SU EMG activity from expiratory muscle. We used a previously published spike sorting algorithm (27) that uses PCA to distinguish voltage waveforms belonging to a single motor unit (magenta dots, top right) from background noise (black dots, top right). The peak amplitude of each single unit waveform and the corresponding noise region (blue shaded region) were used to calculate the SNR, as explained in Methods. (B) Example recording (Table 1: Bird 4, Recording 1, Electrode 3) of the SNR values in a 29-minute continuous recording in the right expiratory muscle (N = 2,585 breath cycles). All SNR values for each complete breath cycle were averaged across one minute. C) Additional examples of single motor unit recordings (note that top and bottom traces come from different subjects but are plotted on the same time scale; Table 1: Bird 8, Recording 1 and Bird 6, Recording 1, Electrode 3; top and bottom, respectively). Colored triangles in (A) and (C) indicate the spike times of single motor units as determined by our spike-sorting algorithm (see Methods).

and SSW bipolar electrodes of the same diameter (Table 2.1: Birds 10-12). There was no difference in SNR distributions between muscle groups (i.e., VS and sVTB; Kolmogorov-Smirnov test, $p = 0.985$), allowing us to combine muscle groups when comparing SNR values between CNTFs and SSW electrodes. The SNR of CNTF recordings was significantly and up to 7.1 times higher compared to SSW (One-way ANOVA, $p = 0.03$; Figure 2.3C). In one animal (Table 2.1: Bird 3), we simultaneously recorded EMG activity from left VS with a CNTF electrode on top of the fascia and a SSW bipolar electrode implanted intramuscularly (red circles in Figure 2.3C). The SNR of this implanted SSW electrode was in the same range as SSW recordings on top of the fascia (SNR: 7.8 ± 1.8) and 4.3 times lower than the CNTF electrode (Supporting Figure 2.1).

The high spatial and temporal resolution and small size of the CNTF bipolar electrodes not only allowed us to record discrete motor unit populations within one muscle, but we were also able to isolate SU activity (Figure 2.6). As described in Methods, we used a well-established spike-sorting algorithm (Sober et al., 2008) to isolate the voltage waveforms of SUs in songbird vocal organ muscles. Briefly, this algorithm performs PCA on each voltage waveform and represents the population of recorded waveforms as points in the space of the first two principal components (PC 1 and PC 2), and then asks whether a "cluster" of similarly shaped waveforms (spikes from a single motor unit, magenta dots in Figure 2.6A, top-right plot) are significantly different from the remainder of the waveforms represented in the PC1-PC2 coordinates. Figure 2.6A shows an example of this spike-sorting method used to extract a single motor unit from one subject (Table 2.1: Bird 4, Recording 1, Electrode 3). In total, we recorded with 25 CNTF electrodes in 9 animals ("Electrode type" CNTF in Table 2.1). Of these 25 CNTF recordings, 12 yielded well-isolated single units (Table 2.1, each recording with SU data shaded in yellow). Of the animals implanted with CNTF electrodes, we recorded at least one single motor unit in 7/9 subjects (Table 2.1,

individual animals with at least one single unit shaded in yellow). Figure 2.6B depicts the SNR for one SU recording from the expiratory muscle group (Bird 4, Electrode 3; N = 2,585 breath cycles). The SNR ranged from 39.3 ± 5.8 to 61.9 ± 5.2. Other examples of SU recordings are shown in Figure 2.6C (Table 2.1: Bird 8, Recording 1 and Bird 6, Recording 1, Electrode 3; top and bottom, respectively). As described in prior work (Schmidt & Martin Wild, 2014; Srivastava et al., 2015; Srivastava et al., 2017; Suthers et al., 1999; Wild et al., 1998), motor unit activity in the expiratory muscle occurs in phasic bursts, which are locked to the respiratory rhythm.

For comparison, we collected 12 recordings with paired SSW in a total of 7 animals ("Electrode type" SSW in Table 2.1). No single motor units were isolatable in any of these 12 recordings (Table 2.1, recordings/animals with no single units isolated are shaded in cyan). Moreover, a prior study that implanted 20 songbirds with intramuscular fine-wire electrodes for chronic recording similarly did not produce any isolatable motor units (Srivastava et al., 2015). The CNTFs electrodes therefore exceed the performance of fine wires for isolating individual motor units.

2.5 Discussion

We showed that CNTFs can be used for acute EMG recording. CNTFs have many characteristics which make them an ideal material to record EMG activity within and across multiple small muscles. First, the high flexibility and high mechanical strength of CNTFs allow for the experimenter to easily handle the electrode without damaging its integrity. Second, because the CNTF bipolar electrodes have a diameter of only ~50 µm, we were able to record different ensembles of motor units from two different bipolar electrodes within the same small vocal muscle (Figure 2.5A). Third, the small diameter of the electrodes and low interface impedance allows for high resolution and quality recordings that result in large SNR (Figures 2.3B,C and 2.6B). Together, these properties yield high-resolution EMG recordings superior to those obtained by the

traditional wire electrodes we tested, including providing what we believe to be the first record of single motor unit spike trains in the muscles of the songbird vocal organ.

For a given electrode design, lower electrode impedances provide higher-fidelity recordings of neural and muscular activity. Although we did not systematically measure the impedance of the CNTF electrodes during the acute recordings, prior work has compared electrical properties of CNTF to other electrode materials *in vitro* (Vitale et al., 2015). The electrochemical impedance for CNTF measured 20.4 ± 8.2 kΩ, which is 2.6-6 times lower than tungsten wires with a similar diameter (Prasad & Sanchez, 2012; Vitale et al., 2015). The low impedance generated by the CNTF in comparison with other electrode materials suggests that the CNTF bipolar electrodes can produce a higher SNR. Indeed, our data confirms that the CNTFs' SNR is up to 7.1 times higher compared to SSW electrodes of similar diameter (Figure 2.3C). The SNR in SSW is comparable to our lowest reported MU SNR value 3.1 ± 0.5 (Bird 1, Electrode 2) and far below our mean MU SNR of 15.5. It is consistent with data from a prior study reporting SNR of fine wire electrodes in reinnervated muscle grafts of 3.8 - 4.6 (Vu et al., 2020). The CNTF electrodes thus compare favorably with traditional fine-wire EMG.

This paper establishes CNTF electrodes as tools for recording EMG activity in acute settings. In addition to the applications shown above, this technology could be expanded by greatly increasing the number of bipolar electrodes placed on the surface of an individual muscle. Increasing the electrode count per muscle would sample data from different subpopulations of motor units. Combining our experimental tools with multichannel spike-sorting algorithms (Pachitariu et al., 2016) would allow us to isolate the waveforms of individual motor units. Moreover, CNTF arrays can easily be used in a wide range of species and muscle groups. Overall, CNTFs allow for EMG recordings in muscles where EMG was previously unattainable. Additionally, CNTFs may reduce

animal discomfort when implanting muscles for chronic data collection, interfering less with natural behaviors.

The flexibility of CNTFs make them an excellent material to build bipolar electrodes for chronic recordings. In chronic recordings, two ways to attach electrodes to a muscle are typically used: on the surface of the muscle or intramuscularly. Using CNTFs in a chronic study would require a biological compliant tissue adhesive to secure the CNTF bipolar electrode on the surface of the muscle. However, the internal use of tissue adhesives, such as cyanoacrylates (specifically short-chain forms), risks disrupting muscle function due to toxicity from formaldehyde release (Ayyildiz & Ayyildiz, 2017; Garcia Cerda et al., 2015). Alternatively, the CNTF electrodes can be implanted intramuscularly. However, because CNTF electrodes lack the stiffness and a sharp tip to penetrate through muscle tissue, they would need a rigid shuttle to push the CNTF through the muscle fascia and into the tissue, such as PEG (Vitale et al., 2015), or could be sutured directly into the muscle. Once the limitation of securing the CNTF bipolar electrode to the targeted muscle is solved, CNTFs could be used in the future for chronic studies that require EMG recording within and across multiple small and deep muscles.

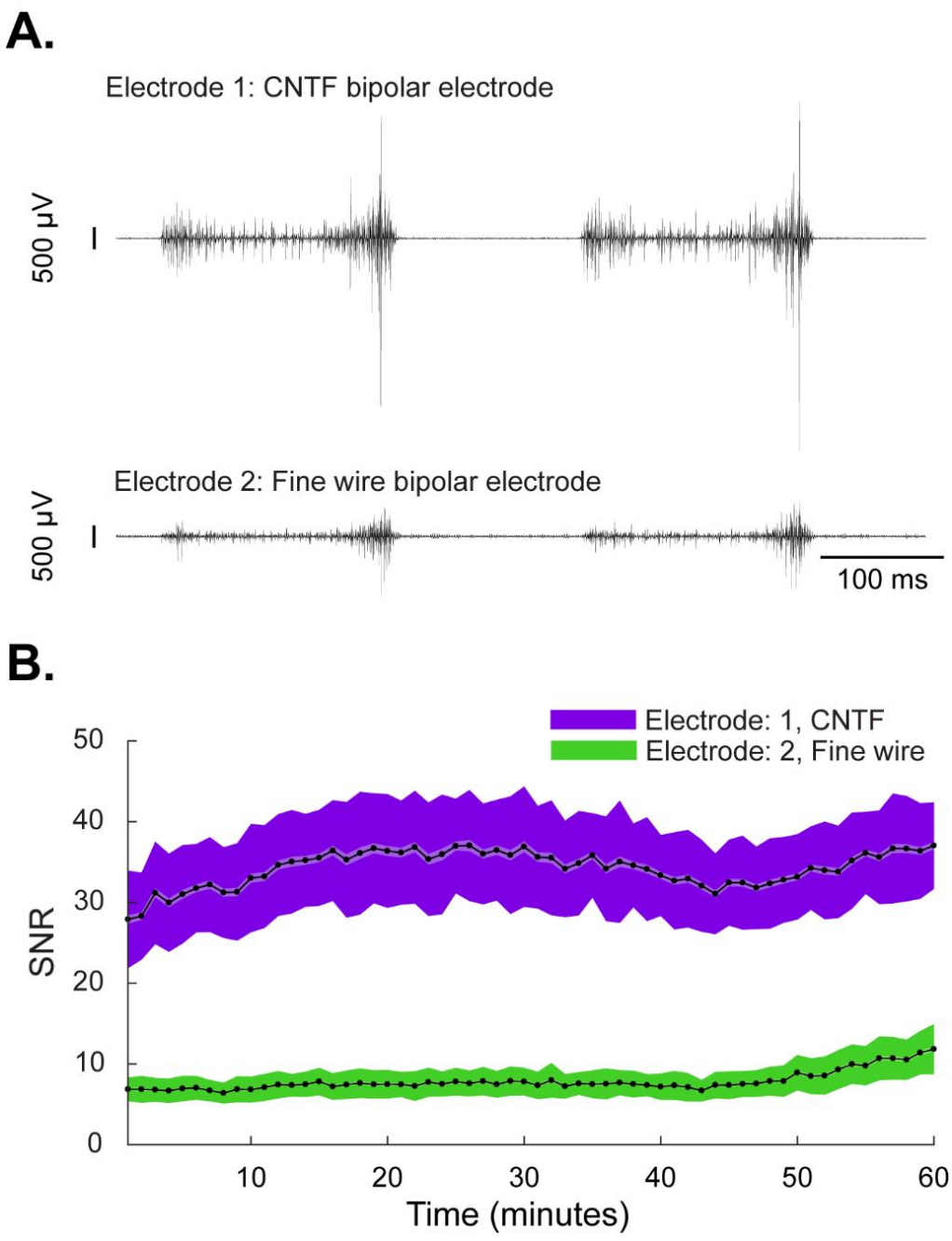

Supporting Figure 2.1: Comparing recording quality and SNR values between CNTF and SSW bipolar electrodes. (A) An example recording (Table 1: Bird 3, Recording 1, Electrodes 1 and 2) of EMG activity from two electrodes simultaneously in the same vocal muscle (L VS). The top panel shows activity recorded from a CNTF electrode, and the bottom panel shows activity recorded intramuscularly from a SSW electrode. (B) The multi-unit SNR values for Bird 3 over a continuous 60-minute period. The CNTF has a higher SNR value when compared to the SSW electrode. The average SNR over this recording for the CNTF was 34.2 ± 6.1, with an average signal = 125.8 ± 31 and an average noise = 3.9 ± 0.3. The average SNR for the SSW was 7.8 ± 1.8, with an average signal = 56.4 ± 11.4 and an average noise = 8.1 ± 2.1. All SNR values for each complete breath cycle were averaged across one minute.

Animal ID	Electrode Type	Recording Number	Electrode Number	Electrode Placement	Recording Length (min)	Total # of Breath Cycles
Bird 1 (F-BF)	CNTF	1	1	R. VS	191	29,255
	CNTF	1	2	L. VS	137*	21,540
	CNTF	1	3	L. sVTB	191	29,311
Bird 2 (F-BF)	CNTF	1	1	L. VS	8	861
	CNTF	2	2	L. VS	70*	9,372
	CNTF	2	3	L. VS	109	14,290
Bird 3 (M-BF)	CNTF	1	1	L. VS	60	8,005
	SSW	1	2	L. VS	60	8,005
Bird 4 (F-BF)	CNTF	1	1	R. Exp	29	3,467
	CNTF	1	2	R. Exp	29	2,551
	CNTF	1	3	R. Exp	29	2,585
Bird 5 (F-BF)	CNTF	1	1	R. Exp	151	14,543
	CNTF	1	2	R. Exp	151	14,557
Bird 6 (F-BF)	CNTF	1	1	L. Exp	249	16,300
	CNTF	1	2	L. Exp	249	17,360
	CNTF	1	3	L. Exp	181*	11,677
Bird 7 (F-ZF)	CNTF	1	1	L. sVTB	11	1,560
	CNTF	1	2	L. sVTB	11	1,509
	CNTF	2	1	L. sVTB	3	328
	CNTF	2	2	L. sVTB	3	353
	CNTF	2	3	L. VS	3	354
	CNTF	3	1	R. sVTB	4	398
Bird 8 (F-ZF)	CNTF	1	1	L. VS	12	1,231
	CNTF	2	2	L. VS	10	718
Bird 9 (M-ZF)	CNTF	1	1	L. VS	13	1,184
	CNTF	1	2	L. sVTB	13	1,192
Bird 10 (M-ZF)	SSW	1	1	sVTB	6	749

Bird 11 (M-ZF)	SSW	1	1	L. sVTB	3	435
Bird 12 (M-ZF)	SSW	1	1	VS	3	334
	SSW	2	1	sVTB	5	252
Bird 13 (M-ZF)	SSW	1	1	sVTB	3	N/A
Bird 14 (M-ZF)	SSW	1	1	L. sVTB	5	N/A
	SSW	1	3	L. VS	5	N/A
	SSW	2	2	L. sVTB	4	N/A
Bird 15 (M-ZF)	SSW	1	1	L. sVTB	5	N/A
	SSW	1	2	L. VS	5	N/A
	SSW	1	3	R. VS	5	N/A

Table 2.1: Summary of data used in analysis. Acronyms: F – female, M – male, BF – Bengalese finch, ZF – Zebra finch, CNTF – carbon nanotube fiber bipolar electrodes, SSW – stainless-steel fine wire bipolar electrodes (Bird 6 – intramuscular recording, Bird 10 – 15 = surface recording), and N/A – unable to differentiate signal region from noise region. Animal IDs shaded yellow represent individual animals with at least one identified SU in the recorded data, and recordings shaded yellow represent the specific recording that had SUs. Animals with no SUs isolated are shaded in cyan. *Recording terminated due to signal loss. All other recordings were terminated by experimenter when the signal SNR was still robust because sufficient data had been collected.

Chapter 3

Millisecond-scale differences in songbird vocal muscle stimulation patterns modulate motor output.

3.1 Abstract

Motor control requires the brain to activate muscles in order to produce the correct behavior. A central objective in neuroscience is to establish how the brain controls muscle activity and modifies muscle output during motor skill learning. Our prior work in songbirds quantified the timescale at which patterns of neural and muscle activity control vocal and respiratory behavior and demonstrated that millisecond-scale variations in spike patterning in cortical neurons (Tang et al., 2014) and respiratory muscle fibers (Srivastava et al., 2017) are correlated with the upcoming motor output. However, it is still unknown whether and how muscle fibers transform these precisely timed spike patterns into variations in behavior. To answer this question, we quantified and compared the effects of activation timing patterns on vocal organ muscles in songbirds *in vitro* to decipher how spike pattern-based strategies can modulate vocal motor output. We experimentally induced two- and three-pulse stimulation patterns in fiber bundles from a Bengalese finch (*Lonchura striata domestica*) vocal muscle *in vitro* and measured the

corresponding changes in force output. These experiments demonstrated that muscles of the songbird vocal organ exhibit strong timing-based nonlinear force output during short IPIs (i.e., IPIs < 15 ms), and suggest that these nonlinearities, along with nonlinearities we have previously described in songbird respiratory muscles, are a crucial feature of vocal behavior.

3.2 Introduction

Motor commands from the brain are translated into behavior through patterns of precisely coordinated activity across multiple muscles. Without the precise integration of neural signals to execute coordinated motor output, animals lose their ability to perform learned behaviors. How the nervous system patterns muscle activation to produce the desired force and behavior output remains a central question in neuroscience. Motor neurons use electrical activity (i.e., action potentials) to transmit information to the muscles, which results in a specific behavior. Here, we define a motor code as the relationship between the electrical activity from individual or ensembles of neurons (i.e., pattern of spikes) and resulting behavior (Gerstner et al., 1997; Kandel et al., 2013; Prescott & Sejnowski, 2008). Understanding the neural code can provide insight into how information (e.g., external stimulus or error correction) is transformed as electrical signals from one area of the brain to another area of the brain or muscles and how the information is represented as a behavior. In theory, neurons can encode information via rate, timing, or a combination of the two. Early theories of brain function relied solely on spike rate (rate code), the total number of action potentials within a time interval, to explain sensory processing and motor control (Figure 1.6). Eventually, researchers studying sensory coding discovered that millisecond-scale spike timing patterns (timing-based or temporal codes) were far more informative about sensory inputs than were spike rates (Strong et al., 1998). Despite the strong evidence for timing codes in sensory systems, however, studies of the motor system have examined neuronal activity almost entirely in

terms of spike rate (Sober et al., 2018). Because the information capacity of rate code is considerably smaller than that of a timing code, rate codes may be insufficient for transmitting information about the control of precise skilled motor behaviors (Hallock & Di Lorenzo, 2006; Prescott & Sejnowski, 2008). In many cases, spike timing-based codes have been shown to offer additional information regarding signaling and encoding neural characteristics unavailable with spike rate (Victor, 2005). For example, two different behaviors could be encoded by the same number of spikes (spike rate) but by different patterns of spike timing (Figure 1.6; left panel).

Previously, our lab combined novel experimental and computational tools to investigate the timescale at which patterns of neural and muscle activity in the motor system control behaviors in songbirds. It was important to establish whether there was a correlation between spike trains and the trial-by-trial variation in behavioral output. Our lab started by investigating the role of spike timing in vocal behavior by recording single neurons in a songbird's cortical vocal motor area (RA) and discovered neurons encode significantly more information about upcoming vocal behavior (i.e., singing) by millisecond-scale spike timing patterns compared with spike rate (Tang, et al., 2014).

Although these results revealed that millisecond-scale differences in spike timing in neurons predict variations in behavior, we wanted to understand whether timing differences caused changes in motor output. Are millisecond-scale differences in spike timing also important in muscles? We approached this question with complimentary *in vivo* and *in vitro* experiments by looking at the respiratory muscles (i.e., the expiratory muscle group) that control the exhale in a breath cycle and the corresponding air sac pressure. We chose the expiratory muscle group first for the following reasons: 1) Respiration is important for birds to perform their vocal behavior. These muscles contract around the abdominal air sacs, controlling pressure through the air sac system that drives

sound production (During et al., 2013; Goller & Cooper, 2004; Hartley, 1990; Schmidt & Martin Wild, 2014; Srivastava et al., 2015; Srivastava et al., 2017) and 2) the expiratory muscle group is typically rhythmically active when the bird is anesthetized making it possible to record the breathing behavior (e.g., expiratory muscle groups and abdominal air sac pressure) during in an acute experimental paradigm. The *in vivo* experiments involved recording single motor units in the respiratory muscles during anesthetized breathing behavior. Respiratory motor units typically fire electrical signals in multiples ("bursts"). Because we wanted to best represent biological processes and understand the interactions between multiple spikes and the corresponding behavioral output, we identified multi-pulse stimulation patterns found in the muscle recording to stimulate the respiratory muscles and record the corresponding air sac pressure during anesthetized breathing behavior. This set of experiments established that most recorded motor units in the expiratory muscle control respiratory muscles with millisecond-time scales and variations in spike timing patterns significantly alter breathing behavior (Figure 1.7A) (Srivastava, et al., 2017). In addition to investigating the role spike timing played in controlling and altering breathing behavior, it was important to understand how millisecond-scale variations in stimulation patterns affect biomechanical properties of muscles. We were specifically interested in the biomechanical relationship between the motor code at the level of the muscle and force output. We extracted a muscle fiber bundle from the respiratory muscle, stimulated the fiber bundle with the same triple-pulse patterns used in the *in vivo* experiments, and measured the force output. We established that variations in activation timing patterns significantly alter muscle force output (Srivastava, et al., 2017).

Activation timing in vocal organ muscles

Our prior work on understanding the importance of spike coding in bird muscles has been solely focused on the expiratory muscle (respiratory muscle that drives exhalation) and the corresponding breathing behavior. Even though breathing is an essential feature in vocalization, we wanted to shift our attention to study syringeal (vocal organ) muscles and the corresponding vocal behavior, which is a main interest in songbird neuroscience. Unlike the expiratory muscle group, vocal organ muscles in songbird's are characterized as a superfast muscle, a muscle that has fast synchronous contraction rates up to 250 Hz and fast isometric contraction speeds around 4.7 ± 0.8 ms (Elemans et al., 2008; Mead et al., 2017). This property suggests that the vocal muscle could use millisecond-scale spike timing patterns to produce precise and complex motor behaviors (e.g., singing). To address whether millisecond-scale changes in activation timing affect force output in muscles of the songbird vocal organ, we performed *in vitro* experiments by extracting muscle fiber bundles from *musculus syringealis ventralis* (ventral syringeal – VS), a vocal muscle of the songbird vocal organ, and stimulated the muscle with either double-pulse or triple-pulse stimulation patterns with varying IPIs. We measured the force output over many iterations for each pattern and calculated whether double-pulse stimulation patterns caused a nonlinear effect in the force output of the VS muscle. We found that all double- and triple-pulse stimulation patterns produced different force waveforms. Additionally, these experiments demonstrated that songbird vocal organ muscles can exhibit strong timing-based nonlinear force output during short IPIs (i.e., IPIs < 15 ms). These results suggest vocal organ muscles are sensitive to small millisecond differences in motor neuron spiking patterns.

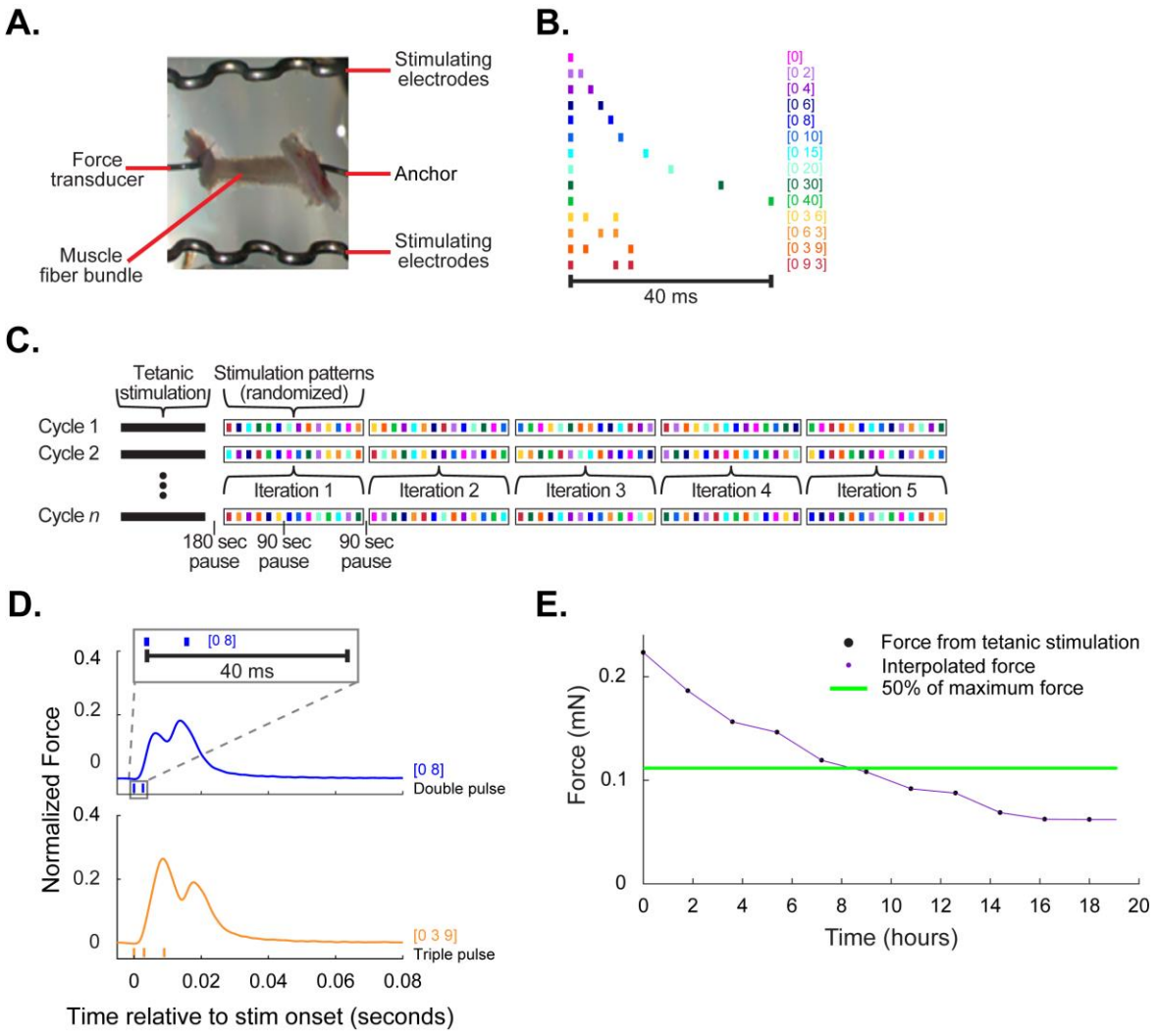

Figure 3.1: Experimental design. (A) In vitro muscle fiber preparation. (B) Stimulation patterns tested in experiment. We tested one single-pulse, nine double-pulse, and four triple-pulse stimulation patterns. (C) Experimental timeline and design schematic. (D) An example of the force waveform (Table 3.1: Bird 2) after delivering a double-pulse stimulation separated by 8 ms (top panel) and a triple-pulse stimulation with the first and middle pulses separated by 6 ms and the middle and last pulses separated by 3 ms (bottom panel). (E) Force from tetanic stimulation (every 5 iterations of all 14 stimulation patterns) interpolated over time (Bird 2). The force waveform for each pattern was normalized to the interpolated value corresponding to the same time. We only analyzed data that were greater than or equal to 50% of the maximum force to account for force decay that occurred over the long experiment.

3.3 Methods

3.3.1 Animals

Six adult (> 90 dph) male Bengalese finches (*Lonchura striata domestica*) were used in this study. Songbirds were bought from a supplier and housed in indoor aviaries at SDU, Denmark. Aviaries were kept on a 12-h:12-h light/dark cycle, and ambient temperature was maintained between 24 to 28°C. Birds were provided with food and water ad libitum. All experimental protocols were approved by SDU Institutional Animal Care and Use Committees. All *in vitro* experiments were done at SDU by Dr. Iris Adam, and all data analysis was done at Emory University by Andrea Pack.

3.3.2 *In vitro* muscle preparation

The muscle fiber bundles were extracted (Figure 3.1A), one bundle from each of the six birds, from a vocal muscle using a previously published technique (Elemans et al., 2008; Srivastava et al., 2017). To summarize, animals were euthanized with an overdose of isoflurane. Birds were placed on their back, and a vertical incision was made from the base of the trachea to the lowest part of the rib cage. The syrinx (i.e., vocal organ) was exposed by cutting through the sternum and then carefully removed from the body cavity. The bundle of muscle fibers was extracted from the surface of the left (n =5) or right (n = 1) VS and then mounted in a test chamber. VS is located on the ventral portion of the syrinx near the midline (see Figure 2.2, Chapter 2). The rostral end of the muscle was connected to a force transducer (Model 400A; Aurora Scientific) and the opposite end was attached to the arm of a servomotor (Model 6023AFM, Cambridge Technology, Cambridge, MA) with a silk suture (Figure 3.1A). The muscle fiber bundle was continuously flushed with oxygenated Ringer's solution at ~39°C for the fiber bundle extraction and entirety of the experiment.

3.3.3 *In vitro* muscle stimulation

Muscle fibers were stimulated through the solution filled chamber using parallel platinum electrodes (Model 701D; Aurora Scientific) (Figure 3.1A). The muscle fibers were stimulated with one, two, or three-pulse stimulation patterns to test whether vocal organ muscles are sensitive to millisecond-scale timing variations. There were a total of 14 stimulation patterns (Figure 3.1C). The nine two-pulse stimulation patterns consisted of two pulses separated by 2, 4, 6, 8, 10, 15, 20, 30, or 40 ms (Figure 3.1D, top panel). There were four three-pulse stimulation patterns. For two of the four patterns, the first and third pulse were separated by 9 ms with the middle pulse either occurring at 3 or 6 ms after the first pulse. The other two three-pulse patterns had 12 ms separating the first and third pulse and the middle pulse occurring at 3 or 9 ms following the first pulse (Figure 3.1D, bottom panel). The one-pulse stimulation pattern was used as a control.

Experimental protocol

First, we applied 50 ms tetanic stimulation (with the exception of Bird 5 – 75 ms tetanic stimulation) at 400 Hz (with the exception of Bird 2 – 300 Hz and Bird 4 – 500 Hz), which was followed by a 180 sec pause. Applying the tetanic stimulation every five iterations of running through all 14 stimulation patterns allowed us to account for force decay that occurred over the long experiment (ranging from 660 to 1,740 minutes). We then went through five iterations of all fourteen stimulation patterns in random order with 90 seconds in between each stimulation pattern (Figure 3.1B). The experiment was repeated over many cycles: Bird 1 – 115 iterations, Bird 2 – 53 iterations, Bird 3 – 45 iterations, Bird 4 – 60 iterations, Bird 5 – 42 iterations, and Bird 6 – 56 iterations (Table 3.1). The total length of the experiments ranged from ~11 – 29 hours. Force and stimulation signals were low-pass filtered at 10 kHz and digitized at 20 kHz via a NIDAq Board

(PCI-MIO-16E4, National Instruments). Custom software in Matlab was used to automatize the experimental protocol.

3.3.4 Data analysis

All six muscle preparations degraded over time, as evidenced by steadily reducing tetanic force (Figure 3.1E), due to multiple iterations of stimulation to the muscle fibers. To account for this, we only analyzed the data from the time before the tetanic force fell to 50% of initial value (Figure 3.1E).

Filtering and normalizing force data

We first filtered the raw force with a low pass Butterworth filter at 200 Hz with 2 poles. As mentioned in 'Experimental protocol', we took a 50 ms tetanic stimulation force measurement between every five iterations of all the stimulation patterns throughout the duration of the experiment. For each tetanic stimulation, we calculated the force difference (tetFdiff) between the maximum force of the previous tetanic stimulation and the baseline force of the current tetanic stimulation (i.e., Maximum Force of tetanic stimulation 1 – baseline force of tetanic stimulation 2). We normalized the force measurements for each stimulus using linear interpolation between all 'tetFdiff' force values across the experiment. For the next step of analysis, we eliminated all data with a force output with an interpolated value less than or equal to 50% of the maximum force determined at the start of the experiment (Figure 3.1E). The remaining number of iterations for each muscle prep after eliminating data was Bird 1 – 55 iterations, Bird 2 – 23 iterations, Bird 3 – 7 iterations, Bird 4 – 28 iterations, Bird 5 – 24 iterations, and Bird 6 – 17 iterations.

Calculating nonlinearity of force output after double-pulse stimulation patterns

The force data derived from the double-pulse stimulation patterns allowed us to calculate the IPI values when the force summation was linear versus nonlinear. To quantify whether any double-pulse stimulation patterns caused a nonlinear effect in the force output of the VS muscle, we calculated the difference between the force output of the real data and the force output from summing two single-pulse responses separated by the corresponding stimulation pattern's IPI. We convolved two copies of the single-pulse waveform (Figure 3.2A, shown in pink as the first stimulation pattern), shifting the waveform by the IPI value. We determined the area under the curve by subtracting the real data and convolved single-pulse waveform (i.e. area under the curve). For each double-pulse stimulation pattern (n = 9), there were six animals, and each animal had a different number of iterations of the experiment varying from 7-55. To determine the statistical significance in our data set, we needed to account for the two-level hierarchical data structure. We used a previously published hierarchical boostrapping method to appropriately account for the error accumulated at different levels of the data (i.e., level 1 = number of birds and level 2 = mumber of iterations) (Saravanan et al., 2020; Saravanan et al., 2019). Briefly, for every stimulation pattern, we generated 1000 random subsamples of the dataset at each level by resampling with replacement from the original data. The mean force data produced by hierarchical bootstrapping was plotted as an empirical distribution function. As detailed previously (Saravanan et al., 2020; Saravanan et al., 2019), the 67% confidence interval range of force values provides a more accurate estimate of the error from the original dataset. The average of the real data for each pattern across all the animals was plotted with the hierarchical bootstrap error. Custom Matlab software was used to analyze the data.

Wavelet-based functional ANOVA analysis

We compared stimulation patterns using a wavelet-based functional ANOVA (wfANOVA), a previously published technique (McKay et al., 2013; Srivastava et al., 2017), to compare stimulation patterns disregarding inter-bird variability. Briefly, wfANOVA identifies statistically significant differences between continuous waveforms by quantifying whether one or more wavelet coefficients used to reconstruct the difference between the waveforms is significantly nonzero ($\alpha = 0.05$, F test with separate post hoc Scheffé tests, with the null hypothesis being that the force waveforms – represented by the coefficients of the wavelet decomposition – are equal). These post hoc tests were conducted using a significance level that was Bonferroni-corrected for the number of significant F-tests corresponding to the initial ANOVA with respect to the stimulation pattern factor (i.e., 0.05 divided by the total number of post hoc tests being conducted). Wavelet coefficients that were significantly different between stimulation patterns were subtracted to find the coefficient corresponding to the difference between the two patterns. Even having one wavelet with significant differences in their coefficients would indicate a significant difference between the two input patterns. After setting all nonsignificant coefficients to zero, the decomposition was transformed back into the time domain (i.e., reconstructed force), which produced a contrast curve between two stimulation patterns. All nonzero data points in the contrast curve revealed significant differences between the two force waveforms. To perform the ANOVA, all iterations of the experiment were grouped by one factor, stimulation pattern. Fixed-effect, one-factor ANOVA was performed on the decomposed wavelet of the force waveforms. Our analysis used an adapted version of the MATLAB code published in (McKay et al., 2013).

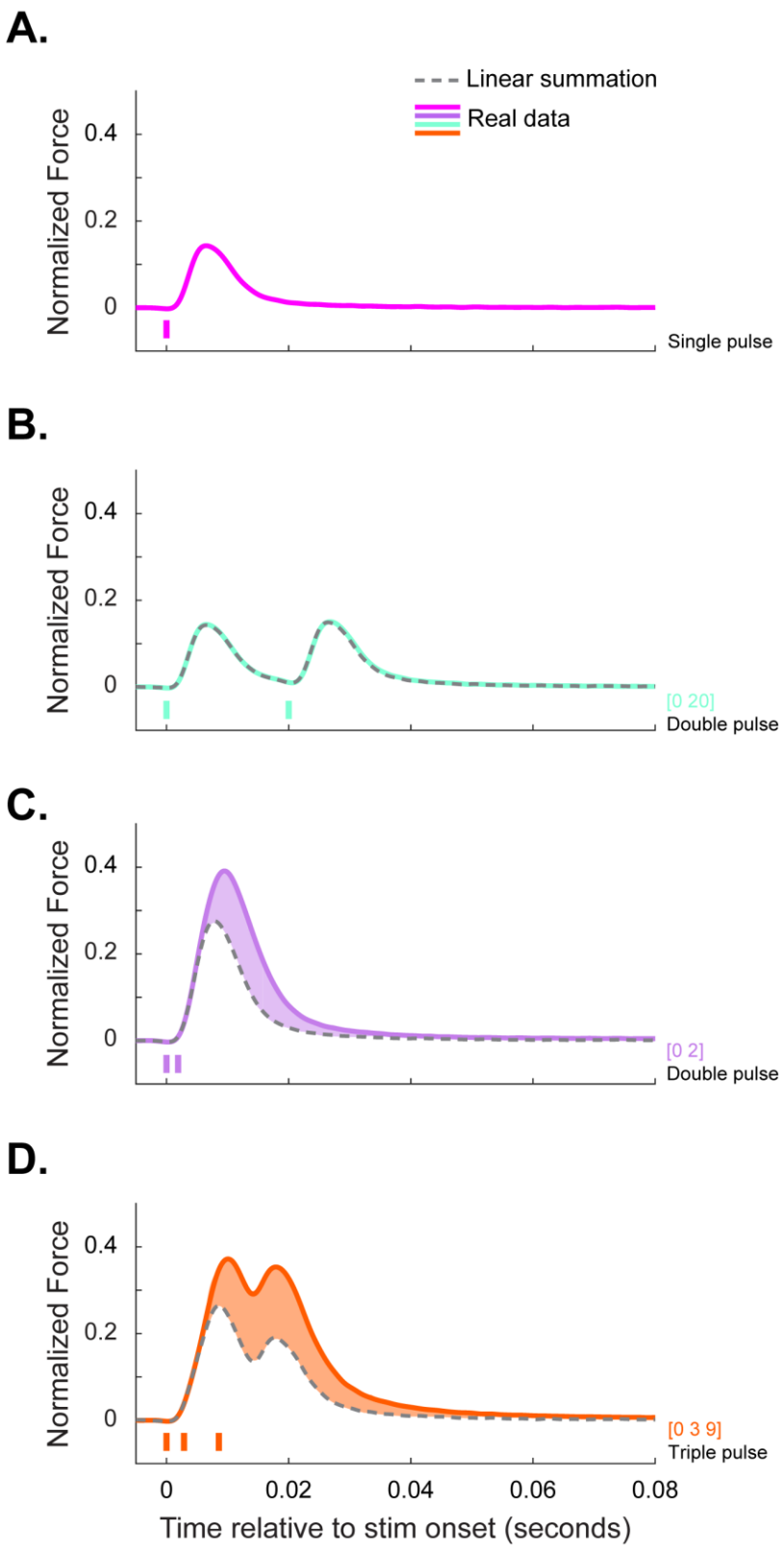

Figure 3.2: Comparing the real force waveform and the corresponding linear summation of the convolved single-pulse waveform. (A) Force wavelength of single-pulse stimulation pattern. This output was used to create the convolved waveform for linear summation. (B) Larger IPIs (20 ms in this example) results in only a 1.3 ± 3.9 mN difference between the real data and linear summation. There is no significant differences between double-pulse stimulation pattern [0 20] and the linear summation of the corresponding convolved waveform. (C) An example when a double-pulse stimulation separated by 2 ms ([0 2]) was 89.9 ± 10.2 mN greater than the linear summation of a the single-pulse waveforms separated by 2 ms, producing a nonlinear effect. (D) Compares the force waveform of a triple-pulse stimulation pattern and the corresponding linear summation of the convolved waveform. At small IPIs, the real data is 73.8 ± 10.7 mN larger than the linear summation. Data presented in this figure were derived from Bird 2. Values presented are mean ± SD. Shaded regions in 3.2C and D represent the difference between the real data and the corresponding convolved waveform.

3.4 Results

This study was completed to 1) determine whether stimulation patterns with varying IPIs cause a supralinear effect on the force output of VS muscle, 2) if so, at what timescale the supralinear effects occurs, and 3) determine whether stimulation patterns with varying IPIs produce significantly different force waveforms. Previous research demonstrated that shorter IPIs (< 20 ms) in respiratory muscles produce supralinear force output and significant behavioral changes, which suggests that millisecond activation timing differences cause changes in force output (Srivastava et al., 2017). We wanted to determine whether millisecond changes in stimulation patterns to fiber bundles from VS vocal muscle also produced supralinear effects on force output. We tested 14 different stimulation patterns (1 single-pulse, 9 double-pulse, 4 triple-pulse) over many iterations varying from 42-115 across 6 muscle fiber bundle preparations.

First, we qualitatively compared the real force waveforms derived from all double- and triple-pulse stimulation patterns to the linear summation of the corresponding convolved single-pulse waveform (Figure 3.2). Figure 3.2A is the waveform for a single-pulse stimulation, which was used to find the linear summation for the other stimulation patterns. Figures 3.2B and 3.2C demonstrate the differences in force waveforms from two double-pulse stimulation patterns with a short IPI (2) and a longer IPI (20) (Figure 3.2B, C). The [0 20] stimulation pattern produced a waveform equivalent to the linear summation of the corresponding convolved waveform, implying that stimulation patterns with larger IPIs do not show supralinearity (Figure 3.2B). Alternatively, double-pulse stimulation patterns with smaller IPIs (Figure 3.2C) produced a force output that was larger when compared to the corresponding linear summation of the convolved waveform (shaded region), demonstrating strong supralinearities at IPIs = 2 in VS muscle. Figure 3.2D demonstrates

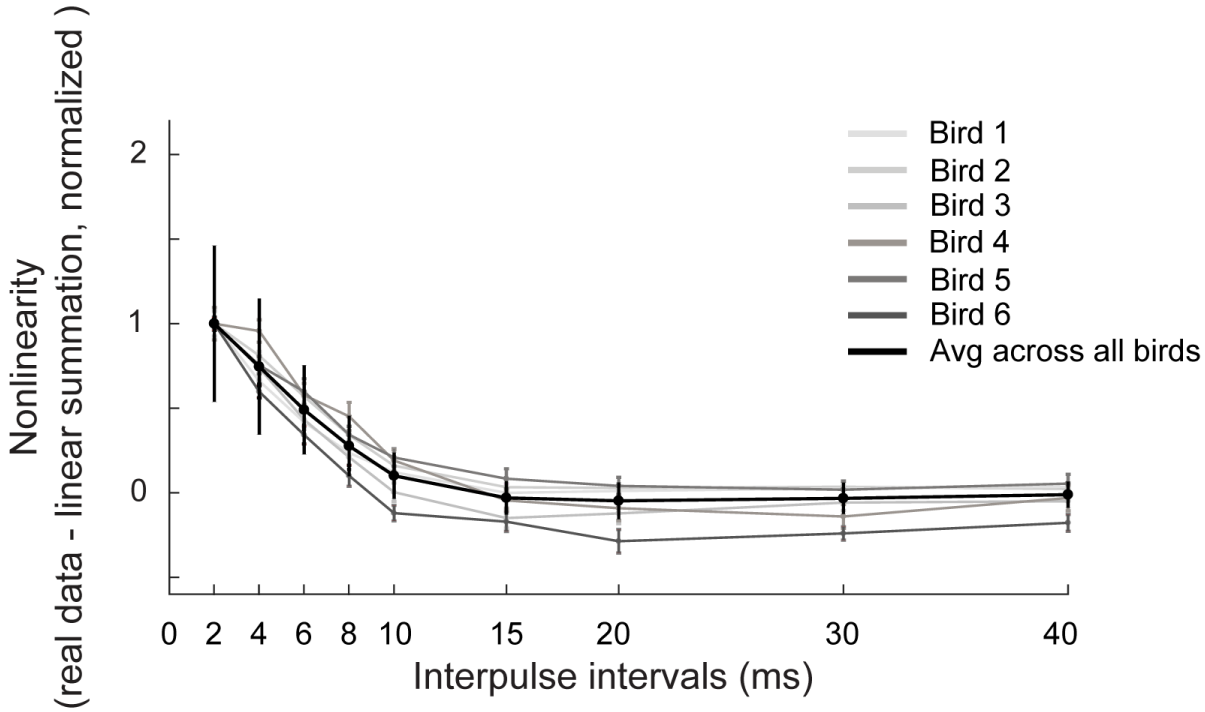

Figure 3.3: Differences between the real force output and the summed response of two-pulse stimulation patterns. Nonlinearity is the difference in area between the real data and the curve predicted from linear summation (shaded regions in Figures 3.2C and D). When the IPI > 15 ms, there was no discernable difference between the real and summed data, suggesting that the VS muscle produced a linear force output at larger IPIs. IPIs < 15 ms resulted in supralinear force output. Data points for mean across all birds are mean of real data ± error derived from the hierarchical bootstrapping method; normalized to maximum value of area under the curve (IPI = 2 ms) across double-pulse stimulation patterns.

the difference between a triple-pulse stimulation pattern and its corresponding linear summation of the single-pulse stimulation.

To quantitatively measure the difference between the real data and linear summation of double-pulse stimulation patterns, we subtracted the area under the curve of the real data from the area under the curve of the convolved waveform, as shown in Figure 3.3. The calculated difference in force, or nonlinearity values, is equivalent to the shaded regions seen in Figure 3.2C and D. A 2 ms IPI produced a waveform that had a higher force magnitude when compared to summing two single-pulse waveforms that are separated by 2 ms. As the IPI increased, the area under the curve

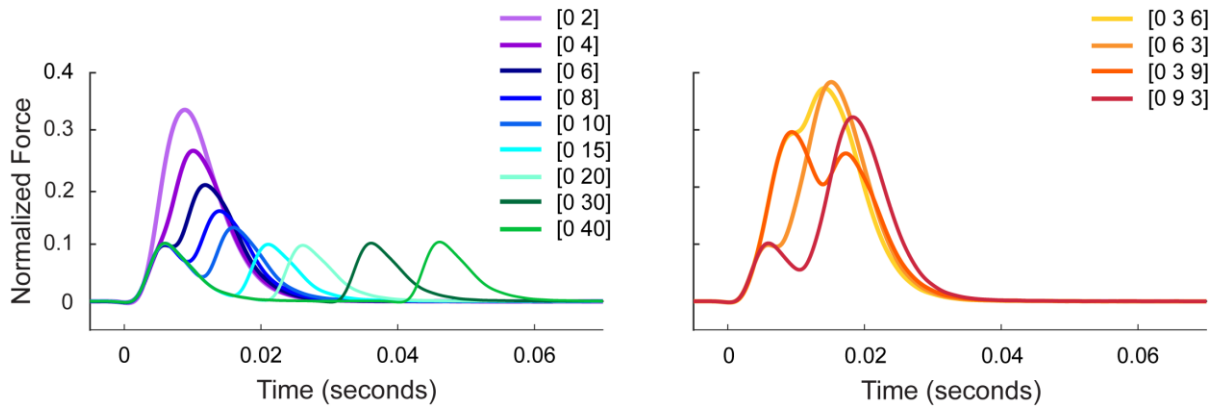

Figure 3.4: Millisecond-scale variation in IPIs affect force output. An example of force waveforms (Table 3.1, Bird 2) for double-pulse stimulation patterns (left panel) and triple-pulse stimulation patterns (right panel). Time is relative to the onset of the stimulation patterns. The force waveform for all double-pulse stimulation patterns differs significantly from each other (wfANOVA). Force waveforms from triple-pulse stimulation patterns [0 3 6] and [0 6 3] differ significantly when compared, and the same holds true when comparing force waveforms from [0 3 9] and [0 9 3] (wfANOVA). The full width of the line indicates mean ± SEM. And all force traces are normalized to peak force during tetanic contraction.

between the real and summed response decreased. As the IPI reached 15 ms or greater, there was no discernible difference between the real and linear summation force output. Although the average nonlinear effect of various IPIs across all preparations did not drop below 0, two of the six animals (Table 3.1: Birds 3 and 4) had a negative value after calculating the nonlinearity of force output with IPIs ≥ 15 ms and one animal (Table 3.1: Bird 6) has a negative value with IPIs ≥ 10 ms. Negative values for area under the curve only occurred when the second force peak was lower than the first force peak (see 'Discussion' section for further detail). These results demonstrated that songbird vocal organ muscles exhibit strong timing-based nonlinear force output with IPIs < 15 ms, and the nonlinear effects become more prominent with smaller IPIs.

We performed a wfANOVA (McKay et al., 2013; Srivastava et al., 2017) to determine whether the force waveforms from different IPIs were significantly different from one another (see section '1.2.4 Superfast Muscles' in introduction for review of Ca^{2+} kinetics). This analysis was performed three times comparing the normalized force output of every trial for: 1) all 2-pulse stimulation

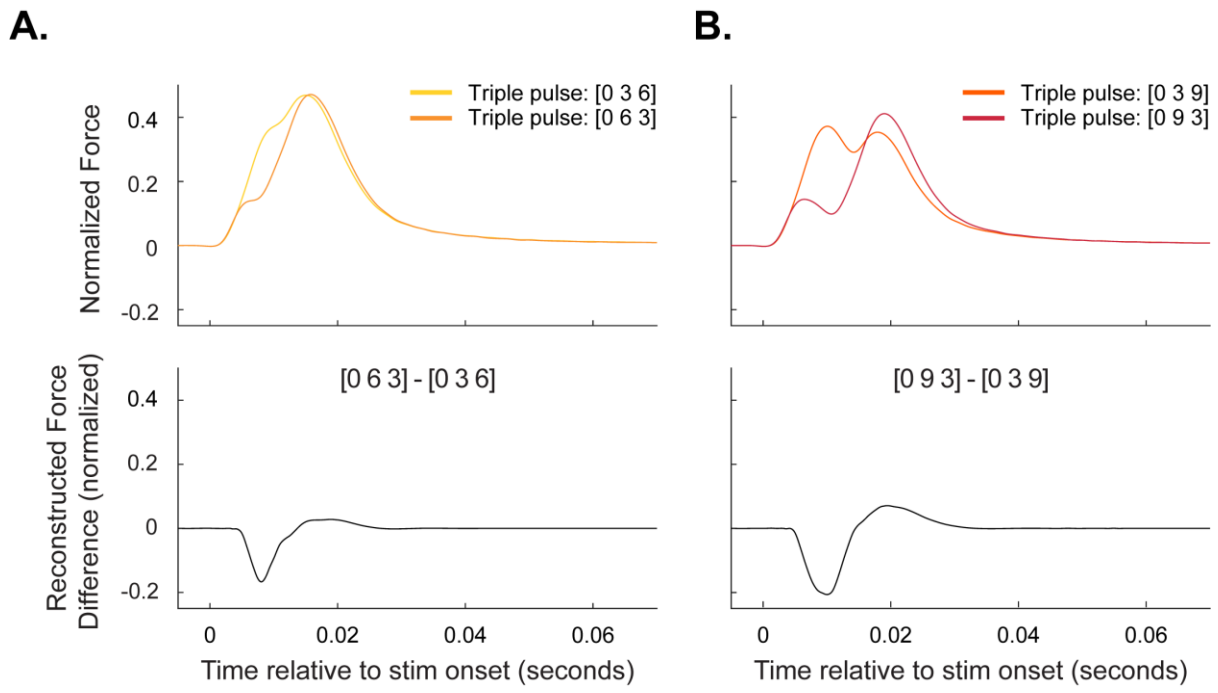

Figure 3.5: Variations in the IPI of triple-pulse stimulation patterns produce significantly different waveforms. (A) The top panel is an example of the force waveform (Table 1: Bird 2) after delivering a single-pulse stimulation pattern and two triple-pulse stimulations patterns: [0 3 6] and [0 6 3]. The reconstructed signal between inverse stimulation patterns [0 3 6] and [0 6 3] from wfANOVA revealed the force output was significantly different between the two patterns for 30.3 ms, starting at time 28.1 ms (# of significant wavelets = 29, post hoc α = 1.7 x 10-3). (B) The top panel and bottom panel show the force waveforms and the corresponding reconstructed signal, respectively, from inverse triple-stimulation patterns [0 3 9] and [0 9 3] (# of significant wavelets = 35, post hoc α = 1.43 x 10-4). The waveforms were significantly different over 23.6 ms. Time is relative to the onset of the stimulation pattern. The full width of the lines in both top panels indicates mean ± SEM.

patterns (Figure 3.4 right panel; # of significant wavelets = 202, post hoc $\alpha = 2.76 \times 10^{-4}$), 2) 3-pulse stimulation patterns [0 3 6] and [0 6 3] (Figure 3.5A; # of significant wavelets = 29, post hoc $\alpha = 1.7 \times 10^{-3}$), and 3) 3-pulse stimulation patterns [0 3 9] and [0 9 3] (Figure 3.5B; # of significant wavelets = 35, post hoc $\alpha = 1.43 \times 10^{-4}$). Every pattern produced a different force waveform as shown in Figure 3.4 (right panel: double-pulse stimulation patterns, left panel: triple-pulse stimulation patterns). We qualitatively determined that every stim pattern produced distinguishable force waveforms, which was supported by our wfANOVA results where all contrast curves derived from the analysis showed a significant effect. As predicted, the largest

changes in peak negative displacement (i.e., first force peak of stim pattern with smaller IPIs is larger than first force peak of stim pattern with larger IPIs) when looking at the double-pulse stimulation contrasts curves occurs when comparing force output between stimulation patterns [0 2] and [0 40]. The positive peak displacement depicts when the second force peak of the stimulation pattern with smaller IPIs is smaller than the second force peak of the stimulation pattern with larger IPIs. As one might assume, these results imply that the peak negative and positive displacements in contrast curves when comparing two stimulation patterns with IPIs close in value will be less and the deflections will occur at a time closer to stimulation onset. Figure 3.5 goes into more detail regarding the interpretation of the contrast curves produced by the wfANOVA when looking at the two comparisons done with the results from the triple-pulse stimulation patterns. The top panel in Figures 3.5A and B show the normalized force waveforms when the second and third pulses are shifted by 3 ms and 6 ms, respectively. The bottom panel shows the corresponding contrast curve derived from the wfANOVA. Any non-zero values in the contrast curve represents every time the compared force waveforms were statistically significant from each other. All time reported is relative to onset of stimulation.

3.5 Discussion

The data presented above demonstrated that millisecond variations in motor neuron activation patterns in a fiber bundle from a songbird's vocal muscle (VS) generated significantly different force waveforms. This was found true for all nine double-pulse and four triple-pulse stimulation patterns (Figures 3.4 and 3.5). Additionally, we determined that IPIs < 15 ms produce a timing-based nonlinear force output for double-pulse stimulation patterns, and the supralinearity of the force output reduces as the IPI gets larger (Figure 3.3).

A double-pulse stimulation typically leads to an increase in motor unit force and the ability of the muscle to maintain high force during long contractions, resulting in a second peak that is commonly larger than the first peak (Mrówczyński et al., 2015). Counterintuitively, there were 3 preparations (Table 3.1: Birds 3, 4, and 6) when looking at the force output from the double-pulse stimulation patterns with larger IPIs that produced a smaller second force peak compared to the first force peak (Figure 3.3). These data ultimately produced negative values when looking at the area under the curve between the real data and the corresponding linear summation of the single-pulse stimulation. Previous research has shown a similar force response where the second force peak in the swimbladder muscle of a toadfish, also a superfast muscle, was reduced by 20% (Harwood et al., 2011; Jong et al., 1995). Briefly, this biological phenomenon can be explained by Ca^{2+} kinetics (see section '1.2.4 Superfast muscles' and '1.2.5 Calcium dynamics' in introduction for review of Ca^{2+} kinetics), which occurs when muscle fiber cells need to pump so much Ca^{2+} that the cells reduce the subsequent amplitude of the Ca^{2+} spikes and buffer the Ca^{2+} to parvalbumin (Harwood et al., 2011). Due to the small size of syringeal muscles (e.g., largest syringeal muscle is 4 mm x 2 mm), we are unable to measure Ca^{2+} buffering. Although we cannot systematically test this, the similarities between syringeal muscles in songbirds and swimbladder muscles in toadfish (e.g., superfast muscle, low fiber stress at maximum tetanic contraction) would suggest that syringeal muscles can also experience these alternative mechanisms for Ca^{2+} kinetics. The finding that small IPIs produce nonlinear force output in muscles of the songbird vocal organ compliments our previous work that demonstrated millisecond differences in spiking patterns in cortical neurons and motor units in the respiratory muscle modulate singing and breathing behavior (Srivastava et al., 2017). Fiber bundles from the respiratory muscles produce nonlinear effects on force output with IPIs < 20 ms, which differs from the vocal organ fiber bundles that only show

nonlinearity with IPIs < 15 ms. Additionally, we know that superfast syringeal muscles (i.e., vocal organ muscles in songbirds) have a twitch half-time of 3.7 ± 0.7 ms, the capability to modulate song acoustics up to 250 Hz (Elemans et al., 2008), syringeal motor units innervate a small number of muscle fibers ranging from 1 to 13.2 ± 2.8 (Adam et al., 2021), and supralinear summation in syringeal muscles increases with muscle contraction speed (Adam & Elemans, 2020). These properties, along with the evidence that millisecond-scale variations in spike patterning in cortical neurons are correlated with the upcoming vocal behavior (Tang et al., 2014), suggest that the vocal organ muscles in songbirds can translate millisecond-scale differences in neural activity to meaningful changes in their vocal behavior. Results demonstrate that while songbird muscles typically show strong timing-based nonlinearities, the time course of these nonlinearities vary substantially across respiratory and vocal organ muscles. Precise pattern-based motor control strategies may therefore reflect a combination of linear and nonlinear summation to modulate motor output, and such strategies might differ across motor effectors.

Although all vocal organ muscles (seven bilateral pairs) are important for producing birdsong, this study focused on VS. This muscle is the largest syringeal muscle (2 mm x 4 mm). Additionally, studies have demonstrated that VS regulates the tension of the vibrating membrane in the bronchi to control and modulate pitch during vocalization, which is the song feature birds care most about. Upcoming experiments will evaluate how double- and triple-pulse stimulation patterns delivered to the VS muscle *in vivo* during ongoing song change singing behavior. We want to determine whether the trial-by-trial variations in vocal behavior are driven by the precise millisecond-scale variations in spike timing patterns found in the corresponding muscles. We predict that millisecond-scale variations in vocal organ muscle stimulation will cause measurable changes in the acoustic properties (e.g., pitch) of the vocal behavior, and the stimulation-induced changes in

behavior are due to non-linear properties in the muscles of the songbird vocal organ. These results will guide future studies to examine how muscle activity is organized across time and space, offering new insights into how the coordination of activity within and across co-active muscles develop as a skilled behavior is learned.

Animal ID	Amplitude of Tetanic Stimulation (hz)	Length of Experiment (# of Iterations)	Analyzed Data (# of Iterations)
Bird 1	400	115	55
Bird 2	300	53	23
Bird 3	400	45	7
Bird 4	500	60	28
Bird 5	400	42	24
Bird 6	400	56	17

Table 3.1. Summary of data used in analysis. All birds in experiments were male Bengalese Finches. One muscle fiber bundle was extracted from the right VS (Bird 6), all other muscle fiber bundles were extracted from the left VS.

Chapter 4

Discussion and Future Directions

4.1 Thesis discussion

One of the fundamental questions in neuroscience is establishing how patterns of neural and muscle activity in the motor system control complex behavior. Over the past ten years, our lab tackled this monumental question in two ways: 1) identifying the time scales, ranging from spike rate to millisecond timing, at which spiking patterns, at the level of the brain and muscle, are most informative about predicting trial-by-trial variations in the behavior related to producing song, and 2) understanding whether millisecond changes in spiking patterns from neurons and/or motor units caused changes to the corresponding behavior. The work presented in my dissertation determined that songbirds' vocal organ muscles contain precise millisecond-scale spike timing codes, much like we observed in RA, analogous to M1 in mammals, and the expiratory muscle group, the muscles that control the exhalation in a breath cycle (Srivastava et al., 2017; Tang et al., 2014).

To pursue these questions, we first needed to create and test a bipolar microelectrode recording array that could record both SU and MU activity, produce high SNR, and could easily make contact with deep, small muscles. In Chapter 2, we characterized the recording parameters of a novel electrode technology. We used CNTF electrodes to record EMG activity from multiple small (2 mm x 4 mm) muscles of the songbird vocal organ simultaneously (Figure 2.5A) in songbirds during an acute experimental paradigm. The unique properties of CNT electrodes allowed us to record both SU (Figure 2.6) and MU activity (Figures 2.4 and 2.5 and S2.1) with a high SNR,

without damaging muscles or interfering with normal motor function. The remarkable recording parameters (e.g., recording SUs and high SNR) of the CNT bipolar electrodes allowed us to begin researching whether millisecond-scale differences in muscle stimulation patterns modulate muscle force in vocal organ muscles. In Chapter 3, we experimentally induced two- and three-pulse stimulation patterns with varying IPIs in fiber bundles of the VS muscle *in vitro* and measured the corresponding changes in force output. These experiments demonstrated that songbird vocal organ muscles exhibit strong timing-based nonlinear force output during short IPIs (Figures 3.2, 3.3, 3.4 and 3.5).

4.1.2 Chapter 2 - Extended discussion

As mentioned in Chapter 2, ideally the EMG electrode will record low amplitude noise and high amplitude signal, resulting in a high SNR. With a high SNR, we can more reliably discriminate meaningful muscle data, especially at the level of single-motor units, from the baseline noise (Sober et al., 2008; Suarez-Perez et al., 2018). The noise amplitude reflects the stability of the electrode-muscle interface (M. B. Raez et al., 2006). CNTF electrode arrays had SNR values ~7 times higher than the SNR values of the SSW (i.e., traditional fine wire) electrodes. For example, when analyzing the noise levels of EMG recordings in the same muscle (i.e., L VS) between CNTFs and SSW (Chapter 2, Table 2.1, Bird 3), the CNTFs recorded a lower noise level ranging from 3.61 to 4.36 mV over 110 minutes. The noise level for the SSW was more variable ranging from 3.94 to 10.55 mV over 110 minutes. In this same recording, CNTFs had a signal ranging from 82.20 to 160.99 mV and SSW had a signal ranging from 42.116 to 66.24 mV. Although we were not able to systematically analyze the signal and noise amplitudes for all data presented in Chapter 2, we saw a similar trend where CNTFs had higher signal and lower noise amplitude

compared to SSW, demonstrating that CNTFs outperform fine wires as a material for EMG recordings.

Another important characteristic of EMG electrodes is having the probes exceed the flexibility of the targeted muscle (McGlynn et al., 2021). An electrode that is too stiff can introduce significant challenges, such as triggering an immune response. An immune reaction typically results in a buildup of scar tissue around the recording site, resulting in a recording that is noisy and obstructed and little to no long-term (i.e., chronic experiments) recording efficacy (Zhao et al., 2022). Additionally, too much stiffness could result in the electrode breaking upon muscle insertion due to the force exerted when penetrating through a muscle. Lastly, using a flexible and strong material for electrodes is far less likely to disrupt natural behavior. We quantitatively determined that a 4-channel SSW electrode array requires 8.3 times more force to bend when compared to CNTFs array (Figure 2.3), suggesting that CNTFs are less likely to cause an immune response break upon implantation, and disrupt behavior when compared to SSW.

Although the robust flexibility of CNTs make for an excellent material to build bipolar electrodes and record from small, deep muscles in acute experiments, the flexibility makes CNTs a difficult material to secure a bipolar electrode to the targeted muscles in a chronic experiment. As mentioned previously, there are two ways to attach electrodes to a muscle for chronic recordings: on the surface of the muscle or intramuscularly. We would need to use a biological compliant tissue adhesive to secure the CNTF bipolar electrode on the surface of the muscle, but the use of tissue adhesives risks disrupting muscle function due to toxicity. Additionally, the ultra-flexible properties of CNTFs make it difficult to secure the electrode onto the muscle with tissue adhesive. Alternatively, we could implant the CNTF intramuscularly. Because the CNTF are flexible, they lack stiffness and a sharp tip to penetrate through muscle tissue. To circumvent this obstacle, we

could either spread apart two muscle fibers with sharp forceps and secure the electrode between the fibers or implement a removable shuttle system that uses a high gauge needle to penetrate the muscle and pull the electrode into the muscle. Both intramuscular techniques have potential to cause tissue damage or an accumulation of scar tissue around the insertion site, ultimately disrupting the function of a healthy muscle. Once the limitation of securing the CNT bipolar electrode to the targeted muscle is solved, CNTF could be used in the future for chronic studies that require EMG recording within and across multiple muscles.

4.2.2 Chapter 3 - Extended discussion

In chapter 3, we demonstrated that muscles of the songbird vocal organ are sensitive to millisecond-scale differences in spiking patterns and that each variation in stimulation pattern produced a significantly different force waveform (Figure 3.4 and 3.5). Additionally, songbird muscles can exhibit strong nonlinear force output during short IPIs (i.e., IPIs < 15 ms) (Figure 3.3 and 3.5). At this time, we are still collecting *in vivo* data, so we have not yet determined whether inducing stimulation patterns to vocal organ muscles with varying IPIs cause changes in the vocal behavior. We predict millisecond-scale variations in vocal muscle stimulation will cause measurable changes in the acoustic properties (e.g., pitch) of the vocal behavior.

Understanding the timescale that motor neurons use to encode motor skill behavior has many applications outside the laboratory. One immediate application is in the development of brain-machine-interface (BMI) devices, which are used in clinical applications to control limb prosthetics or robotics for persons who have lost motor control due to brain or spinal cord injury. Most BMIs are controlled by computer algorithms based on recorded spike rate activity from multiple motor neurons, which controls the movement of a prosthetic limb (Collinger et al., 2013; Guggenmos et al., 2013; Jarosiewicz et al., 2015; Milovanovic et al., 2015). Motor parameters

necessary for movements, such as velocity, force, and position of limb, can be extracted from SU or local field potential neural recordings (Carmena et al., 2003). Currently, prosthetic limbs controlled by BMIs lack the ability to perform complex movements. Not only will the mechanisms used to coordinate muscle ensembles during learning inform motor strategies used by BMI devices but using spike-timing based codes to program BMI algorithms could also improve the prediction of motor output from cortical spike trains, significantly enhancing the performance and precision of motor prostheses. Additionally, specifically looking at the mechanisms of vocal control in birds can apply outside the birdsong research field. There are many neurological disorders that cause deficits in vocal learning, plasticity, and productions (e.g., stroke, Parkinson's Disease, speech disorders). This can have devastating effects on someone's life because of how critical verbal communication is to our interactions. Understanding the CNS circuitry and biomechanics of the vocal organ muscles will help improve and develop various types of therapies used to treat speech deficits.

Below, we propose several electrophysiological and behavioral experiments that could further investigate the role of spike timing in the motor system, which could fundamentally change our understanding of the neural control of behavior.

4.2 Future directions

4.2.1 Sensorimotor learning

Motor learning requires the brain to rapidly process sensory signals and translate the motor command into behavior through precise patterns of coordinated activity across multiple muscles, which we refer to as "muscle ensembles" (Davies, 1968; Kelso, 2009; Kelso, 1995; Thomas, 1967; Ting, 2007; Ting & Macpherson, 2005; Turvey & Carello, 1996). Many human and animal physiological studies characterize motor cortical map reorganization and anatomical changes of

motor areas relative to motor skill learning (Karni et al., 1998; Kleim, Barbay, et al., 1998; Kleim, Swain, et al., 1998; Krakauer et al., 2019; Papale & Hooks, 2018; Sternad, 2018), but the patterns of task-related neural and muscle activity during learning are unknown. Studying sensorimotor learning not only allows us to better understand the functions and integration of the sensory and motor systems, but can also examine the underlying mechanisms of information extraction, error-detection, and various classes of motor control (e.g., feed forward, reactive, and biomechanical control) (Daniel M. Wolpert et al., 2011).

The majority of our research related to how millisecond-scale spike timing patterns drive behavior has been focused on adult songbirds, at which point the song has been crystalized (i.e., learned). We know that precise-spike timing is used in the primary motor area (RA) (Tang et al., 2014), expiratory muscles (Srivastava et al., 2017), and the vocal organ muscles (Chapter 3 – unpublished work) to control variability in acoustic features (e.g., pitch) when producing song. As mentioned in the introduction, Bengalese finches develop their song during a critical period that lasts approximately 25-90 dph (Solis et al., 2000). Juveniles produce highly variable vocalizations when learning their song, and there is less variability once the song is crystalized. Previous research and preliminary data from our lab demonstrated that the characteristics of activity patterns in RA neurons change over the course of learning. In subsong, RA neurons discharge sporadically and evenly across their motif. By the time the song has been learned, RA neurons become highly stereotyped and precise bursts of activity, typically active in only one part of the song (i.e., increase in sparseness) (Leonardo & Fee, 2005; Olveczky et al., 2005). In addition, the average firing rate of neurons in RA during song increased as the behavior is learned (Olveczky et al., 2005). Although we know muscles in adult songbirds with crystalized song are sensitive to small millisecond differences in motor neuron spiking patterns, it is still unknown whether breathing or

vocal organ muscles use a slower rate code or precise spike timing-based codes to learn their song. Below, I will propose a set of electrophysiological and behavioral experiments that might expand the work presented in this dissertation and continue to advance our understanding of the mechanisms underpinning skilled sensorimotor learning.

4.2.2 How is neural activity translated into muscular coordination during motor learning?

The behavioral and electrophysiological data (e.g., neural and muscle activity) collected from the altered-training paradigm could be used to better understand many questions related to sensorimotor learning. Below I will present the questions, explain how to analyze the data in relation to the question, and expected outcomes based on our prior knowledge.

Future Direction 1

The goal of Project 1 is to investigate whether muscles use a spike timing-based code during the acquisition of a skilled vocal behavior (i.e., sensorimotor learning). For this question, we could

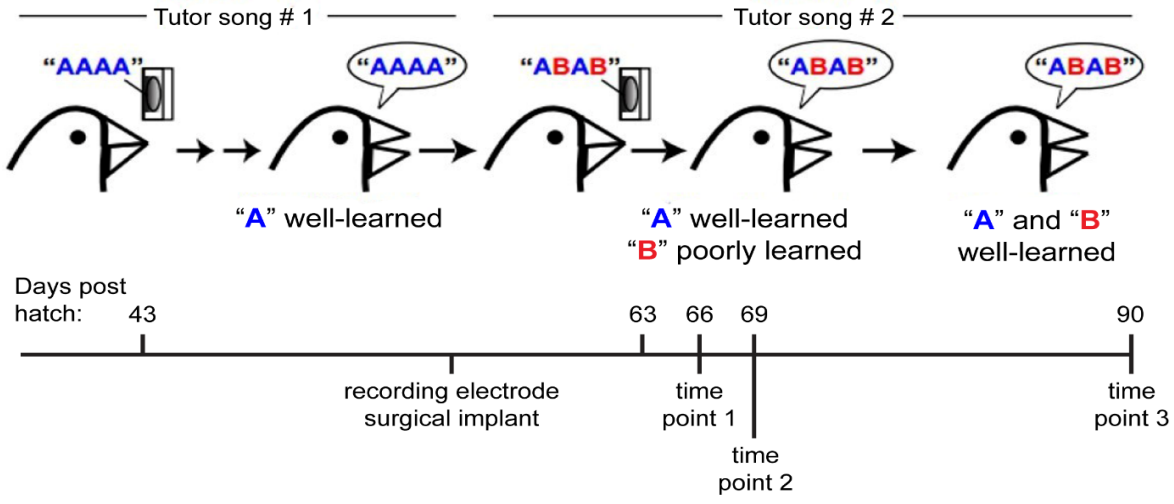

Figure 4.1: Altered-target training paradigm. After a juvenile songbird learns to produce a song consisting of only syllable ("A"), a novel syllable ("B") is presented. EMG recordings from multiple vocal muscles will be collected during the period when syllable "A" is more accurately learned (highly stereotyped syllable) but syllable "B" is less accurately learned (highly variable syllable). Adapted from (Primoz Ravbar et al., 2012).

record single motor units simultaneously from at least 4 bilateral vocal organ muscles via a microelectrode array (Zia et al., 2018). To address the limitations of traditional EMG electrodes (see 'Chapter 1.4.2 Challenges' for overview of limitations), our lab developed flexible multi-electrode arrays with 3-dimensional recording sites that can successfully and reliably record single motor unit activity from muscles.

Typically, it takes finches approximately 60 days to go through the song learning process (Mooney, 2009). It is unlikely one can successfully record muscle activity in birds over a multi-month time period. Here, I will describe a behavioral paradigm that future studies could use to record muscle and/or neural activity during plastic and crystalized syllables. "Altered-target training" will use a manipulated recording of a tutor song to train birds to completely learn one syllable, then have another syllable introduced (Figure 4.1). Experiments using altered-target training could examine the differences of muscle activity during well-learned (equivalent to crystalized song) and poorly learned (equivalent to plastic song) syllables by recording from the same single or multi motor units at two different degrees of learning.

A juvenile bird is first tutored via a recording of a synthetic song, made by splicing together recordings, consisting of a single syllable (e.g. 'AAAA', Figure 4.1). Once syllable 'A' is correctly learned, the recorded tutor song is changed to consist of two alternating syllables, the learned syllable and a novel syllable (e.g. 'ABAB') (Lipkind & Tchernichovski, 2011b). This training technique results in a period of up to two weeks the bird produces a highly stereotyped, crystalized syllable ('A', well-learned syllable) and a highly variable, plastic syllable ('B', poorly learned syllable) before syllable 'B' is learned.

For these experiments, each bird will be audio recorded continuously from 40-90 dph. Birds will begin training the first song ('AAAA') at 43 dph. The playback of the single-syllable recorded

tutor song will be triggered when the songbird pecks at a key placed in the cage (Lipkind & Tchernichovski, 2011a; Tchernichovski et al., 1999). Once the first song is learned, recording electrodes will be implanted into the vocal organ muscles. Approximately two days after surgery, the bird will begin to peck at the key, which now plays the second synthetic tutor song containing the novel syllable ('ABAB'). When the first appearance of the novel syllable ('B') in the song is identified, we will begin recording motor unit activity in vocal organ muscles. Recording will last from approximately 63-90 dph to monitor vocal learning of the novel syllable ('B') (Lipkind & Tchernichovski, 2011a; P. Ravbar et al., 2012; Tchernichovski et al., 1999).

To analyze the vocal behavior, syllable acoustics will be monitored daily with custom-written MatLab software that quantifies acoustic properties, including fundamental frequency (pitch), of specific syllables that are present in both poorly learned and well-learned song. Analysis will be completed for both syllables "A" and "B" to identify three time points: 1) First appearance of novel syllable 'B' (≈ 3 days after being introduced to syllable "B"), 2) When renditions of syllable 'B' become consistent as measured by spectral entropy (≈ 2-4 days after time point 1), and 3) Crystallization of novel syllable 'B' (≈ day 90).

Information-theoretic analysis could be used to calculate the mutual information (MI) between single unit motor neuron recordings and the vocal acoustics of poorly learned (altered-target training = syllable "B") and well-learned (altered-target training = syllable "A") song syllables at various temporal resolutions (Tang et al., 2014). MI, a measure of correlation, could reveal the extent the spiking activity (spike patterns) in vocal organ muscles predicts the vocal output during plastic song. MI is defined as the reduction in one's uncertainty about a variable given the knowledge of another variable. This reduction is expressed mathematically as a difference in entropies, specifically $MI(R;G,dt) = H(R,dt) - H(R|G,dt) = H(G,dt) - H(G|R,dt)$ (Shannon, 1997)

where H is entropy, R is spiking patterns, and *G* is a measure of behavior (e.g. higher pitch vs lower pitch of a song syllable). The estimated entropy indicates the expected uncertainty of the distribution of spiking patterns occurring at each time resolution. When performing our calculations, it is necessary to determine whether there is a sampling bias that underestimates or overestimates the uncertainty of the distribution's entropy (Bialek, 2012). We will first determine if a biased entropy exists using standard techniques (Strong et al., 1998). If a bias is found, we will use methods developed in our lab and elsewhere to correct for the sampling bias (Fisher & Mehta, 2015; Nemenman et al., 2004; Srivastava et al., 2017). A higher MI at smaller time resolutions would demonstrate that a timing code provides more information about upcoming vocal behavior compared with a rate code.

Recent data revealed that syringeal muscle properties related to the NMT change over vocal development in male songbirds. More specifically, there is an increase in speed parameters for tetanic and twitch contractions, a development and increase of supralinear summation, and the sensitivity to millisecond-scale differences in spike timing increases with speed (Adam & Elemans, 2020). Based on these characteristics of syringeal muscles and our previous knowledge regarding precise-millisecond spike timing in vocal muscles during crystalized song, we predict that learned syllables will show more mutual information at finer time scales, indicating a more precise timing code in vocal muscle motor neurons is needed to produce well-learned syllables compared with poorly learned syllables. We expect: 1) Syllable "A" (crystalized syllable) will be encoded by millisecond-scale spike timing patterns, and the MI found for syllable "A" will not change between the three time points (first time point = first appearance of novel syllable 'B', second time point = when renditions of syllable 'B' become consistent, third time point = crystallization of syllable 'B'). 2) Syllable "B" will be encoded by rate code at early stages of

learning (first and second time points). A millisecond-scale spike timing pattern will be used once the syllable is learned (third time point), correlating with an increase in MI as time resolutions decrease (Adrian & Zotterman, 1926b; Hallock & Di Lorenzo, 2006). These results will reveal how the motor code changes during motor skill learning. Finding that the motor code shifts from spike rate to precise spike timing over the course of learning would suggest differences in motor timing induce changes in vocal acoustics, providing strong evidence that the motor system has multiple patterns of spike timing during sensorimotor learning. Contrary to the predicted results, it is possible that the MI will increase as time resolutions decrease from 40 ms to 1 ms in both poorly learned and well-learned syllables. This result would still provide valuable information, suggesting that a timing code is important throughout the entirety of motor skill learning and not only used to encode learned behaviors. Further analysis would discern whether differences existed in the number of spike patterns used to produce a poorly learned and well-learned syllable.

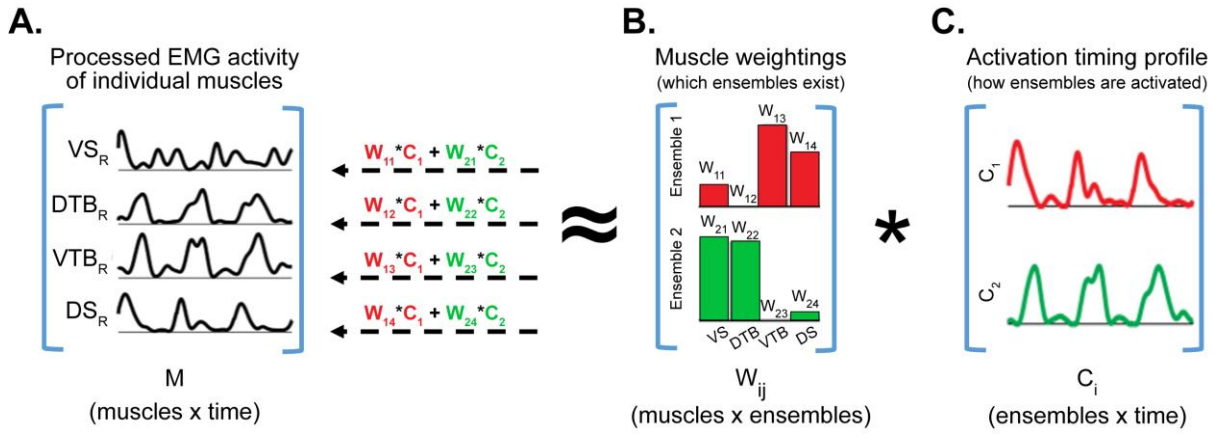

Figure 4.2: Identifying muscle ensembles via NMF analysis. A) Simulated EMG activity from four bird vocal muscles (left panel) is decomposed into a lower dimensional space made up of 2 components: patterns of activity across each muscle (Muscle Weightings, Wij) multiplied by the time-varying levels of ensemble activation (Activation Timing Profile, Ci) (right panel). B) In this example, there are two muscle ensembles (red and green bar graphs). Each bar in the graph represents the relative contribution of each muscle (j) in ensemble (i). C) Ci is how much the corresponding ensemble i was activated across time. Adapted from (Gowland et al., 1992).

Future direction 2

After determining whether the muscles rely more on a rate code or temporal code during learning, an important next question would be investigating whether changes in muscle ensembles accompany motor learning. Previous experiments show how muscle ensembles are activated during motor performance, but there is little research exploring how muscle ensembles develop and change during motor skill learning. For this experiment, we will need to record muscle activity from all muscles of the vocal organ (see section '1.2.3 Vocal organ anatomy and function' for more details) simultaneously during song acquisition. The "altered target training paradigm" can be used again to investigate and identify the differences in muscle coordination between poorly learned (i.e., plastic) and well-learned (i.e., crystalized) syllables.

To understand how muscle stimulation patterns produce various motor behaviors, it is necessary to apply a decomposition technique, such as sammon mapping (Allen et al., 2017) or non-negative matrix factorization (NMF) (Ting & Chvatal, 2010) that identifies groups of co-activated muscles rather than looking at individual muscles. Past research has shown that the complex stimulation patterns observed across muscles can be explained by time-varying combinations of a muscle ensemble representing a consistent pattern of activity across multiple muscles (Ting, 2007). NMF is a computational technique that allows one to visualize and quantitatively interpret variations in patterns of coordination between multiple muscles. In general, this method decomposes a large data set consisting of EMG activity from multiple muscles (Figure 4.2A) into two smaller data sets, represented as two components: spatial patterns of activity across multiple muscles (Figure 4.2B; the ensembles) and a scalar coefficient (Figure 4.2C; their time-varying levels of activation) (Ting & Chvatal, 2010). Mathematically this is defined as M = W x C, where M is the processed EMG data for each muscle across time (matrix M = muscles x time), the columns of W represent

the relative contribution of each muscle to each ensemble (matrix W = muscles x ensembles), and C is how much the corresponding ensemble was activated across time (matrix C = ensembles x time) (Ting & Chvatal, 2010). Custom-written MatLab code will use an iterative procedure to modify the initial values of W and C so that the product approaches the original data in M, eventually creating a reconstructed M (Allen et al., 2017; Sawers et al., 2015). The goodness of fit of reconstructed M for each number of motor ensembles will be measured by the variance accounted for (VAF), which illustrates how much of the variability in the original EMG data is accounted for by the reconstructed M. The number of muscle ensembles selected will account for at least 90% of the VAF (Ting & Chvatal, 2010). The number of extracted muscle ensembles can then be compared between poorly learned and well-learned syllables.

Sammon mapping, an algorithm that maps a data set in high-dimensional space to a lower dimensional space (typically two-dimensional space) while preserving the Euclidean distances of the original data set (de Ridder & Duin, 1997), could be used to quantitatively describe how the structure of the muscle ensemble changes between poorly learned and well-learned syllables (Figure 4.3). NMF will be run 500 times on resampled permutations of the EMG data. The new sets of muscle ensembles will be plotted into 2-D space forming clusters, where the number of clusters are set equal to the number of muscle

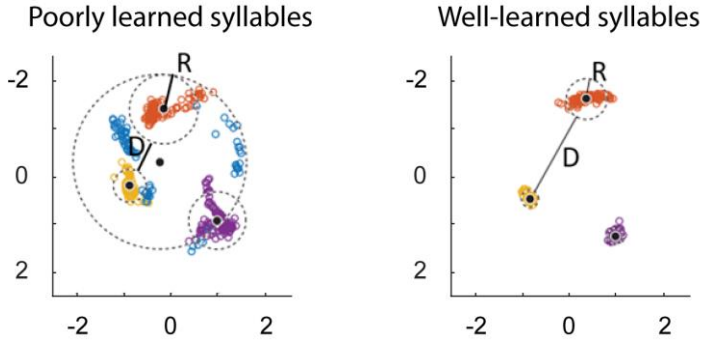

Figure 4.3: Expected results for project 2; Sammon Mapping. Each color and associated circle represents a different muscle ensemble. Poorly learned syllables (left panel) have less stability, or higher variability (larger R) and less consistency, or "distinctness" between iterations of the syllable (smaller D) compared with learned syllables (right panel), Adapted from (Allen et al., 2017).

ensembles defined above (Allen et al., 2017). Lastly, a circle will be drawn around the cluster points to 95% confidence, allowing us to measure: 1) muscle ensemble variability – the variability of muscle ensemble structure across different iterations of vocal behavior and 2) muscle ensemble "distinctness" – the ability to produce more well-defined and consistent muscle ensembles for a specific syllable (Figure 4.3) (Allen et al., 2017; Sawers et al., 2015). The radius (R) of the circle will quantify the variability of each muscle ensemble, where a decrease in muscle ensemble variability is represented by a decrease in radius size. The distance between the circle surrounding each cluster will (D) define muscle ensemble distinctness, where a greater distance represents a more defined muscle ensemble and a smaller distance represents an inconsistent activation of muscle ensembles.

If the altered-target training paradigm is used in this set of experiments, we predict that: 1) The R and D values for each cluster representing syllable "A" will not change between the three time points. 2) The R values will decrease and the D values will increase over the three time points for all the clusters representing syllable "B". These results would suggest that an increase in muscle ensemble stability and distinctness is necessary to learn a complex motor skill. Alternatively, the results could show that the number of muscle ensembles decreases as song syllables develop from poorly learned to well-learned syllables, correlating with a decrease in R value and increase in D value as the syllable is learned. This outcome would further our understanding of how muscles organize patterns of activity, suggesting that fewer muscle ensembles are needed to produce a less variable, well-learned syllable.

Additional studies can involve disrupting the millisecond-scale timing of spikes in RA neurons while recording EMG from vocal organ muscles to determine the causative role of spike timing in song learning. This will allow us to understand how changes in RA spike timing patterns directly

affects muscle ensemble formation and the vocal output. These proposed experiments aim to understand how neural and motor unit activity is coordinated within and across neurons and muscles during the learning of a skilled behavior. To our knowledge, these series of experiments would be the first to establish how muscles modulate spike timing patterns to learn a skilled behavior and offer new insights into how muscle ensembles develop and are refined as a skilled behavior is learned. These studies will allow us to further demonstrate the link between spike timing, motor performance, and complex skill learning.

References

Aamodt, C. M., Farias-Virgens, M., & White, S. A. (2019). Birdsong as a window into language origins and evolutionary neuroscience. *Philosophical Transactions of the Royal Society B*, *375*.

Adam, I., & Elemans, C. P. H. (2020). *Increasing muscle speed drives changes in the neuromuscular transform of motor commands during postnatal development in songbirds*. Cold Spring Harbor Laboratory. https://dx.doi.org/10.1101/2020.02.19.955799

Adam, I., Maxwell, A., Rossler, H., Hansen, E. B., Vellema, M., Brewer, J., & Elemans, C. P. H. (2021). One-to-one innervation of vocal muscles allows precise control of birdsong. *Curr Biol*, *31*(14), 3115-3124 e3115. https://doi.org/10.1016/j.cub.2021.05.008

Adnan, M., Pinnick, R. A., Tang, Z., Taylor, L. W., Pamulapati, S. S., Carfagni, G. R., & Pasquali, M. (2018). Bending behavior of CNT fibers and their scaling laws. *Soft Matter*, *14*(41), 8284-8292. https://doi.org/10.1039/c8sm01129j

Adrian, E. D. (1926). The impulses produced by sensory nerve endings. Part I. *Journal of Physiology-London*, *61*(1), 49-72. <Go to ISI>://WOS:000201354400003

Adrian, E. D., & Bronk, D. W. (1929). The discharge of impulses in motor nerve fibres: Part II. The frequency of discharge in reflex and voluntary contractions. *J Physiol*, *67*(2), i3-151. https://www.ncbi.nlm.nih.gov/pubmed/16994025

Adrian, E. D., & Zotterman, Y. (1926a). The impulses produced by sensory nerve-endings. Part 2. The response of a single end-organ. *Journal of Physiology-London*, *61*(2), 151-171. <Go to ISI>://WOS:000201354500001

Adrian, E. D., & Zotterman, Y. (1926b). The impulses produced by sensory nerve-endings: Part II. The response of a Single End-Organ. *J Physiol*, *61*(2), 151-171. https://doi.org/10.1113/jphysiol.1926.sp002281

Alcazar, J., Csapo, R., Ara, I., & Alegre, L. M. (2019). On the Shape of the Force-Velocity Relationship in Skeletal Muscles: The Linear, the Hyperbolic, and the Double-Hyperbolic. *Frontiers in physiology*, *10*, 769. https://doi.org/10.3389/fphys.2019.00769

Allen, J. L., McKay, J. L., Sawers, A., Hackney, M. E., & Ting, L. H. (2017). Increased neuromuscular consistency in gait and balance after partnered, dance-based rehabilitation in Parkinson's disease. *J Neurophysiol*, *118*(1), 363-373. https://doi.org/10.1152/jn.00813.2016

Alvarez, N. T., Buschbeck, E., Miller, S., Le, A. D., Gupta, V. K., Ruhunage, C., Vilinsky, I., & Ma, Y. (2020). Carbon Nanotube Fibers for Neural Recording and Stimulation. *ACS Appl Bio Mater*, *3*(9), 6478-6487. https://doi.org/10.1021/acsabm.0c00861

Amrutha, N., Arual V.H. . (2017). A Review on Noises in EMG Signal and its Removal.

An, K. H., Kim, W. S., Park, Y. S., Moon, J.-M., Bae, D. J., Lim, S. C., Lee, Y. S., & Lee, Y. H. (2001). Electrochemical Properties of High-Power Supercapacitors Using Single-Walled Carbon Nanotube Electrodes. *Advanced Functional Materials*, *11*(5), 387-392. https://doi.org/https://doi.org/10.1002/1616-3028(200110)11:5<387::AID-ADFM387>3.0.CO;2-G

Andalman, A. S., Foerster, J. N., & Fee, M. S. (2011). Control of vocal and respiratory patterns in birdsong: dissection of forebrain and brainstem mechanisms using temperature. *PLoS ONE*, *6*(9), e25461. https://doi.org/10.1371/journal.pone.0025461

Arabzadeh, E., Panzeri, S., & Diamond, M. E. (2006). Deciphering the spike train of a sensory neuron: counts and temporal patterns in the rat whisker pathway. *J Neurosci*, *26*(36), 9216-9226. https://doi.org/10.1523/JNEUROSCI.1491-06.2006

Ayyildiz, S. N., & Ayyildiz, A. (2017). Cyanoacrylic tissue glues: Biochemical properties and their usage in urology. *Turk J Urol*, *43*(1), 14-24. https://doi.org/10.5152/tud.2017.09465

Basmajian, J. V. L. C. J. d. (1985). *Muscles Alive : their functions revealed by electromyography*. Williams & Wilkins.

Baylor, S. M., & Hollingworth, S. (2012). Intracellular calcium movements during excitation-contraction coupling in mammalian slow-twitch and fast-twitch muscle fibers. *J Gen Physiol*, *139*(4), 261-272. https://doi.org/10.1085/jgp.201210773

Beck, T. W., Housh, T. J., Cramer, J. T., Malek, M. H., Mielke, M., Hendrix, R., & Weir, J. P. (2007). A comparison of monopolar and bipolar recording techniques for examining the patterns of responses for electromyographic amplitude and mean power frequency versus isometric torque for the vastus lateralis muscle. *J Neurosci Methods*, *166*(2), 159-167. https://doi.org/10.1016/j.jneumeth.2007.07.002

Behabtu, N., Young, C. C., Tsentalovich, D. E., Kleinerman, O., Wang, X., Ma, A. W., Bengio, E. A., ter Waarbeek, R. F., de Jong, J. J., Hoogerwerf, R. E., Fairchild, S. B., Ferguson, J. B., Maruyama, B., Kono, J., Talmon, Y., Cohen, Y., Otto, M. J., & Pasquali, M. (2013). Strong, light, multifunctional fibers of carbon nanotubes with ultrahigh conductivity. *Science*, *339*(6116), 182-186. https://doi.org/10.1126/science.1228061

Bengio, E., Senic, D., Taylor, L., Headrick, R., King, M., Chen, P., Little, C., Ladbury, J., Long, C., Holloway, C., Babakhani, A., Booth, J., Orloff, N., & Pasquali, M. (2019). Carbon nanotube thin film patch antennas for wireless communications. *Applied Physics Letters*, *114*, 203102. https://doi.org/10.1063/1.5093327

Berchtold, M. W., Brinkmeier, H., & Müntener, M. (2000). Calcium Ion in Skeletal Muscle: Its Crucial Role for Muscle Function, Plasticity, and Disease. *Physiological Reviews*, *80*(3), 1215-1265. https://doi.org/10.1152/physrev.2000.80.3.1215

Berniker, M., Jarc, A., Bizzi, E., & Tresch, M. C. (2009). Simplified and effective motor control based on muscle synergies to exploit musculoskeletal dynamics. *Proceedings of the National Academy of Sciences*, *106*(18), 7601-7606. https://doi.org/doi:10.1073/pnas.0901512106

Bernshteĭn, N. A. (1967). *The co-ordination and regulation of movements* (Vol. 1). Pergamon Press.

Bethune, D. S., Kiang, C. H., de Vries, M. S., Gorman, G., Savoy, R., Vazquez, J., & Beyers, R. (1993). Cobalt-catalysed growth of carbon nanotubes with single-atomic-layer walls. *Nature*, *363*(6430), 605-607. https://doi.org/10.1038/363605a0

Bialek, W. S. (2012). *Biophysics: Searching for Principles*. Princeton University Press. https://books.google.com/books?id=5In_FKA2rmUC

Bogey, R. A., Perry, J., Bontrager, E. L., & Gronley, J. K. (2000). Comparison of across-subject EMG profiles using surface and multiple indwelling wire electrodes during gait. *J Electromyogr Kinesiol*, *10*(4), 255-259. https://doi.org/10.1016/s1050-6411(00)00015-8

Bottjer, S. W., Miesner, E. A., & Arnold, A. P. (1984). Forebrain lesions disrupt development but not maintenance of song in passerine birds. *Science*, *224*(4651), 901-903. https://doi.org/10.1126/science.6719123

Boughman, J. W. (1998). Vocal learning by greater spear-nosed bats. *Proc Biol Sci*, *265*(1392), 227-233. https://doi.org/10.1098/rspb.1998.0286

Boughman, J. W., & Wilkinson, G. S. (1998). Greater spear-nosed bats discriminate group mates by vocalizations. *Anim Behav*, *55*(6), 1717-1732. https://doi.org/10.1006/anbe.1997.0721

Brainard, M. S., & Doupe, A. J. (2000). Auditory feedback in learning and maintenance of vocal behaviour. *Nat Rev Neurosci*, *1*(1), 31-40. https://doi.org/10.1038/35036205

Brainard, M. S., & Doupe, A. J. (2002). What songbirds teach us about learning. *Nature*, *417*(6886), 351-358. https://doi.org/10.1038/417351a

Brainard, M. S., & Doupe, A. J. (2013). Translating birdsong: songbirds as a model for basic and applied medical research. *Annu Rev Neurosci*, *36*, 489-517. https://doi.org/10.1146/annurev-neuro-060909-152826

Buchthal, F., & Schmalbruch, H. (1980). Motor unit of mammalian muscle. *Physiol Rev*, *60*(1), 90-142. https://doi.org/10.1152/physrev.1980.60.1.90

Burke, R. E., Levine, D. N., Tsairis, P., & Zajac, F. E., 3rd. (1973). Physiological types and histochemical profiles in motor units of the cat gastrocnemius. *J Physiol*, *234*(3), 723-748. https://doi.org/10.1113/jphysiol.1973.sp010369

Burke, R. E., & Tsairis, P. (1974). Trophic functions of the neuron. II. Denervation and regulation of muscle. The correlation of physiological properties with histochemical

characteristics in single muscle units. *Ann N Y Acad Sci*, *228*(0), 145-159. https://doi.org/10.1111/j.1749-6632.1974.tb20507.x

Calabrese, A., & Woolley, S. M. (2015). Coding principles of the canonical cortical microcircuit in the avian brain. *Proc Natl Acad Sci U S A*, *112*(11), 3517-3522. https://doi.org/10.1073/pnas.1408545112

Carmena, J. M., Lebedev, M. A., Crist, R. E., O'Doherty, J. E., Santucci, D. M., Dimitrov, D. F., Patil, P. G., Henriquez, C. S., & Nicolelis, M. A. (2003). Learning to control a brain-machine interface for reaching and grasping by primates. *PLoS Biol*, *1*(2), E42. https://doi.org/10.1371/journal.pbio.0000042

Cavalcanti Garcia, M. A., & Vieira, T. M. M. (2011). Surface electromyography: Why, when and how to use it. *Revista Andaluza de Medicina del Deporte*, *4*(1), 17-28. https://www.elsevier.es/es-revista-revista-andaluza-medicina-del-deporte-284-articulo-surface-electromyography-why-when-how-X1888754611201253

Chowdhury, R. H., Reaz, M. B., Ali, M. A., Bakar, A. A., Chellappan, K., & Chang, T. G. (2013). Surface electromyography signal processing and classification techniques. *Sensors (Basel)*, *13*(9), 12431-12466. https://doi.org/10.3390/s130912431

Clark, D. J., Ting, L. H., Zajac, F. E., Neptune, R. R., & Kautz, S. A. (2010). Merging of healthy motor modules predicts reduced locomotor performance and muscle coordination complexity post-stroke. *J Neurophysiol*, *103*(2), 844-857. https://doi.org/10.1152/jn.00825.2009

Collinger, J. L., Wodlinger, B., Downey, J. E., Wang, W., Tyler-Kabara, E. C., Weber, D. J., McMorland, A. J., Velliste, M., Boninger, M. L., & Schwartz, A. B. (2013). High-performance neuroprosthetic control by an individual with tetraplegia. *Lancet*, *381*(9866), 557-564. https://doi.org/10.1016/S0140-6736(12)61816-9

Cram, J. R. K. G. S. H. J. (1998). *Introduction to surface electromyography*. Aspen Publishers.

Dale, H. H. (1914). The action of certain esters and ethers of choline, and their relation to muscarine. *Journal of Pharmacology and Experimental Therapeutics*, *6*(2), 147-190. https://jpet.aspetjournals.org/content/jpet/6/2/147.full.pdf

Davies, B. T. (1968). A review of " The Co-ordination and Regulation of Movements" By N. Bernstein. (Pergamon Press, 1967.) [Pp. xii + 196.] 505. *Ergonomics*, *11*(1), 95-97. https://doi.org/10.1080/00140136808930945

Davis, V. A., Ericson, L. M., Parra-Vasquez, A. N. G., Fan, H., Wang, Y., Prieto, V., Longoria, J. A., Ramesh, S., Saini, R. K., Kittrell, C., Billups, W. E., Adams, W. W., Hauge, R. H., Smalley, R. E., & Pasquali, M. (2004). Phase Behavior and Rheology of SWNTs in Superacids. *Macromolecules*, *37*(1), 154-160. https://doi.org/10.1021/ma0352328

De Luca, C. J. (1997). The Use of Surface Electromyography in Biomechanics. *Journal of Applied Biomechanics*, *13*(2), 135-163. https://doi.org/10.1123/jab.13.2.135

de Ridder, D., & Duin, R. P. W. (1997). Sammon's mapping using neural networks: A comparison. *Pattern Recognition Letters*, *18*(11), 1307-1316. https://doi.org/https://doi.org/10.1016/S0167-8655(97)00093-7

Devoogd, T. J., Krebs, J. R., Healy, S. D., & Purvis, A. (1993). Relations between song repertoire size and the volume of brain nuclei related to song: comparative evolutionary analyses amongst oscine birds. *Proceedings of the Royal Society of London. Series B: Biological Sciences*, *254*(1340), 75-82.

Dominici, N., Ivanenko, Y. P., Cappellini, G., d'Avella, A., Mondi, V., Cicchese, M., Fabiano, A., Silei, T., Di Paolo, A., Giannini, C., Poppele, R. E., & Lacquaniti, F. (2011). Locomotor primitives in newborn babies and their development. *Science*, *334*(6058), 997-999. https://doi.org/10.1126/science.1210617

dos Santos, E. B. (2018). Critical Period for Song Learning. In J. Vonk & T. Shackelford (Eds.), *Encyclopedia of Animal Cognition and Behavior* (pp. 1-7). Springer International Publishing. https://doi.org/10.1007/978-3-319-47829-6_1650-1

Doupe, A., & Kuhl, P. (1999). Birdsong and human speech: Common themes and mechanisms. Annual Review of Neuroscience, 22, 567-631. *Annual review of neuroscience*, *22*, 567-631. https://doi.org/10.1146/annurev.neuro.22.1.567

Doupe, A. J., & Kuhl, P. K. (1999). Birdsong and human speech: common themes and mechanisms. *Annu Rev Neurosci*, *22*, 567-631. https://doi.org/10.1146/annurev.neuro.22.1.567

Dresselhaus, M. S., Dresselhaus, G. F., & Avouris, P. (2001). Carbon nanotubes : synthesis, structure, properties, and applications.

Duchateau, J., & Enoka, R. M. (2011). Human motor unit recordings: origins and insight into the integrated motor system. *Brain Res*, *1409*, 42-61. https://doi.org/10.1016/j.brainres.2011.06.011

Dunn, A. M., & Zann, R. A. (1996a). Undirected Song Encourages the Breeding Female Zebra Finch to Remain in the Nest. *Ethology*, *102*(4), 540-548. https://doi.org/https://doi.org/10.1111/j.1439-0310.1996.tb01146.x

Dunn, A. M., & Zann, R. A. (1996b). Undirected Song in Wild Zebra Finch Flocks: Contexts and Effects of Mate Removal. *Ethology*, *102*(4), 529-539. https://doi.org/https://doi.org/10.1111/j.1439-0310.1996.tb01145.x

Düring, D. N., Knörlein, B. J., & Elemans, C. P. H. (2017). In situ vocal fold properties and pitch prediction by dynamic actuation of the songbird syrinx. *Scientific Reports*, *7*(1), 11296. https://doi.org/10.1038/s41598-017-11258-1

During, D. N., Ziegler, A., Thompson, C. K., Ziegler, A., Faber, C., Muller, J., Scharff, C., & Elemans, C. P. (2013). The songbird syrinx morphome: a three-dimensional, high-

resolution, interactive morphological map of the zebra finch vocal organ. *BMC Biol*, *11*, 1. https://doi.org/10.1186/1741-7007-11-1

Düring, D. N., Ziegler, A., Thompson, C. K., Ziegler, A., Faber, C., Müller, J., Scharff, C., & Elemans, C. P. (2013). The songbird syrinx morphome: a three-dimensional, high-resolution, interactive morphological map of the zebra finch vocal organ. *BMC Biol*, *11*, 1. https://doi.org/10.1186/1741-7007-11-1

Ebashi, S., Maruyama, K., & Endo, M. (1980). *Muscle contraction: its regulatory mechanisms*. Springer.

Ebashi, S., & Ohtsuki, I. (2007). *Regulatory mechanisms of striated muscle contraction* (Vol. 592). Springer Science & Business Media.

Elemans, C. P., Spierts, I. L., Müller, U. K., Van Leeuwen, J. L., & Goller, F. (2004). Bird song: superfast muscles control dove's trill. *Nature*, *431*(7005), 146. https://doi.org/10.1038/431146a

Elemans, C. P., Zaccarelli, R., & Herzel, H. (2008). Biomechanics and control of vocalization in a non-songbird. *J R Soc Interface*, *5*(24), 691-703. https://doi.org/10.1098/rsif.2007.1237

Elemans, C. P. H., Mead, A. F., Jakobsen, L., & Ratcliffe, J. M. (2011). Superfast Muscles Set Maximum Call Rate in Echolocating Bats. *Science*, *333*(6051), 1885-1888. https://doi.org/doi:10.1126/science.1207309

Elemans, C. P. H., Mead, A. F., Rome, L. C., & Goller, F. (2008). Superfast Vocal Muscles Control Song Production in Songbirds. *PLoS ONE*, *3*(7), e2581. https://doi.org/10.1371/journal.pone.0002581

Engelhardt, W. A., & Liubimova, M. N. (1994). [Myosin and adenosine triphosphatase (Nature, 144, 688, Oct. 14, 1939)]. *Mol Biol (Mosk)*, *28*(6), 1229-1230. (Miozin i adenozintrifosfataza. (Nature, 144, 688, Oct. 14, 1939).)

Enoka, R. M., Amiridis, I. G., & Duchateau, J. (2020). Electrical Stimulation of Muscle: Electrophysiology and Rehabilitation. *Physiology*, *35*(1), 40-56. https://doi.org/10.1152/physiol.00015.2019

Farina, D., & Negro, F. (2012). Accessing the neural drive to muscle and translation to neurorehabilitation technologies. *IEEE Rev Biomed Eng*, *5*, 3-14. https://doi.org/10.1109/RBME.2012.2183586

Farrell, T. R., & Weir, R. F. (2008). A comparison of the effects of electrode implantation and targeting on pattern classification accuracy for prosthesis control. *IEEE Trans Biomed Eng*, *55*(9), 2198-2211. https://doi.org/10.1109/TBME.2008.923917

Faunes, M., Botelho, J. F., & Wild, J. M. (2017). Innervation of the syrinx of the zebra finch (Taeniopygia guttata). *J Comp Neurol*, *525*(13), 2847-2860. https://doi.org/10.1002/cne.24236

Fee, M. S. (2002). Measurement of the linear and nonlinear mechanical properties of the oscine syrinx: implications for function. *J Comp Physiol A Neuroethol Sens Neural Behav Physiol*, *188*(11-12), 829-839. https://doi.org/10.1007/s00359-002-0349-z

Fee, M. S. (2002). Measurement of the linear and nonlinear mechanical properties of the oscine syrinx: Implications for function. *Journal of Comparative Physiology A*, *188*(11), 829-839. https://doi.org/10.1007/s00359-002-0349-z

Fee, M. S., Shraiman, B., Pesaran, B., & Mitra, P. P. (1998). The role of nonlinear dynamics of the syrinx in the vocalizations of a songbird. *Nature*, *395*(6697), 67-71. https://doi.org/10.1038/25725

Fine, M. L., Malloy, K. L., King, C. B., Mitchell, S. L., & Cameron, T. M. (2001). Movement and sound generation by the toadfish swimbladder. *J Comp Physiol A*, *187*(5), 371-379. https://doi.org/10.1007/s003590100209

Fischer, W. J., Hirn, U., Bauer, W., & Schennach, R. (2012). Testing of individual fiber-fiber joints under biaxial load and simultaneous analysis of deformation. *Nordic Pulp & Paper Research Journal*, *27*(2), 237-244.

Fisher, C. K., & Mehta, P. (2015). Bayesian feature selection for high-dimensional linear regression via the Ising approximation with applications to genomics. *Bioinformatics*, *31*(11), 1754-1761. https://doi.org/10.1093/bioinformatics/btv037

Fox, E. J., Tester, N. J., Kautz, S. A., Howland, D. R., Clark, D. J., Garvan, C., & Behrman, A. L. (2013). Modular control of varied locomotor tasks in children with incomplete spinal cord injuries. *J Neurophysiol*, *110*(6), 1415-1425. https://doi.org/10.1152/jn.00676.2012

Fye, W. B. (1995). Albrecht von Haller. *Clin Cardiol*, *18*(5), 291-292. https://doi.org/10.1002/clc.4960180513

Gahr, M., Sonnenschein, E., & Wickler, W. (1998). Sex difference in the size of the neural song control regions in a dueting songbird with similar song repertoire size of males and females. *J Neurosci*, *18*(3), 1124-1131. https://www.ncbi.nlm.nih.gov/pubmed/9437032

Garcia Cerda, D., Ballester, A. M., Aliena-Valero, A., Caraben-Redano, A., & Lloris, J. M. (2015). Use of cyanoacrylate adhesives in general surgery. *Surg Today*, *45*(8), 939-956. https://doi.org/10.1007/s00595-014-1056-4

Gehlert, S., Bloch, W., & Suhr, F. (2015). Ca2+-dependent regulations and signaling in skeletal muscle: from electro-mechanical coupling to adaptation. *Int J Mol Sci*, *16*(1), 1066-1095. https://doi.org/10.3390/ijms16011066

Gergely, J. (1950). Relation of ATP-ase and myosin. Federation Proceedings,

Gobes, S., & Bolhuis, J. (2007). Birdsong Memory: A Neural Dissociation between Song Recognition and Production. *Current biology : CB*, *17*, 789-793. https://doi.org/10.1016/j.cub.2007.03.059

Gobes, S. M., Zandbergen, M. A., & Bolhuis, J. J. (2010). Memory in the making: localized brain activation related to song learning in young songbirds. *Proc Biol Sci*, *277*(1698), 3343-3351. https://doi.org/10.1098/rspb.2010.0870

Gobes, S. M. H., Jennings, R. B., & Maeda, R. K. (2019). The sensitive period for auditory-vocal learning in the zebra finch: Consequences of limited-model availability and multiple-tutor paradigms on song imitation. *Behav Processes*, *163*, 5-12. https://doi.org/10.1016/j.beproc.2017.07.007

Goller, F., & Cooper, B. G. (2004). Peripheral motor dynamics of song production in the zebra finch. *Ann N Y Acad Sci*, *1016*, 130-152. https://doi.org/10.1196/annals.1298.009

Goller, F., & Larsen, O. N. (1997). A new mechanism of sound generation in songbirds. *Proc Natl Acad Sci U S A*, *94*(26), 14787-14791. https://doi.org/10.1073/pnas.94.26.14787

Goller, F., & Larsen, O. N. (2002). New perspectives on mechanisms of sound generation in songbirds. *J Comp Physiol A Neuroethol Sens Neural Behav Physiol*, *188*(11-12), 841-850. https://doi.org/10.1007/s00359-002-0350-6

Goller, F., & Suthers, R. A. (1995). Implications for lateralization of bird song from unilateral gating of bilateral motor patterns. *Nature*, *373*, 63-66. https://doi.org/10.1038/373063a0

Goller, F., & Suthers, R. A. (1996). Role of syringeal muscles in controlling the phonology of bird song. *J Neurophysiol*, *76*(1), 287-300. https://doi.org/10.1152/jn.1996.76.1.287

Gowland, C., deBruin, H., Basmajian, J. V., Plews, N., & Burcea, I. (1992). Agonist and antagonist activity during voluntary upper-limb movement in patients with stroke. *Phys Ther*, *72*(9), 624-633. https://www.ncbi.nlm.nih.gov/pubmed/1508970

Greenewalt, C. H. (1968). *Bird Song: Acoustics and Physiology*. Smithsonian Institution Press. https://books.google.com/books?id=c8I9AAAAIAAJ

Guggenmos, D. J., Azin, M., Barbay, S., Mahnken, J. D., Dunham, C., Mohseni, P., & Nudo, R. J. (2013). Restoration of function after brain damage using a neural prosthesis. *Proc Natl Acad Sci U S A*, *110*(52), 21177-21182. https://doi.org/10.1073/pnas.1316885110

Hahnloser, R. H., Kozhevnikov, A. A., & Fee, M. S. (2002). An ultra-sparse code underlies the generation of neural sequences in a songbird. *Nature*, *419*(6902), 65-70. https://doi.org/10.1038/nature00974

Hallock, R. M., & Di Lorenzo, P. M. (2006). Temporal coding in the gustatory system. *Neurosci Biobehav Rev*, *30*(8), 1145-1160. https://doi.org/10.1016/j.neubiorev.2006.07.005

Hanson, J., & Huxley, H. E. (1953). Structural basis of the cross-striations in muscle. *Nature*, *172*(4377), 530-532. https://doi.org/10.1038/172530b0

Hanson, J., & Lowy, J. (1963). The structure of F-actin and of actin filaments isolated from muscle. *Journal of molecular biology*, *6*(1), 46-IN45.

Hartley, R. S. (1990). Expiratory muscle activity during song production in the canary. *Respir Physiol*, *81*(2), 177-187. https://doi.org/10.1016/0034-5687(90)90044-y

Harwood, C. L., Young, I. S., Tikunov, B. A., Hollingworth, S., Baylor, S. M., & Rome, L. C. (2011). Paying the piper: the cost of Ca2+ pumping during the mating call of toadfish. *J Physiol*, *589*(Pt 22), 5467-5484. https://doi.org/10.1113/jphysiol.2011.211979

Herzog, W., & ter Keurs, H. E. (1988). Force-length relation of in-vivo human rectus femoris muscles. *Pflugers Arch*, *411*(6), 642-647. https://doi.org/10.1007/bf00580860

Hill, A. V. (1938). The heat of shortening and the dynamic constants of muscle. *Proceedings of the Royal Society of London. Series B-Biological Sciences*, *126*(843), 136-195.

Hoffmann, L. A., Kelly, C. W., Nicholson, D. A., & Sober, S. J. (2012). A lightweight, headphones-based system for manipulating auditory feedback in songbirds. *J Vis Exp*(69), e50027. https://doi.org/10.3791/50027

Hu, H., Ni, Y., Montana, V., Haddon, R. C., & Parpura, V. (2004). Chemically Functionalized Carbon Nanotubes as Substrates for Neuronal Growth. *Nano Lett*, *4*(3), 507-511. https://doi.org/10.1021/nl035193d

Huxley, A. F., & Niedergerke, R. (1954). Structural changes in muscle during contraction; interference microscopy of living muscle fibres. *Nature*, *173*(4412), 971-973. https://doi.org/10.1038/173971a0

Huxley, H., & Hanson, J. (1954). Changes in the cross-striations of muscle during contraction and stretch and their structural interpretation. *Nature*, *173*(4412), 973-976. https://doi.org/10.1038/173973a0

Huxley, H. E. (1957). The double array of filaments in cross-striated muscle. *J Biophys Biochem Cytol*, *3*(5), 631-648. https://doi.org/10.1083/jcb.3.5.631

Huxley, H. E. (1969). The mechanism of muscular contraction. *Science*, *164*(3886), 1356-1365. https://doi.org/10.1126/science.164.3886.1356

Iijima, S. (1991). Helical microtubules of graphitic carbon. *Nature*, *354*(6348), 56-58. https://doi.org/10.1038/354056a0

Iijima, S., & Ichihashi, T. (1993). Single-shell carbon nanotubes of 1-nm diameter. *Nature*, *363*(6430), 603-605. https://doi.org/10.1038/363603a0

Israely, S., Leisman, G., & Carmeli, E. (2018). Neuromuscular synergies in motor control in normal and poststroke individuals. *Rev Neurosci*, *29*(6), 593-612. https://doi.org/10.1515/revneuro-2017-0058

Jamal, M. Z. (2012). Signal Acquisition Using Surface EMG and Circuit Design Considerations for Robotic Prosthesis.

Jan, E., & Kotov, N. A. (2007). Successful differentiation of mouse neural stem cells on layer-by-layer assembled single-walled carbon nanotube composite. *Nano Lett*, *7*(5), 1123-1128. https://doi.org/10.1021/nl0620132

Janik, V. M. (2014). Cetacean vocal learning and communication. *Curr Opin Neurobiol*, *28*, 60-65. https://doi.org/10.1016/j.conb.2014.06.010

Jarosiewicz, B., Sarma, A. A., Bacher, D., Masse, N. Y., Simeral, J. D., Sorice, B., Oakley, E. M., Blabe, C., Pandarinath, C., Gilja, V., Cash, S. S., Eskandar, E. N., Friehs, G., Henderson, J. M., Shenoy, K. V., Donoghue, J. P., & Hochberg, L. R. (2015). Virtual typing by people with tetraplegia using a self-calibrating intracortical brain-computer interface. *Sci Transl Med*, *7*(313), 313ra179. https://doi.org/10.1126/scitranslmed.aac7328

Jarque-Bou, N. J., Sancho-Bru, J. L., & Vergara, M. (2021). A Systematic Review of EMG Applications for the Characterization of Forearm and Hand Muscle Activity during Activities of Daily Living: Results, Challenges, and Open Issues. *Sensors*, *21*(9), 3035. https://www.mdpi.com/1424-8220/21/9/3035

Jarvis, E. D. (2004). Learned birdsong and the neurobiology of human language. *Ann N Y Acad Sci*, *1016*, 749-777. https://doi.org/10.1196/annals.1298.038

Jarvis, E. D., Scharff, C., Grossman, M. R., Ramos, J. A., & Nottebohm, F. (1998). For Whom The Bird Sings: Context-Dependent Gene Expression. *Neuron*, *21*(4), 775-788. https://doi.org/https://doi.org/10.1016/S0896-6273(00)80594-2

Jiang, J., Lin, E., & Hanson, D. G. (2000). Vocal fold physiology. *Otolaryngologic Clinics of North America*, *33*(4), 699-718.

Jong, D. S., Pape, P. C., Baylor, S. M., & Chandler, W. K. (1995). Calcium inactivation of calcium release in frog cut muscle fibers that contain millimolar EGTA or Fura-2. *Journal of General Physiology*, *106*(2), 337-388. https://doi.org/10.1085/jgp.106.2.337

Josephson, R. K. (1999). Dissecting muscle power output. *J Exp Biol*, *202*(Pt 23), 3369-3375. https://doi.org/10.1242/jeb.202.23.3369

Julian, F. J., & Morgan, D. L. (1979). The effect on tension of non-uniform distribution of length changes applied to frog muscle fibres. *J Physiol*, *293*, 379-392. https://doi.org/10.1113/jphysiol.1979.sp012895

Julian, F. J., & Moss, R. L. (1980). Sarcomere length-tension relations of frog skinned muscle fibres at lengths above the optimum. *J Physiol*, *304*, 529-539. https://doi.org/10.1113/jphysiol.1980.sp013341

Kam, N. W., Jan, E., & Kotov, N. A. (2009). Electrical stimulation of neural stem cells mediated by humanized carbon nanotube composite made with extracellular matrix protein. *Nano Lett*, *9*(1), 273-278. https://doi.org/10.1021/nl802859a

Kandel, E. R., Jessell, T. M., Schwartz, J. H., Siegelbaum, S. A., & Hudspeth, A. J. (2013). *Principles of Neural Science, Fifth Edition*. McGraw-Hill Education. https://books.google.com/books?id=s64z-LdAIsEC

Kao, M. H., & Brainard, M. S. (2006). Lesions of an avian basal ganglia circuit prevent context-dependent changes to song variability. *J Neurophysiol*, *96*(3), 1441-1455. https://doi.org/10.1152/jn.01138.2005

Karni, A., Meyer, G., Rey-Hipolito, C., Jezzard, P., Adams, M. M., Turner, R., & Ungerleider, L. G. (1998). The acquisition of skilled motor performance: fast and slow experience-driven changes in primary motor cortex. *Proc Natl Acad Sci U S A*, *95*(3), 861-868. https://doi.org/10.1073/pnas.95.3.861

Kazamel, M., & Warren, P. P. (2017). History of electromyography and nerve conduction studies: A tribute to the founding fathers. *J Clin Neurosci*, *43*, 54-60. https://doi.org/10.1016/j.jocn.2017.05.018

Kelley, D. B., & Nottebohm, F. (1979). Projections of a telencephalic auditory nucleus-field L-in the canary. *J Comp Neurol*, *183*(3), 455-469. https://doi.org/10.1002/cne.901830302

Kelso, J. A. (2009). Synergies: atoms of brain and behavior. *Adv Exp Med Biol*, *629*, 83-91. https://doi.org/10.1007/978-0-387-77064-2_5

Kelso, S. (1995). Dynamic Patterns: The Self-Organization of Brain and Behavior. In.

King, A. P., West, M. J., & Goldstein, M. H. (2005). Non-Vocal Shaping of Avian Song Development: Parallels to Human Speech Development. *Ethology*, *111*, 101-117. https://doi.org/10.1111/j.1439-0310.2004.01039.x

Kittelberger, J. M., & Mooney, R. (1999). Lesions of an avian forebrain nucleus that disrupt song development alter synaptic connectivity and transmission in the vocal premotor pathway. *J Neurosci*, *19*(21), 9385-9398. https://www.ncbi.nlm.nih.gov/pubmed/10531443

Kleim, J. A., Barbay, S., & Nudo, R. J. (1998). Functional reorganization of the rat motor cortex following motor skill learning. *J Neurophysiol*, *80*(6), 3321-3325. https://doi.org/10.1152/jn.1998.80.6.3321

Kleim, J. A., Swain, R. A., Armstrong, K. A., Napper, R. M., Jones, T. A., & Greenough, W. T. (1998). Selective synaptic plasticity within the cerebellar cortex following complex motor skill learning. *Neurobiol Learn Mem*, *69*(3), 274-289. https://doi.org/10.1006/nlme.1998.3827

Konishi, M. (1965). The role of auditory feedback in the control of vocalization in the white-crowned sparrow. *Z Tierpsychol*, *22*(7), 770-783.

Konishi, M. (1989). Birdsong for neurobiologists. *Neuron*, *3*(5), 541-549. https://doi.org/10.1016/0896-6273(89)90264-x

Krakauer, J. W., Hadjiosif, A. M., Xu, J., Wong, A. L., & Haith, A. M. (2019). Motor learning. *Compr Physiol*, *9*(2), 613-663.

Krashen, S. D. (1973). "Lateralization, language learning, and the critical period: Some new evidence": Errata. *Language Learning*, *23*, 297-297. https://doi.org/10.1111/j.1467-1770.1973.tb00665.x

Kroodsma, D. E. (1980). Winter Wren Singing Behavior: A Pinnacle of Song Complexity. *The Condor*, *82*(4), 357-365. https://doi.org/10.2307/1367556

Kroodsma, D. E., & Pickert, R. (1980). Environmentally dependent sensitive periods for avian vocal learning. *Nature*, *288*(5790), 477-479. https://doi.org/10.1038/288477a0

Kuhl, P. K., & Meltzoff, A. N. (1996). Infant vocalizations in response to speech: vocal imitation and developmental change. *J Acoust Soc Am*, *100*(4 Pt 1), 2425-2438. https://doi.org/10.1121/1.417951

Lapatki, B. G., Eiglsperger, U., Schindler, H. J., Radeke, J., Holobar, A., & van Dijk, J. P. (2019). Three-dimensional amplitude characteristics of masseter motor units and representativeness of extracted motor unit samples. *Clinical Neurophysiology*, *130*(3), 388-395. https://doi.org/https://doi.org/10.1016/j.clinph.2018.12.008

Larsen, O. N., & Goller, F. (2002). Direct observation of syringeal muscle function in songbirds and a parrot. *J Exp Biol*, *205*(Pt 1), 25-35. https://doi.org/10.1242/jeb.205.1.25

Lee, J. R., Ryu, S., Kim, S., & Kim, B. S. (2015). Behaviors of stem cells on carbon nanotube. *Biomater Res*, *19*, 3. https://doi.org/10.1186/s40824-014-0024-9

Leonardo, A., & Fee, M. S. (2005). Ensemble coding of vocal control in birdsong. *J Neurosci*, *25*(3), 652-661. https://doi.org/10.1523/JNEUROSCI.3036-04.2005

Liddell, E. G. T., & Sherrington, C. S. (1925). Recruitment and some other features of reflex inhibition. *Proceedings of the Royal Society of London. Series B, Containing Papers of a Biological Character*, *97*(686), 488-518. https://doi.org/doi:10.1098/rspb.1925.0016

Lipkind, D., Marcus, G. F., Bemis, D. K., Sasahara, K., Jacoby, N., Takahasi, M., Suzuki, K., Feher, O., Ravbar, P., Okanoya, K., & Tchernichovski, O. (2013). Stepwise acquisition of vocal combinatorial capacity in songbirds and human infants. *Nature*, *498*(7452), 104-108. https://doi.org/10.1038/nature12173

Lipkind, D., & Tchernichovski, O. (2011a). Quantification of developmental birdsong learning from the subsyllabic scale to cultural evolution. *Proc Natl Acad Sci U S A*, *108 Suppl 3*, 15572-15579. https://doi.org/10.1073/pnas.1012941108

Lipkind, D., & Tchernichovski, O. (2011b). Quantification of developmental birdsong learning from the subsyllabic scale to cultural evolution. *Proc Natl Acad Sci U S A*, *108 Suppl 3*(Suppl 3), 15572-15579. https://doi.org/10.1073/pnas.1012941108

Lissandrello, C. A., Gillis, W. F., Shen, J., Pearre, B. W., Vitale, F., Pasquali, M., Holinski, B. J., Chew, D. J., White, A. E., & Gardner, T. J. (2017). A micro-scale printable nanoclip for electrical stimulation and recording in small nerves. *J Neural Eng*, *14*(3), 036006. https://doi.org/10.1088/1741-2552/aa5a5b

Loeb G.E, a. G. C. (1988). ELECTROMYOGRAPHY FOR EXPERIMENTALISTS. By Gerald E. Loeb and Carl Gans. Published by University of Chicago Press, 1986. 373 pages. *Canadian Journal of Neurological Sciences*, *15*(1), 92-92.

London, S. E. (2019). Developmental song learning as a model to understand neural mechanisms that limit and promote the ability to learn. *Behav Processes*, *163*, 13-23. https://doi.org/10.1016/j.beproc.2017.11.008

Long, M. A., & Fee, M. S. (2008). Using temperature to analyse temporal dynamics in the songbird motor pathway. *Nature*, *456*(7219), 189-194. https://doi.org/10.1038/nature07448

Ludlow, C. L. (2005). Central nervous system control of the laryngeal muscles in humans. *Respir Physiol Neurobiol*, *147*(2-3), 205-222. https://doi.org/10.1016/j.resp.2005.04.015

MacDougall-Shackleton, S. A., & Ball, G. F. (1999). Comparative studies of sex differences in the song-control system of songbirds. *Trends in neurosciences*, *22*(10), 432-436.

MacIntosh, B. R. (2003). Role of Calcium Sensitivity Modulation in Skeletal Muscle Performance. *Physiology*, *18*(6), 222-225. https://doi.org/10.1152/nips.01456.2003

MacLennan, D. H., Rice, W. J., & Green, N. M. (1997). The mechanism of Ca2+ transport by sarco(endo)plasmic reticulum Ca2+-ATPases. *J Biol Chem*, *272*(46), 28815-28818. https://doi.org/10.1074/jbc.272.46.28815

Marler, P. (1970). Birdsong and speech development: could there be parallels? *Am Sci*, *58*(6), 669-673.

Marler, P., & Sherman, V. (1983). Song structure without auditory feedback: emendations of the auditory template hypothesis. *J Neurosci*, *3*(3), 517-531. https://doi.org/10.1523/jneurosci.03-03-00517.1983

Marler, P., & Sherman, V. (1985). Innate differences in singing behaviour of sparrows reared in isolation from adult conspecific song. *Animal Behaviour*, *33*(1), 57-71. https://doi.org/https://doi.org/10.1016/S0003-3472(85)80120-2

Marler, P. R. (1970). A comparative approach to vocal learning: Song development in white-crowned sparrows. *Journal of Comparative and Physiological Psychology*, *71*, 1-25.

Martinez-Valdes, E., Negro, F., Laine, C., Falla, D., Mayer, F., & Farina, D. (2017). Tracking motor units longitudinally across experimental sessions with high-density surface electromyography. *The Journal of physiology*, *595*(5), 1479-1496.

McGlynn, E., Nabaei, V., Ren, E., Galeote-Checa, G., Das, R., Curia, G., & Heidari, H. (2021). The Future of Neuroscience: Flexible and Wireless Implantable Neural Electronics. *Advanced Science*, *8*(10), 2002693. https://doi.org/https://doi.org/10.1002/advs.202002693

McGregor, J. N., Grassler, A. L., Jaffe, P. I., Jacob, A. L., Brainard, M. S., & Sober, S. J. (2022). Shared mechanisms of auditory and non-auditory vocal learning in the songbird brain. *eLife*, *11*. https://doi.org/10.7554/eLife.75691

McKay, J. L., Welch, T. D., Vidakovic, B., & Ting, L. H. (2013). Statistically significant contrasts between EMG waveforms revealed using wavelet-based functional ANOVA. *J Neurophysiol*, *109*(2), 591-602. https://doi.org/10.1152/jn.00447.2012

Mead, A. F., Osinalde, N., Ortenblad, N., Nielsen, J., Brewer, J., Vellema, M., Adam, I., Scharff, C., Song, Y., Frandsen, U., Blagoev, B., Kratchmarova, I., & Elemans, C. P. (2017). Fundamental constraints in synchronous muscle limit superfast motor control in vertebrates. *eLife*, *6*. https://doi.org/10.7554/eLife.29425

Mead, A. F., Osinalde, N., Ørtenblad, N., Nielsen, J., Brewer, J., Vellema, M., Adam, I., Scharff, C., Song, Y., Frandsen, U., Blagoev, B., Kratchmarova, I., & Elemans, C. P. H. (2017). Fundamental constraints in synchronous muscle limit superfast motor control in vertebrates. *eLife*, *6*, e29425. https://doi.org/10.7554/eLife.29425

Merlo, A., Farina, D., & Merletti, R. (2003). A fast and reliable technique for muscle activity detection from surface EMG signals. *IEEE Trans Biomed Eng*, *50*(3), 316-323. https://doi.org/10.1109/tbme.2003.808829

Mills, K. R. (2005). The basics of electromyography. *Journal of Neurology, Neurosurgery & Psychiatry*, *76*(suppl 2), ii32-ii35. https://doi.org/10.1136/jnnp.2005.069211

Milovanovic, I., Robinson, R., Fetz, E. E., & Moritz, C. T. (2015). Simultaneous and independent control of a brain-computer interface and contralateral limb movement. *Brain Comput Interfaces (Abingdon)*, *2*(4), 174-185. https://doi.org/10.1080/2326263X.2015.1080961

Minozzo, F. C., Baroni, B. M., Correa, J. A., Vaz, M. A., & Rassier, D. E. (2013). Force produced after stretch in sarcomeres and half-sarcomeres isolated from skeletal muscles. *Scientific Reports*, *3*(1), 2320. https://doi.org/10.1038/srep02320

Mohr, M., Schön, T., von Tscharner, V., & Nigg, B. M. (2018). Intermuscular Coherence Between Surface EMG Signals Is Higher for Monopolar Compared to Bipolar Electrode Configurations. *Frontiers in physiology*, *9*, 566-566. https://doi.org/10.3389/fphys.2018.00566

Mooney, R. (2009). Neural mechanisms for learned birdsong. *Learn Mem*, *16*(11), 655-669. https://doi.org/10.1101/lm.1065209

Mrówczyński, W., Celichowski, J., Raikova, R., & Krutki, P. (2015). Physiological consequences of doublet discharges on motoneuronal firing and motor unit force [Mini Review]. *Frontiers in Cellular Neuroscience*, *9*. https://doi.org/10.3389/fncel.2015.00081

Muralidharan, N., Teblum, E., Westover, A. S., Schauben, D., Itzhak, A., Muallem, M., Nessim, G. D., & Pint, C. L. (2018). Carbon Nanotube Reinforced Structural Composite Supercapacitor. *Sci Rep*, *8*(1), 17662. https://doi.org/10.1038/s41598-018-34963-x

Nemenman, I., Bialek, W., & de Ruyter van Steveninck, R. (2004). Entropy and information in neural spike trains: progress on the sampling problem. *Phys Rev E Stat Nonlin Soft Matter Phys*, *69*(5 Pt 2), 056111. https://doi.org/10.1103/PhysRevE.69.056111

Nordeen, K. W., & Nordeen, E. J. (1992). Auditory feedback is necessary for the maintenance of stereotyped song in adult zebra finches. *Behavioral & Neural Biology*, *57*, 58-66. https://doi.org/10.1016/0163-1047(92)90757-U

Nottebohm, F., & Arnold, A. P. (1976). Sexual dimorphism in vocal control areas of the songbird brain. *Science*, *194*(4261), 211-213. https://doi.org/10.1126/science.959852

Nottebohm, F., Stokes, T. M., & Leonard, C. M. (1976). Central control of song in the canary, Serinus canarius. *J Comp Neurol*, *165*(4), 457-486. https://doi.org/10.1002/cne.901650405

Nowicki, S. (1987). Vocal tract resonances in oscine bird sound production: evidence from birdsongs in a helium atmosphere. *Nature*, *325*(6099), 53-55. https://doi.org/10.1038/325053a0

Nubar, Y. (1962). Stress-strain relationship in skeletal muscle. *Ann N Y Acad Sci*, *93*, 859-876. https://doi.org/10.1111/j.1749-6632.1962.tb30512.x

Ojemann, G. A. (1991). Cortical organization of language. *J Neurosci*, *11*(8), 2281-2287. https://doi.org/10.1523/jneurosci.11-08-02281.1991

Olveczky, B. P., Andalman, A. S., & Fee, M. S. (2005). Vocal experimentation in the juvenile songbird requires a basal ganglia circuit. *PLoS Biol*, *3*(5), e153. https://doi.org/10.1371/journal.pbio.0030153

Pachitariu, M., Steinmetz, N. A., Kadir, S. N., Carandini, M., & Harris, K. D. (2016, 2016). Fast and accurate spike sorting of high-channel count probes with KiloSort.

Papale, A. E., & Hooks, B. M. (2018). Circuit changes in motor cortex during motor skill learning. *Neuroscience*, *368*, 283-297. https://doi.org/10.1016/j.neuroscience.2017.09.010

Perry, J., Easterday, C. S., & Antonelli, D. J. (1981). Surface versus intramuscular electrodes for electromyography of superficial and deep muscles. *Phys Ther*, *61*(1), 7-15. https://doi.org/10.1093/ptj/61.1.7

Podos, J. (1996). Motor constraints on vocal development in a songbird. *Animal Behaviour*, *51*(5), 1061-1070. https://doi.org/https://doi.org/10.1006/anbe.1996.0107

Poole, J. H., Tyack, P. L., Stoeger-Horwath, A. S., & Watwood, S. (2005). Animal behaviour: elephants are capable of vocal learning. *Nature*, *434*(7032), 455-456. https://doi.org/10.1038/434455a

Prasad, A., & Sanchez, J. C. (2012). Quantifying long-term microelectrode array functionality using chronic in vivo impedance testing. *J Neural Eng*, *9*(2), 026028. https://doi.org/10.1088/1741-2560/9/2/026028

Prather, J. F., Okanoya, K., & Bolhuis, J. J. (2017). Brains for birds and babies: Neural parallels between birdsong and speech acquisition. *Neuroscience & Biobehavioral Reviews*, *81*, 225-237. https://doi.org/https://doi.org/10.1016/j.neubiorev.2016.12.035

Prescott, S. A., & Sejnowski, T. J. (2008). Spike-rate coding and spike-time coding are affected oppositely by different adaptation mechanisms. *J Neurosci*, *28*(50), 13649-13661. https://doi.org/10.1523/JNEUROSCI.1792-08.2008

Putney, J., Conn, R., & Sponberg, S. (2019). Precise timing is ubiquitous, consistent, and coordinated across a comprehensive, spike-resolved flight motor program. *Proceedings of the National Academy of Sciences*, *116*(52), 26951-26960. https://doi.org/doi:10.1073/pnas.1907513116

Pylatiuk, C., Muller-Riederer, M., Kargov, A., Schulz, S., Schill, O., Reischl, M., & Bretthauer, G. (2009, 23-26 June 2009). Comparison of surface EMG monitoring electrodes for long-term use in rehabilitation device control. 2009 IEEE International Conference on Rehabilitation Robotics,

Raez, M. B., Hussain, M. S., & Mohd-Yasin, F. (2006). Techniques of EMG signal analysis: detection, processing, classification and applications. *Biological procedures online*, *8*, 11-35. https://doi.org/10.1251/bpo115

Raez, M. B. I., Hussain, M. S., & Mohd-Yasin, F. (2006). Techniques of EMG signal analysis: detection, processing, classification and applications. *Biological procedures online*, *8*, 11-35. https://doi.org/10.1251/bpo115

Ravbar, P., Lipkind, D., Parra, L. C., & Tchernichovski, O. (2012). Vocal Exploration Is Locally Regulated during Song Learning. *The Journal of Neuroscience*, *32*(10), 3422-3432. https://doi.org/10.1523/jneurosci.3740-11.2012

Ravbar, P., Lipkind, D., Parra, L. C., & Tchernichovski, O. (2012). Vocal exploration is locally regulated during song learning. *J Neurosci*, *32*(10), 3422-3432. https://doi.org/10.1523/JNEUROSCI.3740-11.2012

Rdest, M., & Janas, D. (2021). Carbon Nanotube Wearable Sensors for Health Diagnostics. *Sensors*, *21*(17), 5847. https://www.mdpi.com/1424-8220/21/17/5847

Reiner, A., Perkel, D. J., Mello, C. V., & Jarvis, E. D. (2004). Songbirds and the revised avian brain nomenclature. *Ann N Y Acad Sci*, *1016*, 77-108. https://doi.org/10.1196/annals.1298.013

Reiner, A., Yamamoto, K., & Karten, H. J. (2005). Organization and evolution of the avian forebrain. *Anat Rec A Discov Mol Cell Evol Biol*, *287*(1), 1080-1102. https://doi.org/10.1002/ar.a.20253

Riede, T., Fisher, J. H., & Goller, F. (2010). Sexual Dimorphism of the Zebra Finch Syrinx Indicates Adaptation for High Fundamental Frequencies in Males. *PLoS ONE*, *5*(6), e11368. https://doi.org/10.1371/journal.pone.0011368

Riede, T., & Goller, F. (2010a). Functional morphology of the sound-generating labia in the syrinx of two songbird species. *J Anat*, *216*(1), 23-36. https://doi.org/10.1111/j.1469-7580.2009.01161.x

Riede, T., & Goller, F. (2010b). Peripheral mechanisms for vocal production in birds - differences and similarities to human speech and singing. *Brain Lang*, *115*(1), 69-80. https://doi.org/10.1016/j.bandl.2009.11.003

Riede, T., Suthers, R. A., Fletcher, N. H., & Blevins, W. E. (2006). Songbirds tune their vocal tract to the fundamental frequency of their song. *Proc Natl Acad Sci U S A*, *103*(14), 5543-5548. https://doi.org/10.1073/pnas.0601262103

Riede, T., Thomson, S. L., Titze, I. R., & Goller, F. (2019). The evolution of the syrinx: An acoustic theory. *PLoS Biol*, *17*(2), e2006507. https://doi.org/10.1371/journal.pbio.2006507

Rome, L. C. (2006). DESIGN AND FUNCTION OF SUPERFAST MUSCLES: New Insights into the Physiology of Skeletal Muscle. *Annual Review of Physiology*, *68*(1), 193-221. https://doi.org/10.1146/annurev.physiol.68.040104.105418

Rome, L. C., Syme, D. A., Hollingworth, S., Lindstedt, S. L., & Baylor, S. M. (1996). The whistle and the rattle: the design of sound producing muscles. *Proc Natl Acad Sci U S A*, *93*(15), 8095-8100. https://doi.org/10.1073/pnas.93.15.8095

Ryu, S., Lee, P., Chou, J. B., Xu, R., Zhao, R., Hart, A. J., & Kim, S.-G. (2015). Extremely Elastic Wearable Carbon Nanotube Fiber Strain Sensor for Monitoring of Human Motion. *ACS Nano*, *9*(6), 5929-5936. https://doi.org/10.1021/acsnano.5b00599

Sanches, P. R. S., Muller, A. F., Carro, L., Susin, A. A., & Nohama, P. (2007). Analog reconfigurable technologies for EMG signal processing.

Saravanan, V., Berman, G. J., & Sober, S. J. (2020). Application of the hierarchical bootstrap to multi-level data in neuroscience. *Neuron Behav Data Anal Theory*, *3*(5). https://www.ncbi.nlm.nih.gov/pubmed/33644783

Saravanan, V., Hoffmann, L. A., Jacob, A. L., Berman, G. J., & Sober, S. J. (2019). Dopamine Depletion Affects Vocal Acoustics and Disrupts Sensorimotor Adaptation in Songbirds. *eNeuro*, *6*(3). https://doi.org/10.1523/ENEURO.0190-19.2019

Sawers, A., Allen, J. L., & Ting, L. H. (2015). Long-term training modifies the modular structure and organization of walking balance control. *J Neurophysiol*, *114*(6), 3359-3373. https://doi.org/10.1152/jn.00758.2015

Scharff, C., & Nottebohm, F. (1991). A comparative study of the behavioral deficits following lesions of various parts of the zebra finch song system: implications for vocal learning. *J Neurosci*, *11*(9), 2896-2913. https://www.ncbi.nlm.nih.gov/pubmed/1880555

Schiaffino, S., & Reggiani, C. (2011). Fiber Types in Mammalian Skeletal Muscles. *Physiological Reviews*, *91*(4), 1447-1531. https://doi.org/10.1152/physrev.00031.2010

Schmidt, M. F., & Martin Wild, J. (2014). The respiratory-vocal system of songbirds: anatomy, physiology, and neural control. *Prog Brain Res*, *212*, 297-335. https://doi.org/10.1016/B978-0-444-63488-7.00015-X

Scholz, J. P., & Schöner, G. (1999). The uncontrolled manifold concept: identifying control variables for a functional task. *Experimental Brain Research*, *126*(3), 289-306. https://doi.org/10.1007/s002210050738

Scovel, T. (2000). A CRITICAL REVIEW OF THE CRITICAL PERIOD RESEARCH. *Annual Review of Applied Linguistics*, *20*, 213-223. https://doi.org/10.1017/S0267190500200135

Shannon, C. E. (1997). The mathematical theory of communication. 1963. *MD Comput*, *14*(4), 306-317. https://www.ncbi.nlm.nih.gov/pubmed/9230594

Sharif Razavian, R., Ghannadi, B., & McPhee, J. (2019). On the Relationship Between Muscle Synergies and Redundant Degrees of Freedom in Musculoskeletal Systems [Original Research]. *Frontiers in Computational Neuroscience*, *13*. https://doi.org/10.3389/fncom.2019.00023

Shoshan-Barmatz, V., & Ashley, R. H. (1998). The structure, function, and cellular regulation of ryanodine-sensitive Ca2+ release channels. *Int Rev Cytol*, *183*, 185-270. https://doi.org/10.1016/s0074-7696(08)60145-x

Simonyan, K. (2014). The laryngeal motor cortex: its organization and connectivity. *Curr Opin Neurobiol*, *28*, 15-21. https://doi.org/10.1016/j.conb.2014.05.006

Sober, S. J., & Brainard, M. S. (2009). Adult birdsong is actively maintained by error correction. *Nat Neurosci*, *12*(7), 927-931. https://doi.org/10.1038/nn.2336

Sober, S. J., Sponberg, S., Nemenman, I., & Ting, L. H. (2018). Millisecond Spike Timing Codes for Motor Control. *Trends Neurosci*, *41*(10), 644-648. https://doi.org/10.1016/j.tins.2018.08.010

Sober, S. J., Wohlgemuth, M. J., & Brainard, M. S. (2008). Central contributions to acoustic variation in birdsong. *J Neurosci*, *28*(41), 10370-10379. https://doi.org/10.1523/JNEUROSCI.2448-08.2008

Soderberg, G. L. (1992). Selected topics in surface electromyography for use in the occupational setting; expert perspectives [Book]. https://stacks.cdc.gov/view/cdc/6906 (DHHS publication ; no. (NIOSH) 91-100)

Sohrabji, F., Nordeen, E. J., & Nordeen, K. W. (1990). Selective impairment of song learning following lesions of a forebrain nucleus in the juvenile zebra finch. *Behav Neural Biol*, *53*(1), 51-63. https://doi.org/10.1016/0163-1047(90)90797-a

Solis, M. M., Brainard, M. S., Hessler, N. A., & Doupe, A. J. (2000). Song selectivity and sensorimotor signals in vocal learning and production. *Proceedings of the National Academy of Sciences*, *97*(22), 11836-11842. https://doi.org/doi:10.1073/pnas.97.22.11836

Srivastava, K. H., Elemans, C. P., & Sober, S. J. (2015). Multifunctional and Context-Dependent Control of Vocal Acoustics by Individual Muscles. *J Neurosci*, *35*(42), 14183-14194. https://doi.org/10.1523/JNEUROSCI.3610-14.2015

Srivastava, K. H., Holmes, C. M., Vellema, M., Pack, A. R., Elemans, C. P., Nemenman, I., & Sober, S. J. (2017). Motor control by precisely timed spike patterns. *Proc Natl Acad Sci U S A*, *114*(5), 1171-1176. https://doi.org/10.1073/pnas.1611734114

Stein, R. B., Bobet, J., Oğuztöreli, M. N., & Fryer, M. (1988). The kinetics relating calcium and force in skeletal muscle. *Biophys J*, *54*(4), 705-717. https://doi.org/10.1016/s0006-3495(88)83006-6

Sternad, D. (2018). It's not (only) the mean that matters: variability, noise and exploration in skill learning. *Current Opinion in Behavioral Sciences*, *20*, 183-195. https://doi.org/https://doi.org/10.1016/j.cobeha.2018.01.004

Straub, F. (1943). Actin, ii. *Stud. Inst. Med. Chem. Univ. Szeged*, *3*, 23-37.

Strong, S. P., Koberle, R., de Ruyter van Steveninck, R. R., & Bialek, W. (1998). Entropy and Information in Neural Spike Trains. *Physical Review Letters*, *80*(1), 197-200. https://link.aps.org/doi/10.1103/PhysRevLett.80.197

Suarez-Perez, A., Gabriel, G., Rebollo, B., Illa, X., Guimerà-Brunet, A., Hernández-Ferrer, J., Martínez, M. T., Villa, R., & Sanchez-Vives, M. V. (2018). Quantification of Signal-to-Noise Ratio in Cerebral Cortex Recordings Using Flexible MEAs With Co-localized Platinum Black, Carbon Nanotubes, and Gold Electrodes [Original Research]. *Frontiers in Neuroscience*, *12*. https://doi.org/10.3389/fnins.2018.00862

Sun, C.-F., Zhu, H., Baker Iii, E. B., Okada, M., Wan, J., Ghemes, A., Inoue, Y., Hu, L., & Wang, Y. (2013). Weavable high-capacity electrodes. *Nano Energy*, *2*(5), 987-994. https://doi.org/https://doi.org/10.1016/j.nanoen.2013.03.020

Suthers, R. A., Goller, F., & Pytte, C. (1999). The Neuromuscular Control of Birdsong. *Philosophical Transactions: Biological Sciences*, *354*(1385), 927-939. http://www.jstor.org/stable/56780

Suthers, R. A., Vallet, E., Tanvez, A., & Kreutzer, M. (2004). Bilateral song production in domestic canaries. *J Neurobiol*, *60*(3), 381-393. https://doi.org/10.1002/neu.20040

Suthers, R. A., & Zollinger, S. A. (2004). Producing song: the vocal apparatus. *Ann N Y Acad Sci*, *1016*, 109-129. https://doi.org/10.1196/annals.1298.041

Szent-Gyorgyi, A. (1949). Free-energy relations and contraction of actomyosin. *Biol Bull*, *96*(2), 140-161.

Szent-Györgyi, A. G. (1975). Calcium regulation of muscle contraction. *Biophys J*, *15*(7), 707-723. https://doi.org/10.1016/s0006-3495(75)85849-8

Szent-Györgyi, A. G. (2004). The early history of the biochemistry of muscle contraction. *J Gen Physiol*, *123*(6), 631-641. https://doi.org/10.1085/jgp.200409091

Tang, C., Chehayeb, D., Srivastava, K., Nemenman, I., & Sober, S. J. (2014). Millisecond-scale motor encoding in a cortical vocal area. *PLoS Biol*, *12*(12), e1002018. https://doi.org/10.1371/journal.pbio.1002018

Tankisi, H., Burke, D., Cui, L., de Carvalho, M., Kuwabara, S., Nandedkar, S. D., Rutkove, S., Stålberg, E., van Putten, M. J. A. M., & Fuglsang-Frederiksen, A. (2020). Standards of instrumentation of EMG. *Clinical Neurophysiology*, *131*(1), 243-258. https://doi.org/https://doi.org/10.1016/j.clinph.2019.07.025

Taylor, L. W., Williams, S. M., Yan, J. S., Dewey, O. S., Vitale, F., & Pasquali, M. (2021). Washable, Sewable, All-Carbon Electrodes and Signal Wires for Electronic Clothing. *Nano Letters*, *21*(17), 7093-7099. https://doi.org/10.1021/acs.nanolett.1c01039

Tchernichovski, O., Lints, T., Mitra, P. P., & Nottebohm, F. (1999). Vocal imitation in zebra finches is inversely related to model abundance. *Proc Natl Acad Sci U S A*, *96*(22), 12901-12904. https://www.ncbi.nlm.nih.gov/pubmed/10536020

Tchernichovski, O., Mitra, P. P., Lints, T., & Nottebohm, F. (2001). Dynamics of the Vocal Imitation Process: How a Zebra Finch Learns Its Song. *Science*, *291*(5513), 2564-2569. https://doi.org/doi:10.1126/science.1058522

Thomas, G. J. (1967). The Co-ordination and Regulation of Movements. *Psyccritiques*, *12*.

Thorpe, W. H. (2008). THE LEARNING OF SONG PATTERNS BY BIRDS, WITH ESPECIAL REFERENCE TO THE SONG OF THE CHAFFINCH FRINGILLA COELEBS. *Ibis*, *100*, 535-570.

Tikunov, B. A., & Rome, L. C. (2009). Is high concentration of parvalbumin a requirement for superfast relaxation? *J Muscle Res Cell Motil*, *30*(1-2), 57-65. https://doi.org/10.1007/s10974-009-9175-z

Ting, L., & Chvatal, S. (2010). *Decomposing Muscle Activity in Motor TasksMethods and Interpretation*. https://doi.org/10.1093/acprof:oso/9780195395273.003.0005

Ting, L. H. (2007). Dimensional reduction in sensorimotor systems: a framework for understanding muscle coordination of posture. *Prog Brain Res*, *165*, 299-321. https://doi.org/10.1016/S0079-6123(06)65019-X

Ting, L. H., & Chiel, H. J. (2017). Muscle, Biomechanics, and Implications for Neural Control. In *Neurobiology of Motor Control* (pp. 365-416). https://doi.org/https://doi.org/10.1002/9781118873397.ch12

Ting, L. H., & Macpherson, J. M. (2005). A limited set of muscle synergies for force control during a postural task. *J Neurophysiol*, *93*(1), 609-613. https://doi.org/10.1152/jn.00681.2004

Ting, L. H., & McKay, J. L. (2007). Neuromechanics of muscle synergies for posture and movement. *Curr Opin Neurobiol*, *17*(6), 622-628. https://doi.org/10.1016/j.conb.2008.01.002

Titze, I. R. (1980). Comments on the myoelastic - aerodynamic theory of phonation. *J Speech Hear Res*, *23*(3), 495-510. https://doi.org/10.1044/jshr.2303.495

Titze, I. R. (1988). The physics of small-amplitude oscillation of the vocal folds. *The journal of the acoustical society of America*, *83*(4), 1536-1552.

Titze, I. R. a. A., F. (2006). *The myoelastic aerodynamic theory of phonation.*

Torres-Oviedo, G., & Ting, L. H. (2007). Muscle synergies characterizing human postural responses. *J Neurophysiol*, *98*(4), 2144-2156. https://doi.org/10.1152/jn.01360.2006

Tsentalovich, D. E., Headrick, R. J., Mirri, F., Hao, J., Behabtu, N., Young, C. C., & Pasquali, M. (2017). Influence of Carbon Nanotube Characteristics on Macroscopic Fiber Properties. *ACS Appl Mater Interfaces*, *9*(41), 36189-36198. https://doi.org/10.1021/acsami.7b10968

Turker, K. S. (1993). Electromyography: some methodological problems and issues. *Phys Ther*, *73*(10), 698-710. https://doi.org/10.1093/ptj/73.10.698

Turvey, M. T., & Carello, C. (1996). Dynamics of Bernstein's level of synergies. *Dexterity and its development*, 339-376.

Tyack, P. L. (2020). A taxonomy for vocal learning. *Philos Trans R Soc Lond B Biol Sci*, *375*(1789), 20180406. https://doi.org/10.1098/rstb.2018.0406

Van den Berg, J. (1958). Myoelastic-aerodynamic theory of voice production. *Journal of speech and hearing research*, *1*(3), 227-244.

Van den Berg, J., Zantema, J., & Doornenbal Jr, P. (1957). On the air resistance and the Bernoulli effect of the human larynx. *The journal of the acoustical society of America*, *29*(5), 626-631.

Vates, G. E., Broome, B. M., Mello, C. V., & Nottebohm, F. (1996). Auditory pathways of caudal telencephalon and their relation to the song system of adult male zebra finches. *J Comp Neurol*, *366*(4), 613-642. https://doi.org/10.1002/(sici)1096-9861(19960318)366:4<613::Aid-cne5>3.0.Co;2-7

Vicario, D. S. (1991a). Contributions of syringeal muscles to respiration and vocalization in the zebra finch. *J Neurobiol*, *22*(1), 63-73. https://doi.org/10.1002/neu.480220107

Vicario, D. S. (1991b). Neural mechanisms of vocal production in songbirds. *Curr Opin Neurobiol*, *1*(4), 595-600. https://doi.org/10.1016/s0959-4388(05)80034-0

Victor, J. D. (2005). Spike train metrics. *Curr Opin Neurobiol*, *15*(5), 585-592. https://doi.org/10.1016/j.conb.2005.08.002

Vitale, F., Summerson, S. R., Aazhang, B., Kemere, C., & Pasquali, M. (2015). Neural stimulation and recording with bidirectional, soft carbon nanotube fiber microelectrodes. *ACS Nano*, *9*(4), 4465-4474. https://doi.org/10.1021/acsnano.5b01060

Vitale, F., Vercosa, D. G., Rodriguez, A. V., Pamulapati, S. S., Seibt, F., Lewis, E., Yan, J. S., Badhiwala, K., Adnan, M., Royer-Carfagni, G., Beierlein, M., Kemere, C., Pasquali, M., & Robinson, J. T. (2018). Fluidic Microactuation of Flexible Electrodes for Neural Recording. *Nano Lett*, *18*(1), 326-335. https://doi.org/10.1021/acs.nanolett.7b04184

Voge, C. M., & Stegemann, J. P. (2011). Carbon nanotubes in neural interfacing applications. *J Neural Eng*, *8*(1), 011001. https://doi.org/10.1088/1741-2560/8/1/011001

Vromans, M., & Faghri, P. (2017). Electrical Stimulation Frequency and Skeletal Muscle Characteristics: Effects on Force and Fatigue. *Eur J Transl Myol*, *27*(4), 6816. https://doi.org/10.4081/ejtm.2017.6816

Vu, E. T., Mazurek, M. E., & Kuo, Y. C. (1994). Identification of a forebrain motor programming network for the learned song of zebra finches. *J Neurosci*, *14*(11 Pt 2), 6924-6934. https://www.ncbi.nlm.nih.gov/pubmed/7965088

Vu, P. P., Vaskov, A. K., Irwin, Z. T., Henning, P. T., Lueders, D. R., Laidlaw, A. T., Davis, A. J., Nu, C. S., Gates, D. H., Gillespie, R. B., Kemp, S. W. P., Kung, T. A., Chestek, C. A., & Cederna, P. S. (2020). A regenerative peripheral nerve interface allows real-time control of an artificial hand in upper limb amputees. *Sci Transl Med*, *12*(533). https://doi.org/10.1126/scitranslmed.aay2857

Wang, X., Jiang, K., & Shen, G. (2015). Flexible fiber energy storage and integrated devices: recent progress and perspectives. *Materials Today*, *18*(5), 265-272. https://doi.org/https://doi.org/10.1016/j.mattod.2015.01.002

Ward, S. R., Davis, J., Kaufman, K. R., & Lieber, R. L. (2007). Relationship between muscle stress and intramuscular pressure during dynamic muscle contractions. *Muscle Nerve*, *36*(3), 313-319. https://doi.org/10.1002/mus.20828

Wild, J. M. (1997). Neural pathways for the control of birdsong production. *J Neurobiol*, *33*(5), 653-670. https://doi.org/10.1002/(sici)1097-4695(19971105)33:5<653::aid-neu11>3.0.co;2-a

Wild, J. M., Goller, F., & Suthers, R. A. (1998). Inspiratory muscle activity during bird song. *Journal of Neurobiology*, *36*(3), 441-453. https://doi.org/https://doi.org/10.1002/(SICI)1097-4695(19980905)36:3<441::AID-NEU11>3.0.CO;2-E

Winkler, H. (2001, 2001//). The Ecology of Avian Acoustical Signals. Ecology of Sensing, Berlin, Heidelberg.

Wolpert, D. M., Diedrichsen, J., & Flanagan, J. R. (2011). Principles of sensorimotor learning. *Nat Rev Neurosci*, *12*(12), 739-751. https://doi.org/10.1038/nrn3112

Wolpert, D. M., Diedrichsen, J., & Flanagan, J. R. (2011). Principles of sensorimotor learning. *Nature Reviews Neuroscience*, *12*(12), 739-751. https://doi.org/10.1038/nrn3112

Yan, J. S., Orecchioni, M., Vitale, F., Coco, J. A., Duret, G., Antonucci, S., Pamulapati, S. S., Taylor, L. W., Dewey, O. S., Di Sante, M., Segura, A. M., Gurcan, C., Di Lisa, F., Yilmazer, A., McCauley, M. D., Robinson, J. T., Razavi, M., Ley, K., Delogu, L. G., & Pasquali, M. (2021). Biocompatibility studies of macroscopic fibers made from carbon nanotubes: Implications for carbon nanotube macrostructures in biomedical applications. *Carbon*, *173*, 462-476. https://doi.org/https://doi.org/10.1016/j.carbon.2020.10.077

Young, I. S., Harwood, C. L., & Rome, L. C. (2003). Cross-bridge blocker BTS permits direct measurement of SR Ca2+ pump ATP utilization in toadfish swimbladder muscle fibers. *Am J Physiol Cell Physiol*, *285*(4), C781-787. https://doi.org/10.1152/ajpcell.00025.2003

Young, I. S., & Rome, L. C. (2001). Mutually exclusive muscle designs: the power output of the locomotory and sonic muscles of the oyster toadfish (Opsanus tau). *Proc Biol Sci*, *268*(1480), 1965-1970. https://doi.org/10.1098/rspb.2001.1731

Yu, A. C., & Margoliash, D. (1996). Temporal hierarchical control of singing in birds. *Science*, *273*(5283), 1871-1875. https://doi.org/10.1126/science.273.5283.1871

Zajac, F. E. (1989). Muscle and tendon: properties, models, scaling, and application to biomechanics and motor control. *Crit Rev Biomed Eng*, *17*(4), 359-411.

Zeisel, S. H. (2012). A brief history of choline. *Ann Nutr Metab*, *61*(3), 254-258. https://doi.org/10.1159/000343120

Zhao, H., Liu, R., Zhang, H., Cao, P., Liu, Z., & Li, Y. (2022). Research Progress on the Flexibility of an Implantable Neural Microelectrode. *Micromachines (Basel)*, *13*(3). https://doi.org/10.3390/mi13030386

Zhu, F., Zhu, J., Zhang, X., Wang, Y., Su, J., McCallum, G. A., Zhang, X., Sui, X., & Durand, D. M. (2019). Flexural characterization of carbon nanotube (CNT) yarn neural electrodes. *Materials Research Express*, *6*(4), 045402. https://doi.org/10.1088/2053-1591/aafbf7

Zhurov, Y., & Brezina, V. (2006). Variability of motor neuron spike timing maintains and shapes contractions of the accessory radula closer muscle of Aplysia. *J Neurosci*, *26*(26), 7056-7070. https://doi.org/10.1523/JNEUROSCI.5277-05.2006

Zia, M., Chung, B., Sober, S. J., & Bakir, M. S. (2018). Fabrication and Characterization of 3D Multi-Electrode Array on Flexible Substrate for In Vivo EMG Recording from Expiratory Muscle of Songbird. *Tech Dig Int Electron Devices Meet*, *2018*, 29.24.21-29.24.24. https://doi.org/10.1109/iedm.2018.8614503